

6-30-2016

Characterization, Synthesis And Stabilization Of AU Based Bimetallic Catalysis For The Hydrochlorination Of Acetylene

Kerry Charles O'Connell
University of South Carolina

Follow this and additional works at: <http://scholarcommons.sc.edu/etd>



Part of the [Chemical Engineering Commons](#)

Recommended Citation

O'Connell, K. C. (2016). *Characterization, Synthesis And Stabilization Of AU Based Bimetallic Catalysis For The Hydrochlorination Of Acetylene*. (Doctoral dissertation). Retrieved from <http://scholarcommons.sc.edu/etd/3438>

This Open Access Dissertation is brought to you for free and open access by Scholar Commons. It has been accepted for inclusion in Theses and Dissertations by an authorized administrator of Scholar Commons. For more information, please contact SCHOLARC@mailbox.sc.edu.

CHARACTERIZATION, SYNTHESIS AND STABILIZATION OF AU BASED BIMETALLIC
CATALYSTS FOR THE HYDROCHLORINATION OF ACETYLENE

by

Kerry Charles O'Connell

Bachelor of Science
University of Illinois-Chicago, 2011

Submitted in Partial Fulfillment of the Requirements

For the Degree of Doctor of Philosophy in

Chemical Engineering

College of Engineering and Computing

University of South Carolina

2016

Accepted by:

John R. Regalbuto, Major Professor

John R. Monnier, Committee Member

Christopher T. Williams, Committee Member

Donna Chen, Committee Member

Lacy Ford, Senior Vice Provost and Dean of Graduate Studies

© Copyright by Kerry Charles O'Connell, 2016
All Rights Reserved.

ACKNOWLEDGEMENTS

I would like to thank all of my collaborators at the University of South Carolina, especially Hye-Ran Cho and John Tengco. My time here would not have been nearly as fulfilling or enjoyable without the help and friendship of all the catalysis group members. I want to thank Dr. John R. Regalbuto, my advisor, for the opportunity to work at CReF and develop a depth of knowledge over the field of catalysis and further my understanding of engineering principles. Thank you also to everyone on my PhD committee, all of the incites and probing questions that helped further all of my research, Dr. John Monnier, Dr. Chris Williams, and Dr. Donna Chen.

Most importantly I wish to thank Susan and Peter O'Connell, my mom and dad. Thank you for all of your love and support and especially for making home never feel so far away. This would have been an impossible task without you as my support network and I am forever grateful for that. Thank you to my fiancé Brooke Grussing for your never-ending support and kind ear when work was stressful and difficult.

ABSTRACT

Polyvinyl chloride (PVC) is the third most-produced plastic polymer world-wide by volume after polypropylene and polyethylene. Vinyl chloride monomer, which is polymerized into PVC, is produced via mercuric chloride catalysts that deactivate as mercury sublimes into the atmosphere from the catalyst surface, resulting in substantial environmental concerns.

In an effort to rationally synthesize non-mercuric catalysts, strong electrostatic adsorption (SEA) was used to prepare highly dispersed and active gold nanoparticles over low point of zero charge (PZC) carbon to increase the active metal surface area. The use of <1.5nm gold clusters did not lead to large increases in activity as there was an increased degree of particle coalescence during reaction for activated carbon supported samples. A pronounced support effect was observed in which oxide supports completely prevented Au sintering, but was virtually inactive. This suggests that the active site for the hydrochlorination reaction involves the carbon surface.

The stabilization of carbon supported gold nanoparticles in the HCl-rich reaction environment was achieved by “high surface free energy anchoring” shells of Au onto stable cores of high surface free energy metals. The synthesis of core-shell nanoparticles with high dispersion is possible by coupling electroless deposition (ED) with SEA. Highly dispersed Pt or Ru cores, which were stable in presence of HCl at elevated temperature (180°C), were prepared via SEA. ED was used to selectively deposit gold at

various surface coverages onto the stable cores. The gold, which had a lower surface free energy than that of either the Pt or Ru, remained on the base metal after 20 hours of reaction time, as no gold (or Pt or Ru) sintering was observed. However, catalytic activity of the core-shell catalysts remained low, even though the amount of exposed Au surface was on the order of twenty times higher than the pure, sintered Au catalyst.

Efforts in catalyst design and synthesis have become increasingly important to ensure high metal utilization in catalysts employing expensive metals such as platinum group metals, and to maintain an active surface at high temperatures and/or extreme chemical environments. The ability to exploit differences in surface free energy of metal species coupled with SEA and ED to control particle morphology opens up a new vein of synthesis to stabilize particles through rational catalyst design that gives unparalleled control over particle morphology and size control.

TABLE OF CONTENTS

ACKNOWLEDGEMENTS	iii
ABSTRACT	iv
LIST OF TABLES	viii
LIST OF FIGURES	ix
CHAPTER 1: INTRODUCTION	1
1.1 Catalysis overview	1
1.2 Catalyst preparation	3
1.3 Vinyl Chloride Monomer (VCM) Synthesis.....	21
1.4 Dissertation Layout	29
CHAPTER 2: HIGH SENSITIVITY SILICON SLIT DETECTORS FOR 1 NM POWDER XRD SIZE DETECTION LIMIT	32
2.1 Abstract	33
2.2 Introduction	33
2.3 Experimental	35
2.4 Results and Discussion.....	37
2.5 Conclusion	45
CHAPTER 3: THE SINTERING AND ACTIVE SITES OF SUPPORTED GOLD CATALYSTS FOR THE HYDROCHLORINATION OF ACETYLENE.....	46
3.1 Introduction	47
3.2 Experimental	50

3.3 Results and Discussion.....	54
3.4 Conclusion	68
CHAPTER 4: THE STABILIZATION OF AU SHELLS BY HIGH SURFACE FREE ENERGY PT AND RU CORE, AND THE EFFECT ON ACTIVITY FOR ACETYLENE HYDROCHLORINATION.....	70
4.1 Introduction.....	71
4.2 Experimental	75
4.3 Results and Discussion.....	80
4.4 Conclusion	94
REFERENCES	98
APPENDIX A: PREMISSION TO REPRINT	109

LIST OF TABLES

Table 1.1 Commonly used metal salt precursors for electroless deposition.....	18
Table 1.2 A positive ΔE for the redox reaction for $\text{Au}(\text{CN})_2^-$ in the presence of hydrazine for the case of Au@Pd is indicative that ED is favorable.	19
Table 2.1 Summary of Particle sizes using XRD and HRTEM.....	40
Table 3.1 Support materials used in catalytic testing, all supports were used as received, except for the oxidized VXC-72.	51
Table 3.2 Particle size before and after 20 hours TOS for Au catalysts at a GHSV of 4500 hr^{-1} with a 1.1:1:1 ratio of $\text{HCl}:\text{C}_2\text{H}_2:\text{He}$	58
Table 4.1 Summary of metal particle size as a function of time on line for Au/C, Pt/C, and Ru/C [139].....	84
Table 4.2 Summary of fractional coverage determined via chemisorption for the Au@Pt and Au@Ru bimetallic samples.....	89

LIST OF FIGURES

Figure 1.1 Simplified illustrations of various impregnation techniques	4
Figure 1.2 Mechanism of electrostatic adsorption for the case of platinum over a charged support surface	8
Figure 1.3 General steps for the method of Strong Electrostatic Adsorption: 1) Support PZC determination, 2) Uptake Survey experiment to determine pH of strongest interaction 3) Catalyst finishing i.e. reduction in Hydrogen.....	9
Figure 1.4 Modeled adsorption curves for CPA and PTA from the RPA model various SL	10
Figure 1.5 Modeled adsorption curves for CPA and PTA from the RPA model with supports of various PZC.....	12
Figure 1.6 Diagram for the selective adsorption of Platinum onto Cobalt oxide supported on silica	14
Figure 1.7 Electroless deposition method for the preparation of Au onto Pt	16
Figure 1.8 Catalytic activity of metals for anodic oxidation	20
Figure 1.9 Industrial routes for the production of VCM.....	22
Figure 1.10 Correlation of initial acetylene hydrochlorination activity with standard electrode potential for supported metal chlorides.....	23
Figure 1.11 Correlation between initial acetylene conversion versus the standard electrode potential. Potentials are obtained from the reduction potentials of the following chloride salts (RhCl_6) ³⁻ , (RuCl_5) ²⁻ , PdCl_2 , (PtCl_6) ²⁻ , (IrCl_6) ³⁻ , and (AuCl_4) ⁻	24
Figure 1.12 Conversion of acetylene (black) and selectivity to vinyl chloride (red) 95 hour run for 1 weight percent Au/C at a GHSV of 4500 hr ⁻¹	26
Figure 1.13 Schematic of the reactor system for VCM synthesis used for catalytic activity and stability studies.....	29

Figure 2.1 XRD profile of various loadings of AuNps/VXC using a.) D/teX Ultra detector, b.) Scintillation detector.	38
Figure 2.2 HRTEM image of a.) 3.0 wt.% AuNp/VXC with the particle size distribution inset. b.) Au/KBB with particle size distribution inset. c.) Au/VXC with particle size distribution inset. d.) Au/Kbb high resolution image.	39
Figure 2.3 XRD analysis of Au/KBB samples at 0.5°/min with D/teX detector.	42
Figure 2.4 XRD profile Au/VXC using D/teX Ultra detector	43
Figure 2.5 XRD pattern at different scan rates for 1% AuNp/VXC for A) D/teX B) Scintillation	43
Figure 2.6 Example of Background subtraction for Au peaks from supported Au/C in which positions and FWHM's were calculated by fitting Gaussian profiles.....	44
Figure 3.1 Au Metal uptake over the pH range of 2-13 for 160 ppm Au over 1000 m ² /L of support for each sample, uptake was determined via ICP-OES of pre and post support contacted samples.	56
Figure 3.2 Metal Free control pH shift (black) over the pH range of 1-13 using NaOH and HNO ₃ to adjust the initial pH with a surface loading of 1000 m ² /L and the metal containing pH shift with 160 ppm of Au in solution (red) adjusted under the same conditions and loading	56
Figure 3.3 XRD patterns at operating condition of 30kV and 15mA. All spectra were taken at a scan rate of 0.5°/min and sampling width of 0.02° over the range of 10-80° 2θ for the fresh (F) and spent (S) catalyst samples. A) P25, B)A300, C)VXC-OX, D)KB-M, E)KB-B, F)CA-1, G)4827 H)VXC-IWI.	59
Figure 3.4 Representative stem images of Au/KBB fresh spent particles after 20 hours on stream.....	60
Figure 3.5 Conversion of acetylene based on (C ₂ H ₂ (in) – C ₂ H ₂ (out))/ C ₂ H ₂ (in)) for each sample tested at a GHSV of 4500 hr ⁻¹ the samples were dried for 1 hour at 110°C in the glass reactor and then prechlorided at 180°C for 1 hour prior to the beginning of catalytic testing.	61
Figure 3.6 XPS spectra of fresh and used Au/C catalysts using HAuCl ₄ prepared via IWI and Au(en) ₂ Cl ₃ prepared via SEA. Fresh and spent catalysts denoted as F and S, respectively. Binding energy values have been referenced to C1s peak at 284.6 eV. Literature values for Au 4f _{7/2} binding energies of Au ⁰ , Au ⁺ , and Au ³⁺ are 84, 85.0, and 86 eV, respectively.....	64

Figure 3.7 XRD patterns for Au/C samples exposed to 1:1 HCl:He at 180°C for times increasing to 60 minutes of pre chlorination at 10 SCCM after drying for 180°C in He (10 SCCM) for 1 hour..	65
Figure 3.8 XRD patterns at operating condition of 30kV and 15mA. All spectra were taken at a scan rate of 0.5°/min and sampling width of 0.02° over the range of 10-80° 2 θ . Profiles of samples after exposure to 10 SCCM total flow rate of HCl diluted in He at 180°C over time. For atomic ratios of 1:3 and 1:9 100 ppm HCl was used, for all other atomic ratios 2000 ppm HCl was used.	67
Figure 4.1 Uptake of Au Pt, and Ru over 1000 m ² /L carbon as a function of the final pH of the adsorption solution.....	80
Figure 4.2 XRD patterns for all freshly prepared SEA catalysts after reduction(top) and XRD pattern of HCl aged catalysts at 180°C for 60 minutes and 15 hours at 1:1 HCl:He at 10 SCCM after drying at 180°C in flowing He for 60 minutes	82
Figure 4.3 STEM of Fresh Au, Ru and Pt/C and a spent Au/C catalyst	83
Figure 4.4 Conversion of Acetylene to VCM over monometallic carbon supported catalysts prepared via SEA at standard conditions, with a GHSV of 4000 hr ⁻¹	86
Figure 4.5 Concentration of Au remaining in the developer bath over time for the deposition of 1 and 2 monolayers of Au onto a) 1 wt. % Pt/C, b) 0.5 wt% Ru/C	88
Figure 4.6 Conversion of acetylene to VCM using Au@Ru/C (Black) and Au@Pt/C (red). GHSV of 4000 hr ⁻¹	91
Figure 4.7 Conversion of acetylene to VCM using Ru@Au/C (Black) and Pt@Au/C (red). GHSV of 4000 hr ⁻¹	92
Figure 4.8 STEM images of 2ML Au over Pt (top) and Ru (bottom) after reaction. Scale bars are 2nm. EDXS maps of Au and either Pt or Ru particles for each image	95
Figure 4.9 STEM images of the Spent Pt@2MLAu samples and fresh and spent 0.5Ru@2MLAu samples	96

CHAPTER 1: INTRODUCTION

1.1 Catalysis overview

The study of catalytic reactions may be dated back to 1835 when Jöns Jacob Berzelius coined the term catalytic power, with the definition of, “the abilities of a substance to awaken affinities, which are asleep at a particular temperature, by their mere presence and not by their own affinity.” Perhaps before catalysis was even thought to be studied, it was practiced through different avenues such as fermentation of sugars to ethanol and production of yogurt via enzymatic catalysis of milk. Further study of the science lead Ostwald to define a catalyst as, “a substance which accelerates a chemical reaction without affecting the position of the equilibrium” as far as the laws of physical chemistry are concerned, in which the study of catalysis is deeply rooted.

Certain properties of a catalyst are of the highest interest when determining the effectiveness for a particular reaction such as activity, stability, selectivity, toxicity, cost, and ability to be regenerated [1]. The scale and importance of catalysis on the world is enormous; it is estimated that catalytic processes are responsible for roughly 75% of all chemical and petroleum products produced annually which was about \$900 billion dollars as of 2006 [2]. Common industries that employ catalytic processes include petroleum and coal refining to value added chemicals, automobile emission control, active pharmaceutical ingredient production, agrochemicals, and the synthesis of numerous organic chemical intermediates which can only be synthesized economically via production by catalytic processes [3].

There are two main branches of catalysis: heterogeneous and homogeneous. During a heterogeneous catalytic reaction, the reactants are in a different phase than the catalyst, e.g. automobile exhaust flowing over a solid catalyst in a catalytic converter. A homogeneous reaction consists of the catalyst being in the same phase as the reactants, e.g. a liquid acid catalyst such as the self-ionization of water. The work presented in this study focuses on heterogeneous catalysis using solid-phase supported metal particles.

There has been significant development over the past several decades with the goal to better produce good catalysts with a high degree of particle morphology control and with high reproducibility. As many of the conventionally employed industrial methods are not well understood, there is a great degree of research taking place to improve and better understand the fundamental mechanisms of these methods. In our group, Strong Electrostatic Adsorption (SEA) is used to produce monometallic particles with high dispersion and this work is coupled with Electroless Deposition (ED) of metal particles to produce a bimetallic system with core-shell morphology for this study. The added degree of control gained when starting with small particles produced via SEA give an inherent advantage when producing bimetallic catalysts with a high degree of reproducibility. The following section contains a brief overview of these two methods and conventional methods of preparation for mono and bimetallic catalysts.

1.2 Catalyst preparation

Heterogeneous catalysts are the most commonly used industrial catalyst, utilized in over 90% of industrial catalytic processes. Typical heterogeneous catalysts contain very small metal nanoparticles, on the scale of nanometers, that are anchored in place by a support material that is porous, refractory, and has a high surface area. The use of small particles on a support with high surface area ensures there is a high dispersion of metal particles which increases the number of active sites per total mass of the catalyst system, thus increasing cost efficiency. The synthesis of highly dispersed metal nanoparticles, especially platinum group metals, depends heavily on a synthesis method that ensures high dispersion of the metal precursor to result in high dispersion of the reduced metal[4, 5].

There are three fundamental branches of catalyst synthesis which are employed to produce supported metal nanoparticles: precipitation, impregnation, and adsorption. These catalyst synthesis methods can be broken down into even more complex preparation methods, with more tuning of variables in the synthetic procedures, among other research groups. The choice of metal and support plays an important role for these three methods. The supports (carbon, alumina, silica, titania, zeolites) used vary as widely as the metals deposited onto them, but the main focus on this study will be carbon supported catalysts.

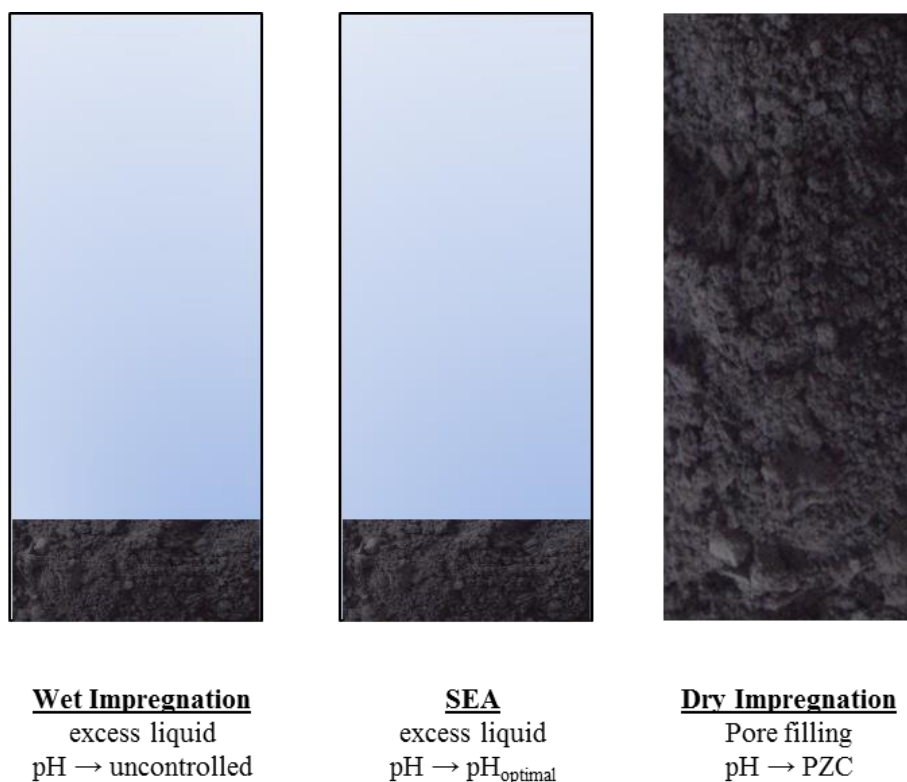


Figure 1.1 Simplified illustrations of various impregnation techniques and the parameters that are controlled during synthesis

1.2.1 Impregnation

Impregnation is by far the most commonly used method for catalyst synthesis method in industry, as well as academic research. It is classified as either dry impregnation (DI) or often incipient wetness impregnation (IWI) when the volume of the impregnation metal containing solution is equal to that of the pore volume of the support and is added to the support [6]. The liquid rapidly diffuses into the macro and micro pores of the support through the convection process which disperses the metal salt on the surface of the support and after catalyst finishing the metal species remains on the support. This method is often used to produce bimetallic catalysts by using two metal precursors in the impregnation solution and has the advantage of not needing to be filtered as the solution is dried from the support in atmosphere and a precise metal

loading is achieved. As pH is often not controlled, there is no way to ensure that strong precursor-support interactions are taking place and this may result in poor dispersion of the metal particles.

Wet impregnation (WI) is another type of impregnation preparation that the metal precursor solution is contacted with the support in excess of the pore volume of the support and the samples are agitated for better precursor distribution and thus better metal particle distribution. The samples are filtered and washed after stirring, which results in any precursors that interact weakly with the support to be washed away. This means the initial and final concentrations of the metal precursor need to be measured. The liquid in the metal-salt and support slurry can also be evaporated over time in atmosphere, at elevated temperature to ensure no complexes are washed from the surface and a homogenous distribution is achieved [7].

1.2.2 Precipitation

Precipitation involves the evolution of a solid phase from a homogenous liquid phase as a result of physical and or chemical transformations. It combines nucleation and agglomeration which are the formation of stable nanoparticles and the growth of these nanoparticle into larger particles. This process is very dependent on the pH of the solution, temperature at which the process occurs, as well as the type of chemical reagents (i.e. a precursor that will precipitate) used as well as presence of nucleation sites. The degree of precursor saturation is the determining step for nucleation and the growth of these particles [8]. This technique is often also used to synthesize multi-phase systems so two metals can be precipitated at the same time. This technique depends heavily on the solubility of the two metals to determine the rate of deposition as well as the degree of

alloying of the multiple species as there is often sequential precipitation of the metals as opposed to pure co-precipitation and there is a large dependence on pH to ensure the complexes precipitate on the support surface after speciation.

A common use of precipitation, especially in the synthesis of supported gold catalysts, is the method of deposition precipitation (DP). This method of preparation dates back to the work of Farben and Gues [9]. DP combines a metal salt precursor commonly HAuCl_4 when gold is deposited [10], with a precipitating agent that is mixed homogeneously throughout the solution that is mixed with the salt and support. Commonly used precipitating agents are urea [5, 11] and sodium hydroxide [10, 12, 13]. After the addition and mixing of the precipitating agent, the support itself becomes sites for nucleation for precipitation of the metal-hydroxide complexes from solution on the surface. After the nucleation of these gold seed particles, growth occurs as the gold atoms start to form larger clusters with the polydispersity index depending on the pH gradient of the solution. The method of DP-urea developed by Geus and further studied by Louis, allows for the limiting of pH gradients in the bath, which promotes the homogeneity of the bath by the slow decomposition of urea at elevated temperatures which ensures deposition onto the support surface in a uniform manner. DP synthesis methods have the advantage of being highly reproducible and allow for high metal loadings for metals such as Pt, Pd, Ni, and Au [10, 12-17]. There is also a thrust of research that applies sequential deposition precipitation for bimetallic catalysts, such as Au-Ag and Au-Cu [18, 19].

1.2.3 Adsorption

Adsorption is an application of the impregnation method when strong metal-support interactions are created between the support material and the metal precursor that

can be anionic or cationic in nature. Three separate subcategories exist for adsorption, strong electrostatic adsorption (SEA), reactive adsorption, which will be covered as electroless deposition (ED) in this chapter, and ion exchange (IE). SEA and ED will be discussed extensively throughout this work. Monometallic gold and bimetallic gold containing catalysts were synthesized via a combination of these methods for the hydrochlorination of acetylene to vinyl chloride monomer (VCM). Ion exchange will be covered briefly to ensure complete coverage of the topic. Ion exchange is a process that unlike SEA or ED occurs independent of the pH of the solution. The driving force for this process is the change in charge of the adsorbing complex, and is often employed for preparing supported catalysts on zeolites. A proton H^+ in the zeolite framework is often exchanged with a cationic metal precursor creating a localized difference in charge and a driving force for adsorption [20]. There are limited amounts of cationic precursors that are favorable for IE, which adds to the difficulty of the technique, but it is a favorable method to ensure strong metal support interactions take place to increase metal dispersion for select systems [4].

1.2.4 Strong Electrostatic Adsorption

SEA is the cornerstone method of catalyst synthesis in the Regalbuto research group. This method accounts for the charging parameter of the support in the adsorbing solution as a function of the pH of that solution. The control of pH and the ability to adjust surface charge differentiates SEA from typical impregnation methods and allows for anionic and cationic precursors to be strongly adsorbed onto the support. This work dates back to the groundbreaking work of Brunelle [21] and Schwarz [22-25], which operated under the hypothesis that the adsorption of noble metal complexes onto metal

oxides, typically used as catalyst supports, was of a columbic nature. Further work found that the adsorption of noble metals over carbon was also columbic in nature [26-29]. The degree of deprotonation or protonation of the surface hydroxyl groups as a function of the adsorbate solution pH determines if there is a driving force for either cationic or anionic complex adsorption onto the surface of the support. The pH at which the net charge on the support becomes zero is dubbed the point of zero charge or PZC. This phenomenon is depicted in figure 1.2 below.

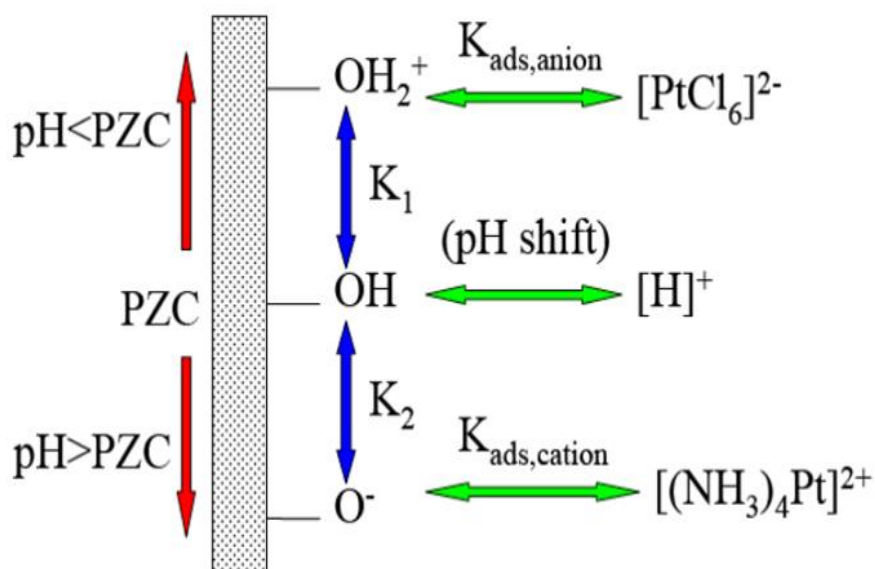


Figure 1.2 Mechanism of electrostatic adsorption for the case of platinum over a charged support surface

According to figure 1.2 when the system is below the PZC of the support, the surface hydroxyl groups protonate and the surface has a net positive charge, which permits the adsorption of anionic metal complexes such as chloroplatinic acid (CPA) or $[\text{PtCl}_6]^{2-}$ in this example. When the system is at a pH above the PZC of the support, the surface hydroxyl groups become deprotonated and there is a net negative charge on the

surface, which is a driving force for the adsorption of cationic metal complexes such as platinum tetraammine (PTA) $[(\text{NH}_3)_4\text{Pt}]^{2+}$.

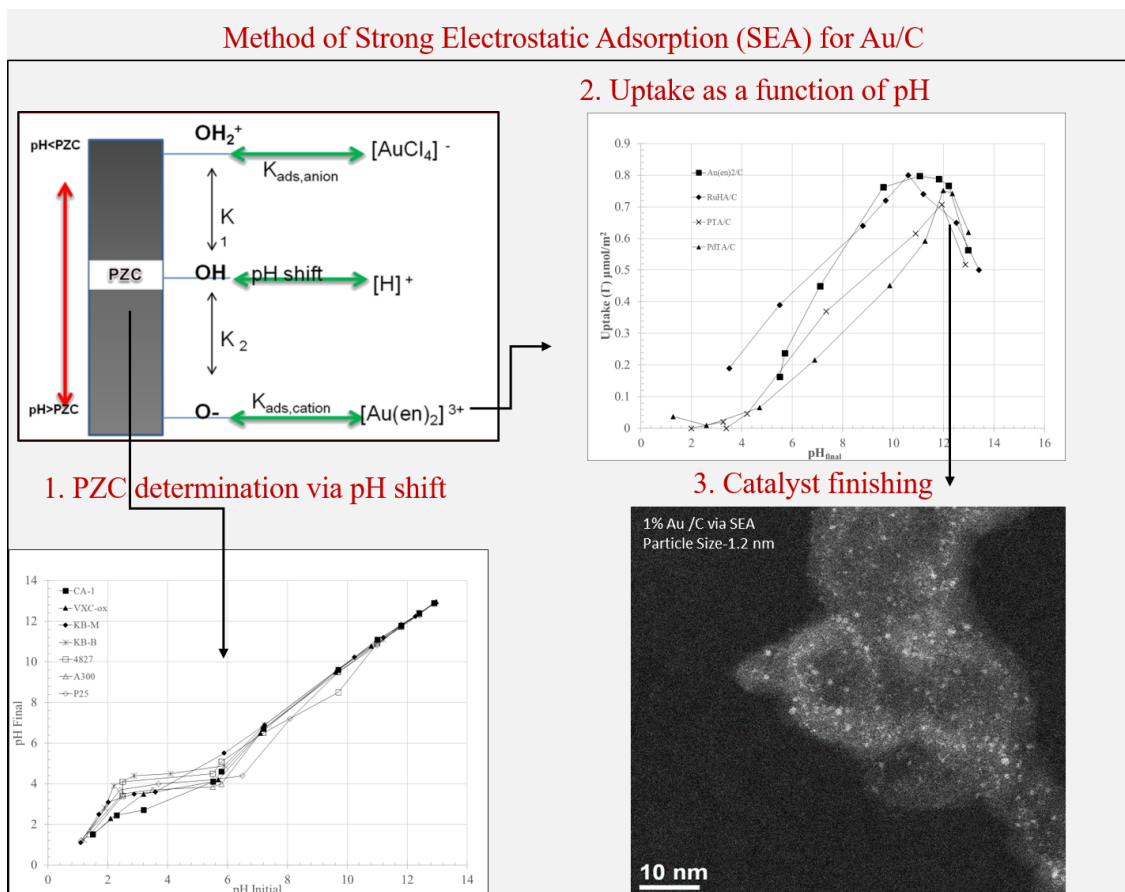


Figure 1.3 General steps for the method of Strong Electrostatic Adsorption: 1) Support PZC determination, 2) Uptake Survey experiment to determine pH of strongest interaction 3) Catalyst finishing i.e. reduction in Hydrogen

To perform SEA synthesis, the first step is to determine the PZC of the desired support material. This can be done very accurately via the measurement of the equilibrium pH as a function of the initial pH of the adsorbing solution at high support surface loading (SL). Surface loading is the amount of support surface per liter of preparation solution and is calculated by the equation below.

$$\text{Surface Loading} \left(\frac{\text{m}^2}{\text{L}} \right) = \frac{\text{surface area of the support} \left(\frac{\text{m}^2}{\text{g}} \right) * \text{mass of support in solution (g)}}{\text{volume of precursor solution (L)}}$$

Surface loading is an important concept, that allows for excellent comparison across experiments, for SEA synthesis as the supports used in catalyst preparation have widely different surface areas. Using a constant surface loading of 1000 m²/L for different supports across multiple experiments ensures that there is similar amount of surface sites for metal precursors to electrostatically adsorb with a high degree of dispersion. This gives a better comparison of uptake values of metal onto the support surface (Γ $\mu\text{mol}/\text{m}^2$) when the surface area may vary significantly the, surface loading is kept constant.

The overarching hypothesis of SEA is that to produce highly dispersed metal nanoparticles on the support, the metal precursors must themselves be highly dispersed onto the support during the adsorption stage of preparation. The hydration sheaths and ligands attached to the metal core of the precursors are removed via catalyst finishing i.e. reduction or calcination to preserve the highly dispersed metal nanoparticles and this process is outlined in Figure 1.3.

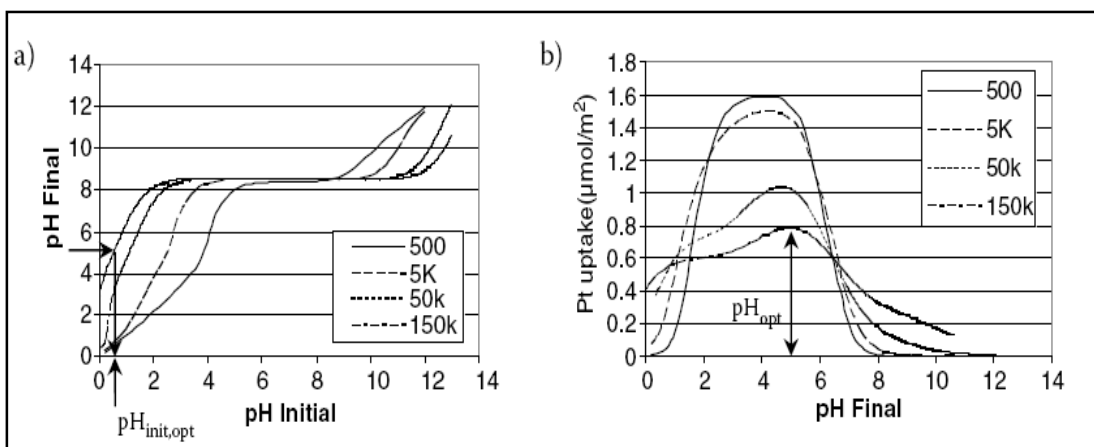


Figure 1.4 Modeled adsorption curves for CPA and PTA from the RPA model various SL [30]

A parameter free model dubbed the revised physical adsorption model has been proposed by this research group as a way to model the adsorption of these complexes with only physical forces, omitting any chemical terms and mechanisms from the adsorption model [31]. The driving force for the RPA model are columbic forces that are generated by the difference in the support surface charge relative to the metal complex in solution as the pH is varied [32]. This model allows for the prediction of the pH shift of metal oxides in solution as a function of surface loading and Park and Regalbuto were the first to simulate the pH shift effect of the bulk solution with the addition of higher loadings of oxide [33]. The RPA model was proposed as a novel technique to accurately measure the PZC of oxides. This measurement is different from a traditional titration experiment, as stated earlier, in that the initial solutions of different pH are contacted with the oxide at various SL. This model predicts that the change in surface loading will have a buffering effect on the equilibrium pH. In Figure 1.4a the, pH final plateau becomes much wider as the surface loading is increased from 500 to 150,000 m²/L. The adsorption of CPA in Figure 1.4b also proceeds to a maximum value and then tapers off. In each case there exists a pH where there is maximum precursor support interaction, this is the optimal pH, the point metal uptake is greatest [34]. Maximum uptake also decreases as the surface loading is increased as the concentration of Pt required to ensure the same surface density increases. At pH extremes, the increased ionic strength retards the metal uptake and this is attributed to electric double layer screening [35].

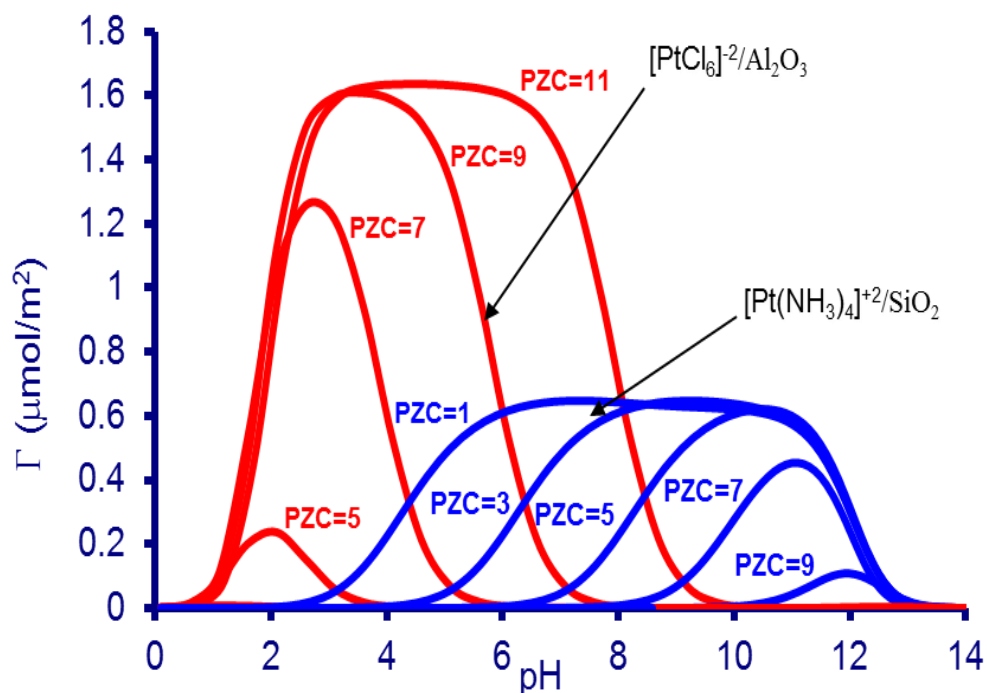


Figure 1.5 Modeled adsorption curves for CPA and PTA from the RPA model with supports of various PZC

From the RPA model the PZC of the support material also plays a large role in complex adsorption (Figure 1.5). Supports with low PZC values have a very broad adsorption peak where the uptake is at a maximum for PTA over low PZC silica, the electrostatic potential develops quickly after the solution passes the PZC and we see more narrow maximum uptake bands for CPA over alumina as the supports PZC increases. The increased adsorption of CPA, compared to PTA, is attributed to the sizes of the complexes as CPA is assumed to retain one hydration sheath when adsorbed on the support surface and PTA retains two thus, the steric limitations may be a contribution to the difference in total uptake [31].

1.2.5 Adsorption for bimetallics

The study of bimetallic catalysts has become omnipresent within academic research. A bimetallic catalyst can promote increased selectivity, stability, or overall

activity when compared to the constituent monometallic samples. The three ways bimetallic catalysts are believed to increase performance are thought to be ensemble effects, electronic effects, and bifunctional effects [36]. Ensemble effects are when a surface component of the bimetallic composition is inactive in the reaction and dilutes the active metal species into discrete ensembles of atoms. This can result in only desirable reactions occurring and limiting side reactions. Electronic effects occur when electron transfer between the two metal components either surface or bulk. Bifunctional effects occur when both metals are catalytically active for the reaction and the surface distribution is uniform in nature. This can allow the activation of multiple different molecules on the surface which allows for increased reaction rates and pathways. Bifunctional effects are of great interest as they can increase catalytic performance greatly and thus creating catalysts with well-defined surface composition is of great interest and the coupling of SEA and ED presents a great opportunity to study this effect.

SEA has also been applied to the synthesis of bimetallic catalysts to produce either a bimetal composition that is highly alloyed by adsorbing two metal complexes of similar charge at once onto a charged surface, this is dubbed co-SEA [37, 38]. A core-shell structure is also possible by exploiting the differences in surface charge between metal oxide and support [38-41]. Schwarz's research [39-41] proposed that if you had a composite support surface that can include a low PZC support such as silica with an adsorbed high PZC metal oxide on the surface, when operating in an acidic range, the hydroxyl groups on the surface of the high PZC oxide will be much larger than that of the silica support. To accomplish this via SEA, a primary metal can be deposited onto the support surface, i.e. cobalt via cobalt hexaammine, and then oxidized by catalyst

finishing to cobalt oxide. After this step the secondary metal, for this example anionic CPA, can be steered to selectively adsorb onto the surface of the cobalt oxide. A schematic of this example is presented in Figure 1.6.

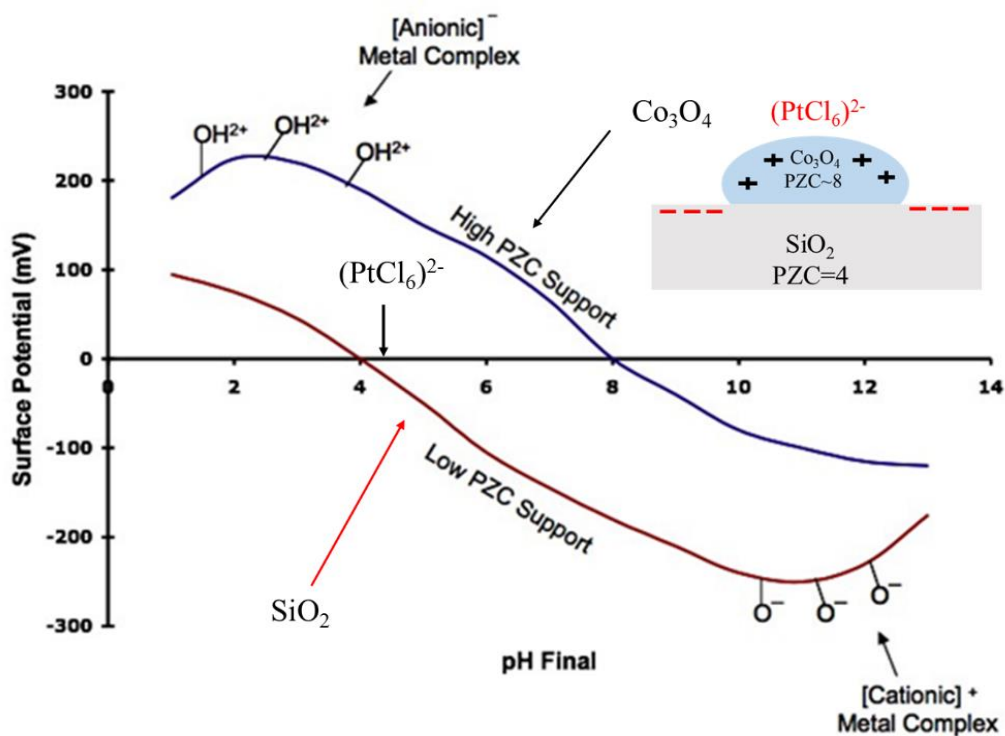


Figure 1.6 Diagram for the selective adsorption of Pt onto Cobalt oxide supported on silica

The work done by Schwarz that attempted to selectively deposit Co^{2+} or Pd^{2+} onto composite oxides [40-41] did not work as expected as they used bare metal ions as the precursors for the secondary metal and these species tend to hydrolyze and precipitate at the pH range used. This can be remedied by using metal-chloride, ammine, or oxide precursors which are stable over a wide pH range and concentration [35]. The main drawback for this technique is that there may be the need for multiple cycles of SEA, as there is limited core metal oxide surface area compared to the bulk support to adsorb complexes.

1.2.6 Electroless Deposition

Electroless deposition (ED) is another type of reactive adsorption preparation that is an excellent method for the preparation of bimetallic catalysts in a core@shell morphology. It is a natural pairing for SEA as the smaller the base metal particles the smaller the particles will be after the deposition of the secondary metal onto the first. ED has deep roots in industrial applications to plate precious metals (e.g. Cu, Co, Pt, Au) onto different metallic substrates. An external powers source is also not required for the plating of metal which differentiates this technique from electrodeposition along with the ability to plate onto non-conductive surfaces. The commercial and industrial applications for ED are vast as it is used in the manufacturing of catalysts, batteries, semiconductors, thin films, and even in corrosion prevention [42].

This study focuses on the plating of gold onto primary metal (Pt and Ru) synthesized via SEA. Gold plating via ED provides a methodology to selectively deposit the Au onto the preexisting metal and not the support in a controlled manner as shown in Figure 1.7 [43-46]. ED gives a way to produce bimetallic catalysts with more precisely controlled surface compositions which allows accurate correlation between surface composition of a bimetallic to catalyst activity and performance which in theory allows for optimization and reduction of total metal used [47]. ED also does not require high temperature catalyst finishing as the reducing agent is used during deposition and this may help avoid nanoparticle sintering that can occur at elevated temperatures. Work done here at the University of South Carolina by the Monnier research group has developed a large array of ED templates with the ability to deposit metals such as Au, Pt, Cu, and Ag onto supported single metal catalysts of Pt, Pd, Co, Ru prepared via traditional catalytic

methods i.e. impregnation. [45-51]. These ED baths have the same structure for each case. A reducing agent, a metal salt that can be reduced i.e. $\text{KAu}(\text{CN})_2$, and a stabilizer such as citrate can be used to stabilize the salt. The developer bath must be kinetically stable while being reactive enough to ensure deposition, sometimes for multiple monolayers, of the secondary metal onto the previously supported single metal surface.

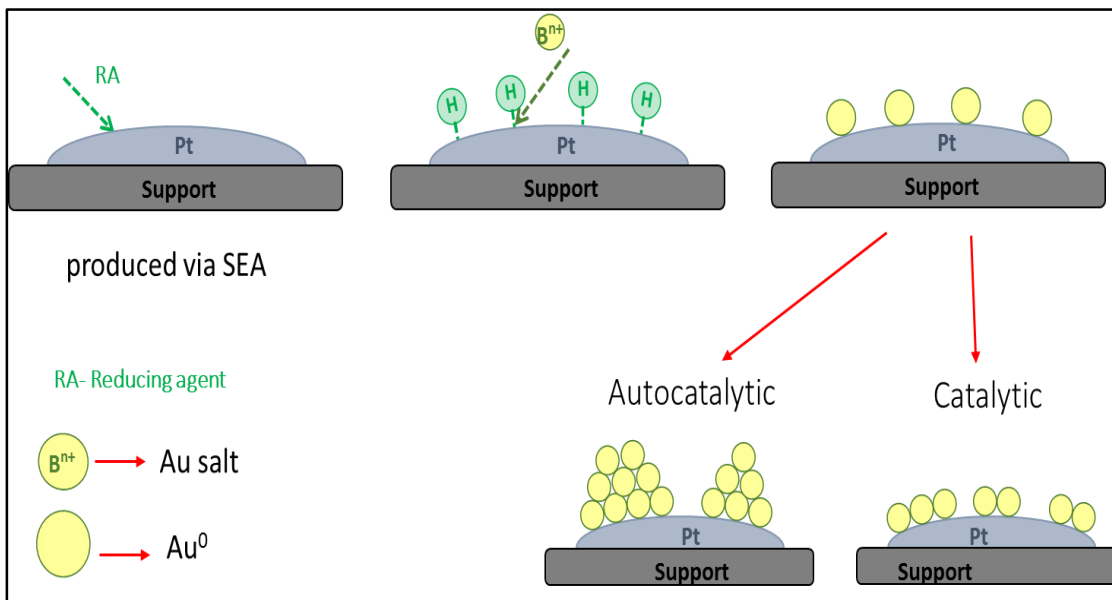


Figure 1.7 Electroless deposition method for the selective adsorption of Au onto Pt

The work presented in this thesis will be focused on the catalytic and autocatalytic deposition of gold atoms onto SEA prepared monometallic catalysts. ED can proceed in one of two manners, catalytically where the metal salt that is in solution is deposited onto the preexisting metal catalyst that is facilitated via the organic reducing agent in the bath that acts on the depositing metal. Autocatalytic deposition can also occur as the newly deposited metal may also activate the reducing agent in solution, this would result in the deposition of the metal in solution on the recently reduced metal particles. The method of electroless deposition begins with catalytic deposition with idea of producing a single

atom thick monolayer, but after some short time in the bath, both methods start to occur in conjunction with one another. This can be controlled to some degree through the choice of the reducing agent, bath conditions (pH and temperature), and the electrochemical properties of the metal substrate and catalyst. Similar to sequential SEA, ED can be used to produce core@shell bimetallic particles such as Au@Pd and Au@Pt in this study [46, 51]. Multiple monolayers of the deposited metal can also be prepared as the metal beings to deposit autocatalytic in a single-step bath after developing the proper conditions, as such it provides a much more time and cost efficient way than SEA to produce core@shell bimetallics with a wide variety of systems, especially in noble metals such as Ir, Au, Pt, Ru, and Rh [43, 45-47, 49, 51].

The key step to a successful ED system for bimetallics is to develop an ED bath. The developer bath is typically aqueous in nature and pH is held constant with a metal source, reducing agent and a monometallic catalyst as the adsorption substrate with particles that have high dispersion of the core metal to ensure small bimetallic particles [52]. The requirements for a successful bath are that it must be kinetically stable with no metal deposition in solution with no substrate present, as well as thermodynamically unstable to ensure deposition goes to completion as the substrate is present.

The metal salt chosen for the ED bath must be one that is soluble in the solvent medium (water) and also does not precipitate or undergo complexation to an unstable species under bath conditions, as this may elicit deposition precipitation or total precipitation of the metal in solution.

Table 1.1 Commonly used metal salt precursors for electroless deposition

Metal	Metal Salt Precursors
Ag	[AgNO ₃], [NaAg(CN) ₂]
Au	[KAu(CN) ₂], [KAuCl ₄], [NaAu(SO ₃) ₂]
Co	[CoSO ₄], [CoCl ₂]
Cu	[CuSO ₄], [KCu(CN) ₂]
Ni	[NiSO ₄], [Ni(H ₂ PO ₂) ₂], [Ni(CH ₃ COO) ₂]
Pd	[PdCl ₂], [Pd(NH ₃) ₄ Cl ₂]
Pt	[NaPt(OH) ₆], [(NH ₃) ₂ Pt(NO ₂) ₂], [Na ₂ PtCl ₆]

The metal salt chosen for the ED bath must be one that is soluble in the solvent medium (water) and also does not precipitate or undergo complexation to an unstable species under bath conditions, as this may elicit deposition precipitation or total precipitation of the metal in solution. In this study, KAu(CN)₂ is used as the metal ion source as cyanide salts have high formation constants and have produced very stable ED baths. Table 1.1 gives a list of commonly used metal salts such as sulfates, chlorides and acetate sources [53]. Each metal source offers different drawbacks for use, as cyanide containing compounds are very toxic and are not industrially favorable. Chlorine containing compounds, though safer, leave residual Cl⁻ on the surface that needs to be removed, as ionic chlorine can induce corrosion on the substrate and are pH sensitive.

The developer bath also requires the use of a reducing agent, which is the source of the electrons that will reduce the metal salt in solution. The selection of reducing agents is largely based on the work of Ohno et al who measured catalytic activity of different noble and non-noble metals with reducing agents [54]. Since the reducing agent

needs a favorable oxidation potential so that it may reduce the metal ion thermodynamically but not before the activation on the primary metal substrate surface. This work by Ohno relates the anodic potential of hydrazine, formaldehyde, hypophosphite, and dimethylamine borane for a variety of metal surfaces and this is shown in Figure 1.8. When the reducing agent is more active for the metal substrate surface, catalytic deposition will be the favored mechanism and vice versa for the secondary metal. Though the chart gives accurate trends for the potential, each bath will require stability and activity checks to ensure secondary metal deposition.

For the cases in this work, the deposition of Au onto noble metal cores KAu(CN)₂ is used as the metal salt with hydrazine (1:10), the reducing agent at the bath pH maintained at pH 10, as this has previously been studied and shown to be an effective method of gold deposition onto Pd [45, 46]. Potassium dicyanoaurate was chosen for the salt as it has a very high formation constant which favors complex stability and the total cell potential for Au(CN)₂⁻ and hydrazine is positive, which is an indication that ED is favorable (Table 1.2).

Table 1.2 A positive ΔE for the redox reaction for Au(CN)₂⁻ in the presence of hydrazine for the case of Au@Pd is indicative that ED is favorable.

$\text{Au(CN)}_2^- + e^- \rightarrow \text{Au}^0 + 2\text{CN}^-$	$E^\circ_r = -0.6\text{V}$
$\text{N}_2\text{H}_4 + 4\text{OH}^- \rightarrow \text{N}_2 + 4\text{H}_2\text{O} + 4e^-$	$E^\circ_{\text{ox}} = 1.16\text{V}$
$\text{Au(CN)}_2^- + x[\text{N}_2\text{H}_4 + 4\text{OH}^-] \rightarrow \text{Au}^0 + 2\text{CN}^- + x[\text{N}_2 + 4\text{H}_2\text{O}]$	$\Delta E^\circ = 0.56\text{V}$

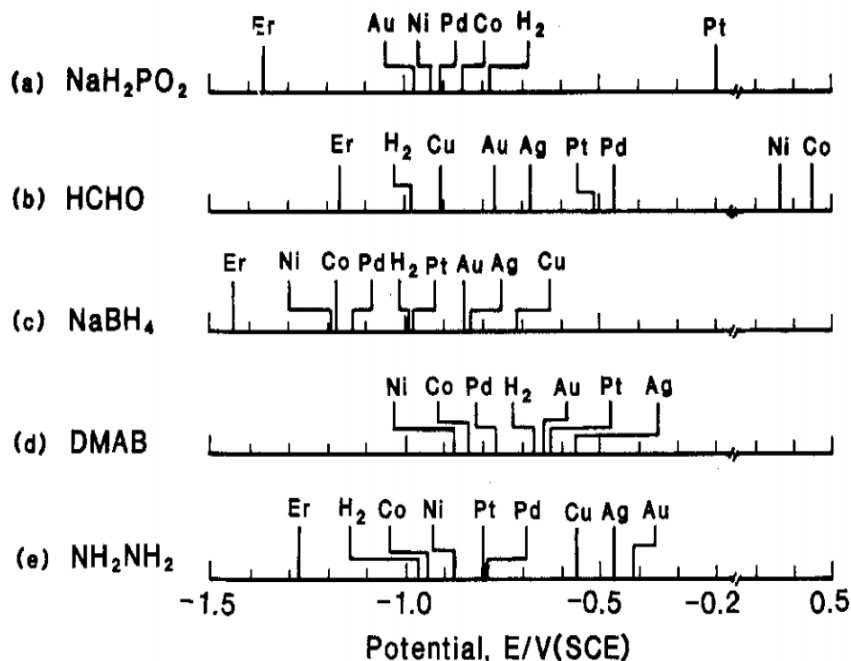


Figure 1.8 Catalytic activity of metals for anodic oxidation

The electroless developer bath can be enhanced to improve the bath stability lifetime, as well as other properties, such as deposition layer thickness and increased support adhesion onto the substrate by adding a multitude of agents to the bath. Compounds that act as a stabilizer or complexing agent may be added to the bath and will be briefly covered in this literature review. A complexing agent reduces the amount of metal reduction, which stabilizes the bath, in solution by forming a complex with the secondary metal salt in solution. The complexing agent can often prevent metal speciation and hydrolysis, which could result in the deposition metal plating out of solution. A commonly employed complexing agent is EDTA, which is often used in copper and cobalt baths and citrate, which is used during noble metal deposition[52]. A stabilizing agent is often employed to increase the life time of the developer bath, which is often not a concern in research lab scale experiments with short time scales. These

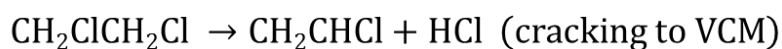
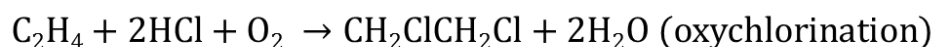
compounds retard the reduction of the metal ions in the developer bath, which stops the formation of precipitates.

1.3 Vinyl Chloride Monomer (VCM) Synthesis

Vinyl chloride monomer (VCM) is the building block monomer from which poly vinyl chloride (PVC) is produced. This reaction is of great industrial importance as PVC has applications that scale a gamut, from plastic use in construction, clothing and packaging, PVC is an important commodity chemical that catalysis plays a large role in. Worldwide demand is projected to reach 40 million tons in 2016, with growth in the market projected until at least 2020 [55, 56]. As the vast majority of VCM produced worldwide is polymerized to form PVC, the growth projections for both are deeply intertwined.

Two main methods of VCM production that exist today are the oxychlorination of ethylene (often called the balanced process) to acetylene, which is a multi-step process that is the most commonly used process in VCM production. Ethylene is an oil-derived feedstock as such, the price is tied to the fluctuations in global oil production and pricing. The second method, common in coal-rich regions where the cost to produce or purchase ethylene is high, is the direct hydrochlorination of acetylene to VCM. This reaction is catalyzed by a mercuric chloride catalyst support on activated carbon.

Oxychlorination “balanced” VCM process



Direct hydrochlorination VCM process

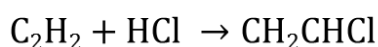


Figure 1.9 Industrial routes for the production of VCM

The oxychlorination process which (Figure 1.9) involves a chlorination step where ethylene is directly chlorided to 1,2-Dichloroethane (DCE) as well as an oxychlorination step that produces DCE as well as water, this product stream must be purified before thermal cracking unlike the directly chlorided step. The hydrochlorination of acetylene, which in a single step process (Figure 1.9) that results in a highly pure stream of VCM that requires little further treatment and no thermal cracking [57]. The direct hydrochlorination process is becoming more popular as the large surplus of coal in china make this route economically more feasible than the balanced process. The catalyst used in this reaction, mercuric chloride supported on carbon, can be reduced under reaction conditions and leaches as well as sublimates from the catalyst surface. This is due to the high vapor pressure at reaction conditions, which promotes the thermal desorption from the carbon surface [58, 59]. This resurgence in the process popularity coupled with the environmental concerns of releasing Hg^0 into the atmosphere have led to increased academic and industrial research for a replacement catalyst that is both catalytically

comparable to the commercial catalyst as well as the removal of any environmental and public health concerns.

The search for a catalytically active replacement catalyst has largely focused on a carbon supported gold catalyst. This work dates back to the initial research of the Hutchings research group and a work on gold catalysis would not be complete without mention of this research group. Hutchings et al. hypothesized that gold would be active for the hydrochlorination of acetylene and by correlating the activity of various supported metal chloride catalysts with their standard electrode potential in a two-electron process (Figure 1.10) [60]. This work was studied further by Conte et al. as the standard electrode potential of the metal chloride salt was used for the correlation [61]. They found that supported Au/C would be highly active for this reaction system and as such most research moving forward has focused on ways to increase the activity of these gold catalysts. It should be noted that Pt is especially inactive for this reaction based on Figure 1.11, which is corroborated by our reaction results for monometallic platinum catalysts.

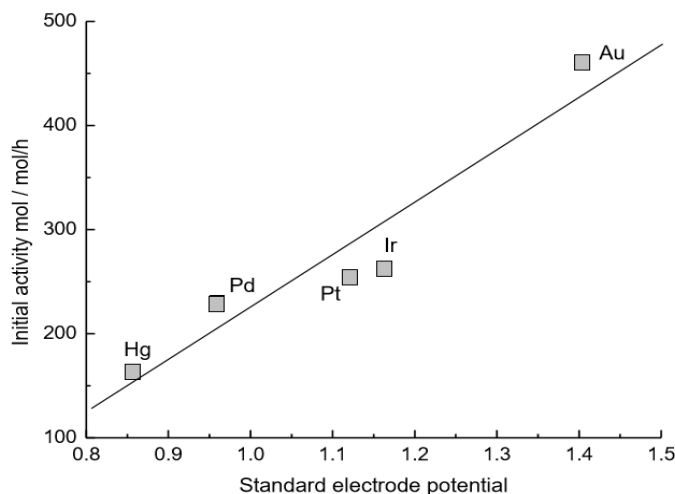


Figure 1.10 Correlation of initial acetylene hydrochlorination activity with standard electrode potential for supported metal chlorides [60]

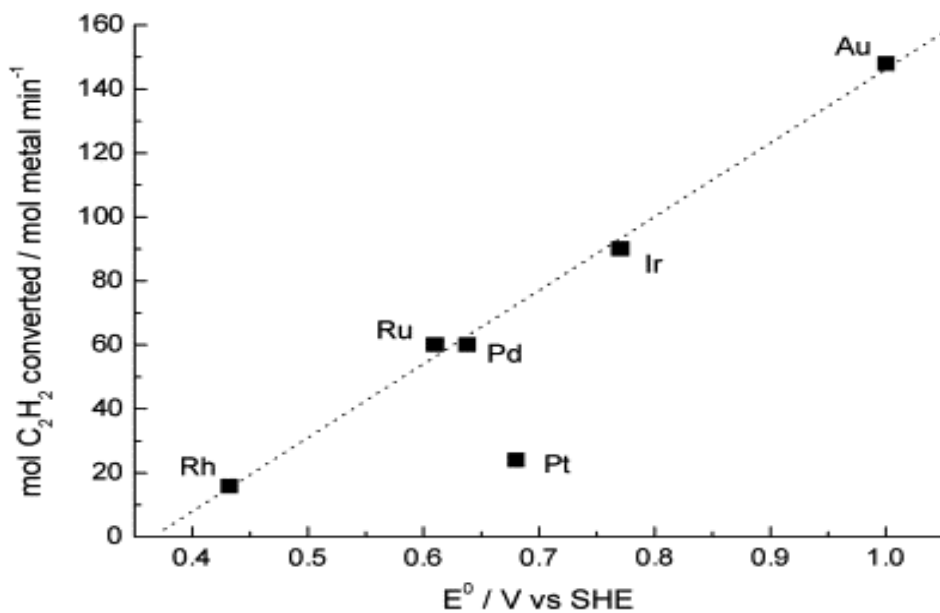


Figure 1.11 Correlation between initial acetylene conversion versus the standard electrode potential. Potentials are obtained from the reduction potentials of the following chloride salts $(RhCl_6)^{3-}$, $(RuCl_5)^{2-}$, $PdCl_2$, $(PtCl_6)^{2-}$, $(IrCl_6)^{3-}$, and $(AuCl_4)^{-}$ [61]

The initial work on supported gold catalysts, using cationic gold species, showed a high degree of promise as a potential industrial replacement. Gold supported on carbon is highly selective to the desired product VCM with selectivity values greater than 99.5 percent. Cationic gold species are electrophilic in nature and react strongly with nucleophiles. The cationic species then coordinates preferentially to alkene and alkynes, which leads to their use in the hydrochlorination reaction [62]. In many of the other metal cases, there is a secondary hydrochlorination step that leads to the formation of DCE and can often lead to further deactivation. The biggest drawback and hence research thrust in this work is that the gold catalyst continues to deactivate over long times on stream (Figure 1.12) and doesn't reach an equilibrium conversion value [63, 64]. Nkosi et al. found that there was no loss of gold metal during the reaction unlike the case of the mercury catalyst. It was instead found that temperature plays a large role on catalyst

deactivation. Catalysts run at low temperatures ($<100^{\circ}\text{C}$), had elevated amounts of carbonaceous coke formation on the gold surface. For reactions run at temperatures above 100°C , the reduction of the active cationic Au^{3+} species to Au^0 was found to be the driving force behind deactivation, as determined via XPS study.

Many studies, this dissertation included, will focus on the use of Au^{3+} as a monometallic environmentally benign replacement [64-67]. There has been considerable further study conducted on single metal catalysts such as Pd^{2+} [68, 69], Pt^{2+} [70, 71], Cu^{2+} [72], Ru^{3+} [73-75], and Bi^{3+} [76] and more recently novel nonmetallic supports such as carbon nitride, boron doped carbon, or graphene [73, 77, 78]. However, these research efforts have not produced results that are satisfactory for commercial production due to stability problems that lead to rapid catalyst deactivation. Literature has indicated that carbon-supported gold catalysts offers high initial normalized activity up to an order of magnitude higher when compared to traditional mercuric chloride based catalysts on a mole basis [64, 79]. Despite the high initial activity, the catalysts deactivate rapidly due to the reduced Au dispersion on the support surface coupled with the reduction of the active species (Au^{3+}) [3,5,6] leading to the need for further fundamental study of the cause for Au sintering on certain supports and the role of the support synthesis in producing stable active catalytic sites, which will be covered in great detail in chapters 3 and 4 of this work.

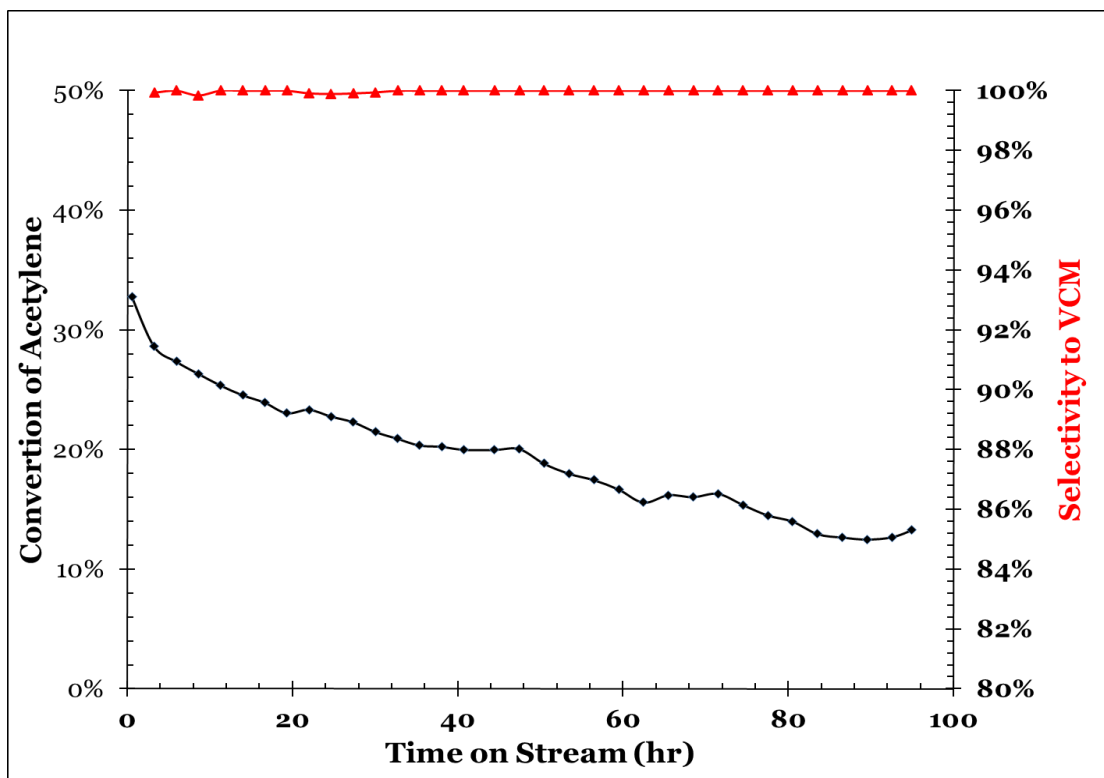


Figure 1.12 Conversion of acetylene (black) and selectivity to vinyl chloride (red) 95 hour run for 1 weight percent Au/C at a GHSV of 4500 hr^{-1}

The concentration of Au^{3+} on the surface, and retardation of reduction to Au^0 , is of great interest to many research groups as it is believed that AuCl_3 or the Au_2Cl_6 dimer is the active species on the surface of the gold clusters. Catalysts are often pretreated in HCl or another oxidizing environment or treatment, such as IWI preparation of catalysts in aqua regia to increase the Au^{3+} concentration on the surface [65, 80]. This pretreatment effect is up for debate, as work done by Wittanadecha et al found that after short time periods (180 min) the effect of pretreatment was negligible on the conversion of acetylene for samples initially rich in Au^{3+} on the surface or a reduced sample with only Au^0 present. This result was confirmed via XPS as samples that had only metallic gold present on the surface had an induction period that mirrored the deactivation of the Au^{3+}

rich samples as the surface reaches some equilibrium composition. Clearly, further study is needed to determine in situ what takes place on the surface of these catalysts, but due to the corrosive nature of HCl, studies of this nature have not yet been performed.

Recent research suggests that the location of the Au^{3+} species on the surface of the catalyst may be more important than having an excess of Au^{3+} compared to Au^0 on the surface, for increased activity and stability [80, 81]. Researchers have reported that Au^0 catalysts, with no pretreatment or oxidization, show activity for this reaction [82]. The on line HCl may be enough to oxidize the metallic gold to proceed with the reaction, which makes the concentration of HCl an important variable. The active site as well as the reaction mechanism for this reaction is still not completely understood. Other variables have recently become of interest for gold catalysts supported on carbon, including the role of the support and support surface groups on particle stabilization [76, 83]. Work on modification of the carbon surface functional groups has shown some promise for increasing catalyst stability, as we will also discuss in chapter 3. Groups have treated activated carbon with thermal or chemical treatments to modify the groups or add them completely [84-86]. Li et al. discovered that the surface functional groups on activated carbons modified via thermal treatment helped to increase gold particle dispersion, but also that phenolic or alcohol groups assisted in Au^{3+} reduction to Au^0 . A wide variety of different variables in the preparation of catalysts, and support treatment, for VCM synthesis among research groups as well as differences in gas hourly space velocity (GHSV) of the reaction make it difficult to draw conclusions on activity studies for this reaction. Space velocity values range widely from group to group from values on the low

end near 80 hr^{-1} ranging to near 4500 hr^{-1} , which are typical conditions used in many of our studies to better reflect real world reactor conditions.

The reactor system used for this study is also important to discuss. A flow reactor system was built at the bench top scale to safely use HCl as a reactant gas (99.9999% Praxair) as well as be able to sample the product gas via online gas chromatography analysis automatically so we can better understand reaction trends by studying this system for long time on stream (TOS). Figure 1.12 give a schematic for this reactor system. A Pyrex glass reactor is used for the reactor cell as HCl is corrosive, HCl is added at the top of the reactor via calibrated mass flow controller, which makes this system different than most and unreacted HCl is scrubbed out in a shelled scrubber containing NaOH and cooled via chiller. Setup of the system in this way allows for removal of HCl from the mass balance as it is added and then removed before GC analysis, coupled with the use of a digital valve sequence programmer and a switching valve for analysis we can set up the system to run for long time scales and only need to change the NaOH scrubbing solution, which can be easily done via three-way valve and the reactor exit. (Figure 1.12)

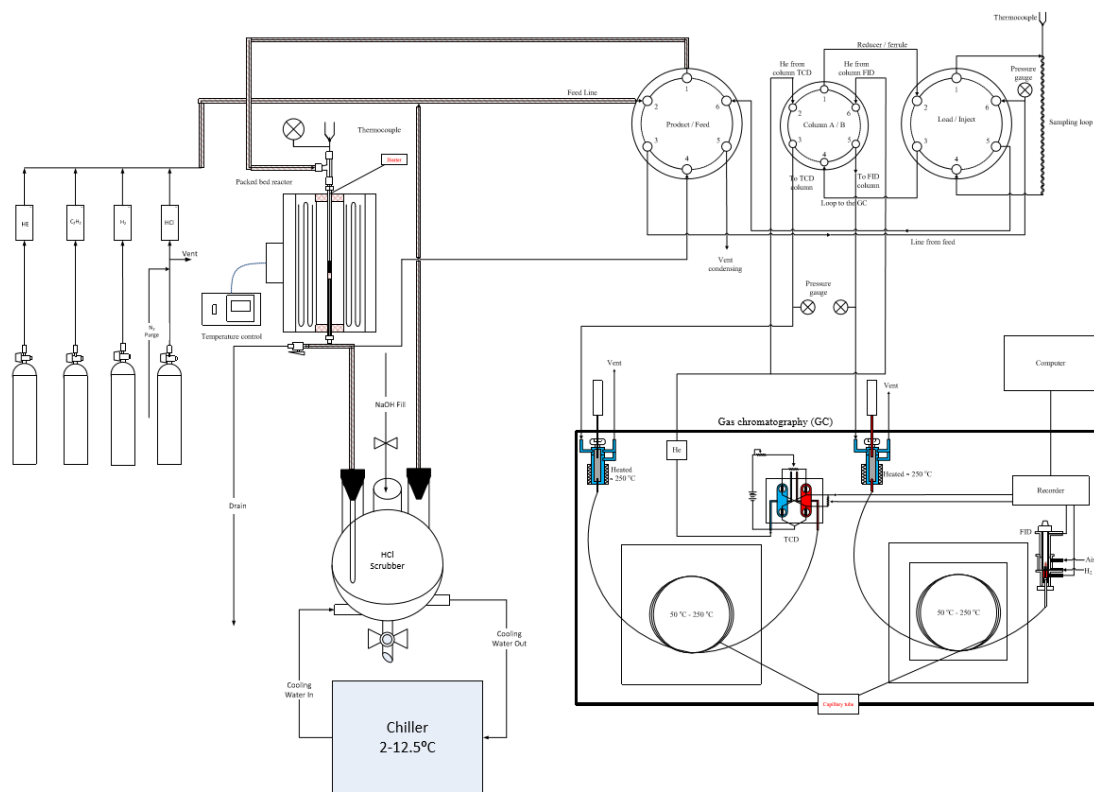


Figure 1.13 Schematic of the reactor system for VCM synthesis used for catalytic activity and stability studies.

1.4 Dissertation Layout

The bulk of this work involves the synthesis, characterization, and reaction testing for gold containing catalysts synthesized via SEA and ED supported on carbon. Acetylene hydrochlorination is used as a method for catalytic testing as a probe reaction to test catalyst synthesis methods. It is also an important industrial reaction that further research is necessary to better understand the reaction pathway and the deactivation mechanism. By the increased control of particle size and surface morphology that can only be obtained through SEA and ED, this research can result in a better understanding of this reaction and solve a real industrial and environmental problem.

Chapter 2 of this work focuses on the characterization of well dispersed nanoparticles supported on carbon via x-ray powder diffraction. Through the use of an advanced silicon-slit detector on a Rigaku Miniflex-II, it enables the characterization of gold particles at sizes as low as 1.24 nm and weight loadings as low as 0.33 %. This is well beyond previous limits of detection of 2-2.5 nm and at elevated scan rates XRD results corroborated very well with STEM. This advancement gives us a way to determine gold particle size rapidly without needing to send many samples for imaging, as chemisorption is not an option to accurately determine gold particle size. This work has been applied to many well defined systems in the research group such as Pt and Pd on carbon and metal oxides to determine particle size and metal oxide content, thanks to the high signal to noise ratio of the data.

Chapter 3 of this work will cover the use of SEA to synthesize monometallic gold catalysts for acetylene hydrochlorination. The method will be applied over a variety of carbon and metal oxide supports to help elucidate the role of the support and support surface on the catalytic activity, as well as determine the role of HCl in gold particle sintering, which appears to be a large barrier to producing stable and active particles for this reaction and makes determining the role of particle size as well as active sites difficult.

Chapter 4 will pair SEA with ED to produce core shell catalysts with gold shells over platinum and ruthenium cores, which are prepared via SEA. The goal is to prepare particles that are stable under reaction conditions including high HCl concentrations. Pt and Ru both have higher surface free energies than Au, so we hypothesize that using ED to deposit a thin shell of gold on the surface will allow for small stable gold particles for

this reaction and we can better understand the role of particle size as well as the effect of bimetallic catalysts on the catalytic activity of this system. This work of surface free energy stabilization has resulted in a patent application as well as funding from the National Science Foundation for future research and is being applied to multiple systems here at USC for further study.

CHAPTER 2: HIGH SENSITIVITY SILICON SLIT DETECTORS FOR 1 NM POWDER XRD SIZE DETECTION LIMIT

Reprinted with permission from [O'Connell, K., and John R. Regalbuto. "High Sensitivity Silicon Slit Detectors for 1 nm Powder XRD Size Detection Limit." *Catalysis Letters* 145.3 (2015): 777-783].

DOI: 10.1007/s10562-015-1479-6

Copyright [2015] Springer US/Catalysis Letters.

2.1 Abstract

The limit of conventional x-ray powder diffraction for the detection of supported nanoparticles is usually taken to be 2 – 2.5 nm, at which size low signal to noise ratios make detection of particles of low weight loading and small particle size difficult. Advancement in drop in XRD detectors such as a high surface area silicon slit detector significantly lowers this limit of detection. In this paper we demonstrate the ability of a Rigaku Miniflex instrument, equipped with a Si slit detector, to characterize Au particles supported on carbon at sizes as small as 1.2 nm and weight loading as low as .33 %. At elevated scan speeds good corroboration between STEM and XRD is maintained. Thus, the latest generation XRD detector allows quick and simple access to the behaviorally rich 1-2 nm particle size range.

2.2 Introduction

The limit of conventional x-ray powder diffraction for the detection of supported nanoparticles is usually taken to be 2 – 2.5 nm [87, 88], at which size low signal to noise ratios and decreased detector sensitivity make detection of particles of low weight loading and small particle size difficult due to instrumental error and broadening [87-90]. Recent advancements in XRD detector technology, however, substantially lower this limit of detection. The Rigaku Corporation has recently developed a drop replacement detector for the Miniflex II system - a 1D silicon strip detector D/teX Ultra - which is 2 orders of magnitude more sensitive compared to a scintillation detector. This is done by increasing the active aperture area for detection which increases the count rate by using a smaller pixel pitch of 0.1mm[90]. This increase in sensitivity and resolution allows for higher signal to noise ratios at higher scan speeds when compared to conventional

detectors, increasing throughput while also allowing for deconvolution of smaller metal nanoparticles using PDXL, a Rigaku software for diffraction pattern analysis, than with scintillation detectors on the same equipment.

A proof of principal experiment was conducted with carbon supported Au nanoparticles synthesized at various weight loadings (0.33-3.0 wt.%) and particles size from 1.2 - 2.5 nm. Au nanoparticles were chosen since they do not readily oxidize at ultrasmall size when exposed to the atmosphere as do platinum and palladium [91, 92]. Supported Au nanoparticles have received increased interest when it was discovered that small gold particles are active for CO oxidation at sub-ambient conditions[93, 94]. Reactions of interest over gold nanoparticles include the water gas shift, reduction of NO, and hydrochlorination of acetylene [63, 95-97]. The activity of Au catalysts generally increases drastically below 3 nm, which is often below the limits of detection for scintillation counter detectors for low weight percent Au catalysts [63, 91, 95-98]. This enhanced activity is suggested to be a function of small metallic particles that have increased fractions of surface sites [99].

Characterization for highly dispersed Au catalysts often relies on STEM and in some cases EXAFS for particles size analysis [100]. These techniques have an increased turnaround time and are more expensive than powder XRD. Thus semiconductor based detectors for XRD analysis such as the Rigaku D/teX Ultra can provide a time and cost effective to characterize ultrasmall nanoparticles. Advanced detectors such as the D/teX system have seen limited use in academic research despite the advantages in signal intensity and noise reduction [89, 101, 102].

In this paper we demonstrate that the limit of detection of the silicon slit detector is close to 1.0 nm for even low metal loadings. Nominal loadings of 0.33 wt.% Au with average particle size as low as 1.6 nm can be detected using the silicon strip detector and at higher loadings (≥ 1 wt.%), particles as small as 1.2 nm produced via Strong Electrostatic Adsorption (SEA) are detected via the deconvolution of the Au (111) peak from the carbon background peak. Colloidal Au nanoparticles capped with decanethiolate and deposited in carbon were used as a control material for their narrow size distribution and small particle size as comparison to SEA-produced samples to limit the possibility of large Au clusters skewing the XRD results[103]. These results are seen to be in good agreement with HRTEM analysis, with much greater accuracy for the D/teX detector compared to a scintillation counter at very slow scan rates. Analysis at faster scan rates shows the greatest increase in accuracy for the D/teX detector over the scintillation counter.

2.3 Experimental

Au/C Nanoparticle Preparation

Bis(ethylenediamine)gold(III) chloride (gold bis-(en)₂, or AuBen) was synthesized by the method of Block and Bailar[104]. The synthesis of AuBen and its monoclinic crystal structure was confirmed by XRD and compared to the previous work by Minacheva in 1988[105]. The method of SEA for AuBen is outlined previously by Barnes [106]. Briefly, fresh AuBen was prepared and dissolved in water at the required concentration to prepare samples over the range of 0.33-3% weight loading confirmed by ICP-OES, the pH was adjusted to that of optimum uptake (~ 12) and 1000m²/L of low PZC carbon support was contacted with the AuBen solution. Darco KBB (surface area

1100 m²/g) and oxidized Vulcan XC72 (180 m²/g) were used as support. The support was filtered from solution after an hour of shaking and dried at room temperature overnight and then reduced in a flowing 5 % H₂ balance He at 160°C for 1 hour with a ramp rate of 2.5°C/min. ICP-OES was used to determine gold uptake by measuring concentration of the impregnation solution before and after support contact.

Gold nanoparticles (AuNps) with a core size of 1.7 nm capped with a decanethiolate (DT) monolayer shell were synthesized using a two-phased method[107-109]. The AuNP solution was dispersed onto Vulcan XC72 carbon with a pore volume of 2.3 ml/g at 0.33, 1.0, and 3.0 % weight loading via dry impregnation (DI). In order to achieve higher weight loadings, the samples were impregnated multiple times after being dried overnight at 100°C between every DI step. The AuNp catalysts were left untreated and characterized via HRTEM and XRD analysis.

Catalyst characterization

X-Ray diffraction measurements of the supported Au particles were performed on a Rigaku Miniflex-II using both a standard scintillation counter detector as well as an advanced silicon strip detector (D/teX Ultra). Diffraction patterns were recorded over a range of 10-80 °2θ using Cu-Kα radiation ($\lambda = 1.5406 \text{ \AA}$) operated at 30mA and 15kV using Bragg-Brentano geometry. A scan rate of 0.5°/min was used for all scans for both detectors with a slit width of 0.2. A sample of annealed gold shavings physically mixed with carbon support was used to correct for instrumental broadening, a possible source of error for such small nano particles. PDXL 2 was used for peak broadening analysis of the XRD profiles and particle size analysis based on the Au (111) peak after correcting for instrumental broadening with a shape factor of 0.94 in the Scherrer equation. Samples of

1.0 and 3.0 wt.% were compared using both detectors at elevated scan speed of 5° and 20° $2\theta/\text{min}$.

High resolution scanning transmission electron microscopy(HRTEM) z-contrast imaging was performed on all samples using a JEOL JEM 2100F HRTEM with CEOS GmbH hexapole STEM probe corrector. The Au/C samples prepared by SEA of AuBen and DI of AuNPs at weight loadings 0.33, 1.0 and 3.0 wt.% particle size distributions were calculated by counting particles over a series of images, approximately 500 particles for each sample, and comparing the volume particle size average to the particle size from FWHM calculation of the Au (111) peak using both the advanced silicon strip detector as well as the standard scintillation counter.

2.4 Results and Discussion

AuNps on carbon

As a proof of principle experiment, gold nanoparticles prepared via a 2-phase synthesis method [107-109] were dispersed into Vulcan-XC72 carbon at weight loadings of 0.33, 1.0, and 3.0%. These samples were dried overnight at 100°C and then characterized using both scintillation and D/teX Ultra detectors as well as HRTEM analysis for particle size distributions using z-contrast imaging.

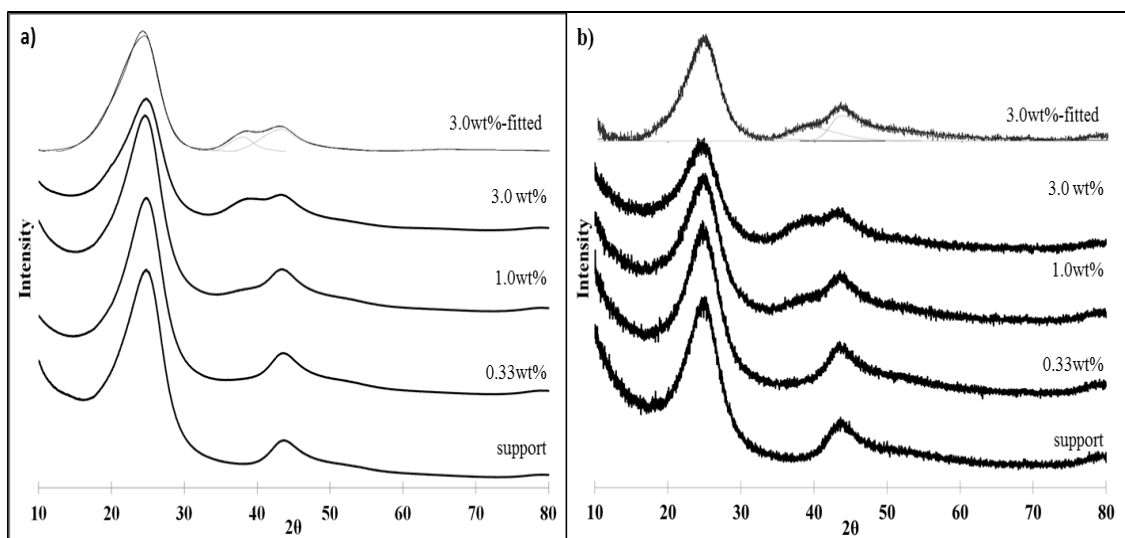


Figure 2.1 XRD profile of various loadings of AuNps/VXC using a.) D/teX Ultra detector, b.) Scintillation detector.

Particle size analysis using the D/teX Ultra detector (Fig. 2.1a) with the increased signal to noise ratio yielded particle sizes of 1.6 nm for of the higher weight loadings. The scintillation count detector (Fig. 2.1b) yielded particles sizes of 2.0 and 1.5 nm for the 3.0 and 1.0 wt.% samples respectively. (That nanoparticles below 2.5 nm could be observed with even the scintillation counter is tribute to the quality of the Rigaku basic instrument.) For the 0.33 wt.% sample a rise in the baseline is observed with the Si slit detector, but is unquantifiable, while this rise is not evident for the scintillation counter. The Gaussian fitted data is shown for 3.0wt% for each detector as diffraction pattern A; all data were fit using PDXL 2 and summarized in table 1.

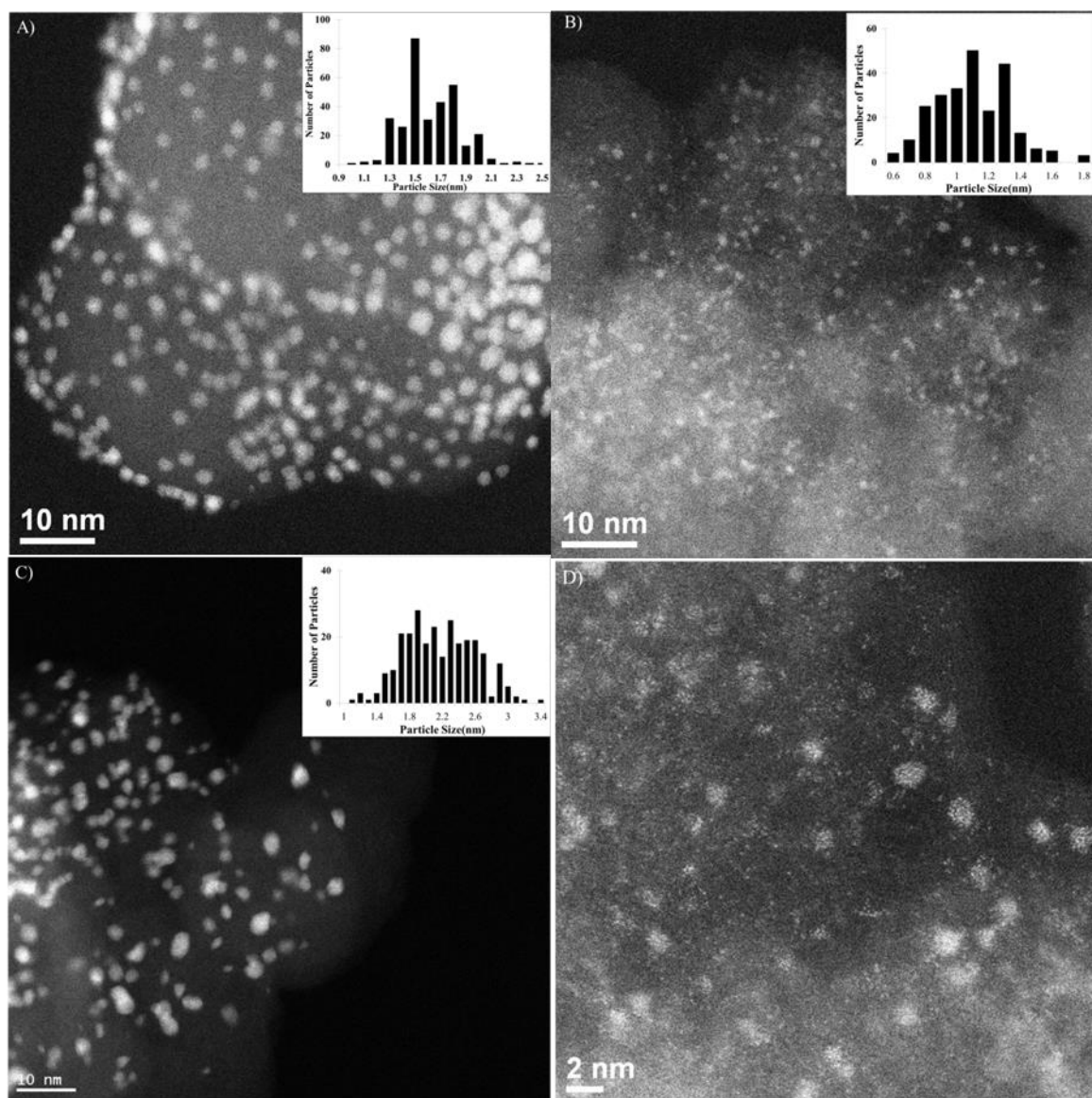


Figure 2.2 HRTEM image of a.) 3.0 wt.% AuNp/VXC with the particle size distribution inset. b.) Au/KBB with particle size distribution inset. c.) Au/VXC with particle size distribution inset. d.) Au/Kbb high resolution image

HRTEM analysis for the 3.0wt% AuNps dispersed on Vulcan carbon yielded average particle size based on a number average particle size of 1.6 nm and a volume average size of 1.7 nm. This value is assumed for the lower loading samples as the AuNp samples were left untreated at the various loadings employed.

With size estimates of 1.6 nm for both the 3.0 and 1.0 wt.% AuNps, respectively, the Si slit detector gave much higher precision as well as more accuracy of the Np size in view of the HRTEM volume-average size estimate of 1.7 nm, compared with the scintillation detector (2.0 and 1.5 nm respectively). The error in particle size calculation for 3.0 wt.% AuNps was 3.5% and 15% for the D/teX detector and scintillation counter respectively; similar differences (5.9 and 14%) were observed for 1.0% weight loading.

Table 2. 1 Summary of Particle sizes using XRD and HRTEM

AuNp/VXC	Particle size in nm via		
	D/teX Ultra	Scintillation counter	HRTEM
3.0 wt. %	1.6	2.0	1.7
1.0wt%	1.6	1.5	1.7
0.33wt%	-	-	1.7
Au/KBB (SEA)			
3.0 wt. %	1.3	-	1.2
1.0 wt. %	≤1.3	-	1.2
0.33 wt. %	-	-	-
Au/VXC (SEA)			
3.0 wt. %	2.5	2.6	2.5
1.0wt%	2.3	2.5	2.5
0.33wt%	-	-	2.4

Au/KBB prepared via SEA

AuBen was adsorbed onto Darco KBB carbon with a PZC of 4.5 and surface area of 1100m²/g using SEA to prepare catalyst samples at loadings of 0.33, 1.0, and 3.0 wt.%. These samples were characterized using XRD and HRTEM after being reduced at 160°C in a flowing 5% H₂/He mixture. HRTEM analysis of the 3.0 wt.% Au/KBB sample gave a volume weighted average particle size of 1.2 nm (Fig. 2.2b).

The XRD patterns of this series using a D/teX Ultra detector are shown in Figure 2.3. The 3.0 wt.% sample exhibits a broad Au (111) peak, indicating small particles.

Using the very clean data collected with the D/teX Ultra detector, the Au (111) peak was deconvoluted from the carbon background peak to yield a particle size of 1.3 nm. This value is within 5% (4.8% larger) than the STEM-obtained value. For the 1.0 wt.% sample a weak shoulder is present for the Au (111) peak and no peak is readily discernable for Au (200). With a scintillation detector the Au (111) peak is indiscernible from the carbon background for the 1 wt.% Au sample. STEM results (not shown) revealed a size of 1.2 nm for this sample. Thus, while qualitatively detectable, 1.2 nm Au particles at 1 wt.% appears to be just below the limit of quantification for the silicon strip detector.

Au/VXC prepared via SEA

Figure 2.4 provides an analysis of a sample possessing nanoparticles of somewhat larger size, produced by SEA of AuBen over an HNO₃-oxidized Vulcan XC-72 (PZC of 4.5 and a surface area from BET of 180m²/g). The 3 wt.% sample of this series is seen in (Fig. 2.2c); for this, the 1.0, and 0.33 wt.% sample, STEM gave volume averaged particle sizes of 2.5, 2.5, and 2.4 nm respectively. Particle sizes determined using the D/teX Ultra detector were 2.5 and 2.3 for the 3.0 and 1.0 % samples respectively while the 0.33% Au sample appears to possess a bimodal distribution as evidenced by the small, sharper (111) peak. This pattern establishes that Au particles can be detected even at the heretofore undetectable loading of 0.33 wt.%. This peak was not observed with the scintillation counter, which gave XRD estimated sizes of 2.6 and 2.5 nm for the 3.0 and 1.0 wt.% samples. The latter value is the only estimate from the scintillation counter which is in better agreement with STEM data than the corresponding Si slit estimate.

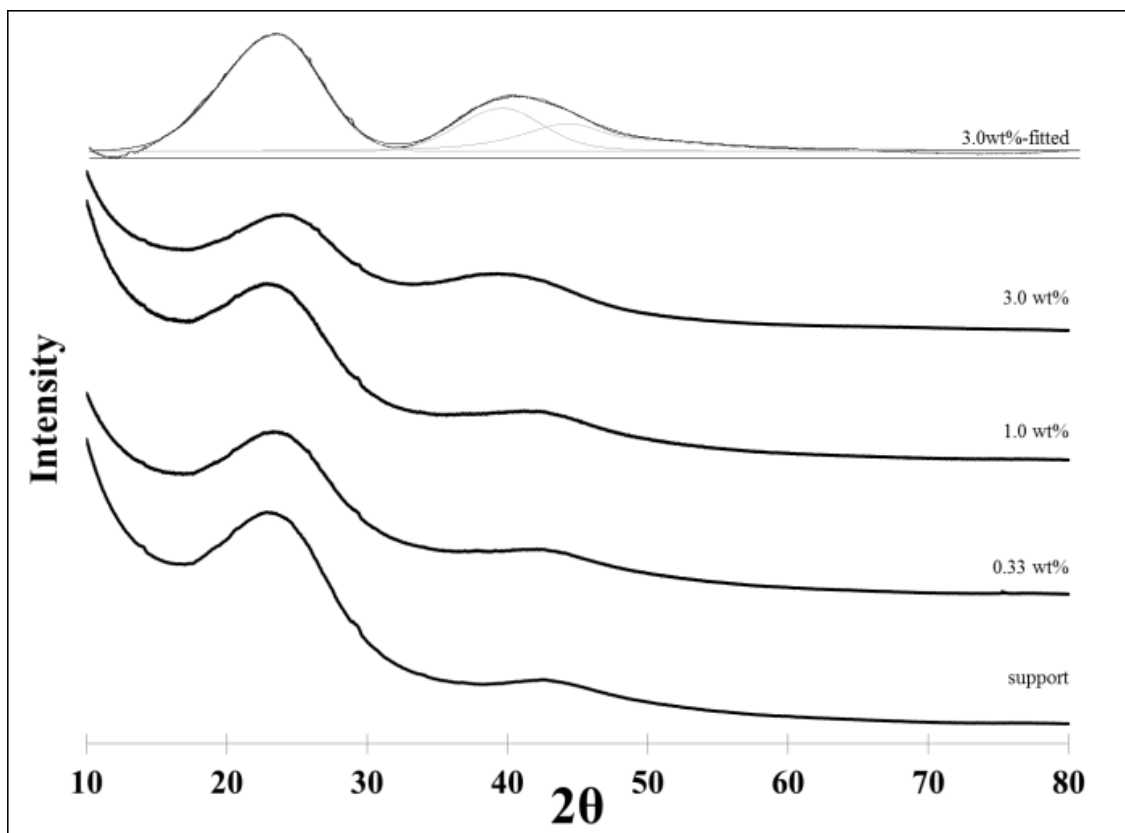


Figure 2.3 XRD analysis of Au/KBB samples at $0.5^\circ/\text{min}$ with D/teX detector

Analysis at increased scan speeds

To illustrate the benefit of the more sensitive Si slit detector at accelerated analysis times, the 1.0 wt.% AuNp/C samples (1.7 nm by STEM) were analyzed at scan rates of 5° and 20° $2\theta/\text{min}$ (increased from the original rate of 0.5° $2\theta/\text{min}$) using both detectors. As the scan rate is increased from 0.5° - $20^\circ/\text{min}$, a relatively small increase in the D/teX Ultra detector noise is seen and particle size remains consistent at 1.6 nm.

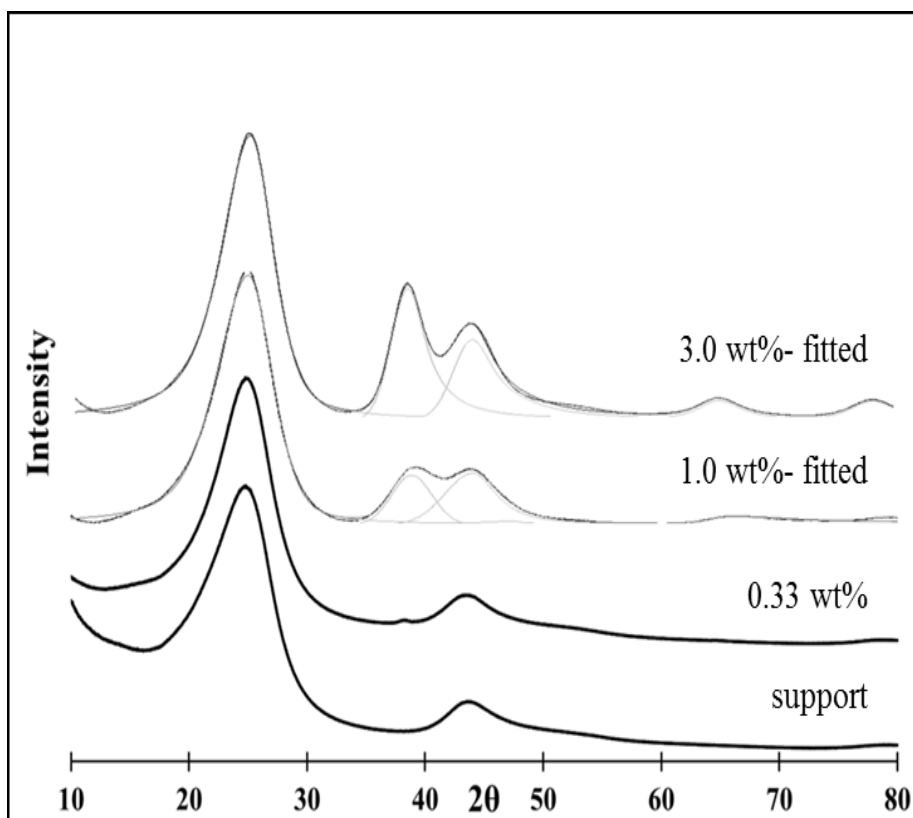


Figure 2.4 XRD profile Au/VXC using D/teX Ultra detector

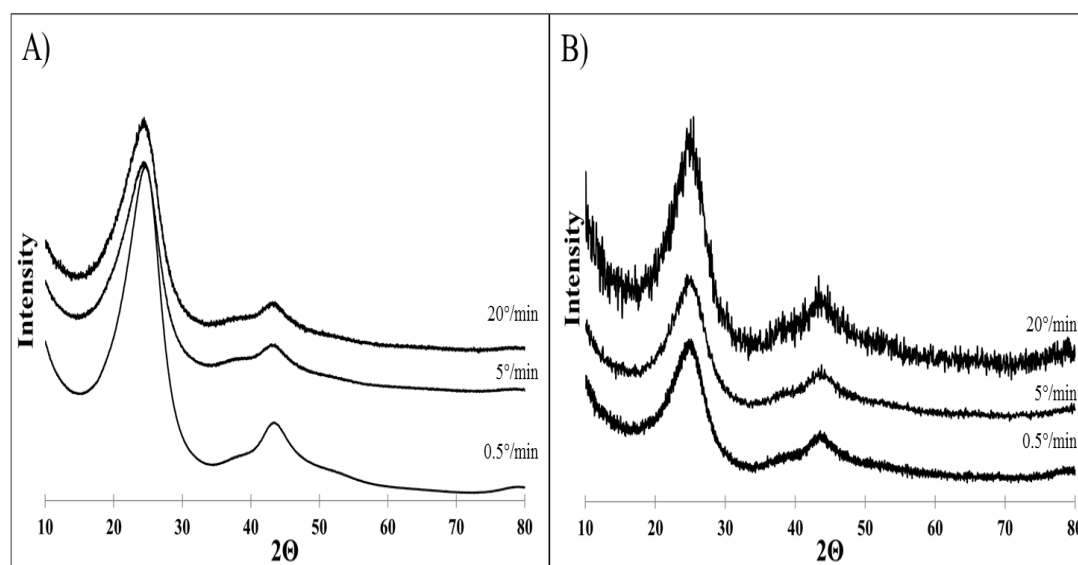


Figure 2.5 XRD pattern at different scan rates for 1% AuNp/VXC for A) D/teX B) Scintillation

The 1.0 wt.% samples analyzed with the scintillation detector at speeds of 0.5, 5, and 20°/min are shown in Figure 2.5b. The poor signal to noise ratio makes it difficult to perform a deconvolution of the Au (111) peak from the carbon background resulting in an artificially large particle size of 2.1 nm for the scan rate of 20°/min. For 5°/min the particle size is more accurate at 1.7 nm.

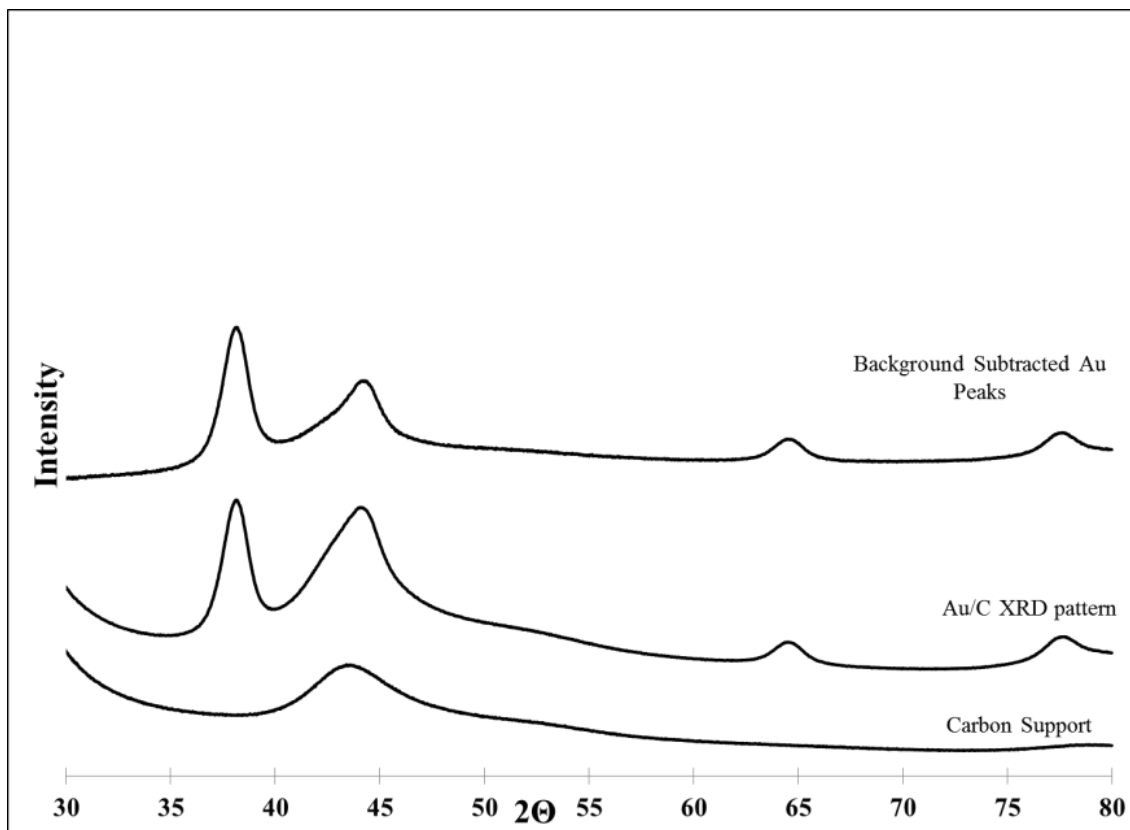


Figure 2.6 Example of Background subtraction for Au peaks from supported Au/C in which positions and FWHM's were calculated by fitting Gaussian shapes to the profiles.

Using PDXL or similar software package we can easily subtract the carbon background signal from the supported Au crystalline signal and fit the resulting Au signal and depending on peak shape use either Lorentzian, Gaussian fitting, or a combinatory method to fit the FWHM values. Au diffraction curves in this study are fit using Pseudo-Voigt shapes which allow for some peak asymmetry from which the FWHM is calculated

and used in the Scherrer equation for crystalline size analysis based on the (111) diffraction peak.

2.5 Conclusion

In this paper we have demonstrated that next generation Si slit detectors extends the limit of reliable size estimation down from the previously held limit of detection of about 2.5 nm with scintillation counters, to about 1 nm. It is noted that the base Rigaku Miniflex instrument, with the standard detector, performs impressively and is capable of detecting particles less than 2 nm, if somewhat inaccurately compared to the Si slit detector. With the latter, using the Au (111) peak and a carbon support, Au particles with average size of 1.2 nm could be detected at loadings as low as 3.0 wt.%, while 1.7 nm particles were detectable at loadings as low as 1.0 wt.%. The advanced detector can be run at much higher scan speed and still produce diffraction patterns with much higher signal to noise ratios than the scintillation counter. Nanoparticle properties such as catalytic reactivity often vary drastically in the size range between 2.5 and 1 nm, and the Si slit detectors now allows this rich regime of behavior to be reliably accessed by the simple, inexpensive, powerful method of powder XRD.

Acknowledgments

The authors would like to acknowledge the support of the NSF for grant CBET-1160023.

CHAPTER 3: THE SINTERING AND ACTIVE SITES OF SUPPORTED GOLD
CATALYSTS FOR THE HYDROCHLORINATION OF ACETYLENE

To be Submitted[K.C. O'Connell, J.R. Monnier, and J.R. Regalbuto]

3.1 Introduction

Acetylene hydrochlorination is a well-studied catalytic synthesis route for the production of vinyl chloride monomer (VCM) that is common in coal-rich regions of the world, due to the abundance of acetylene, which can be synthesized from calcium carbide. The direct hydrochlorination to acetylene has limited need for further separation and processing after reaction, due to high selectivity to VCM [57]. The most common commercial catalyst for this reaction is carbon supported mercuric chloride, which has significant environmental concerns, mainly the sublimation of reduced Hg^0 into the atmosphere due to hotspot formation during reaction. This loss of active metal, due to elevated vapor pressure, has raised environmental concerns as well as reduced the catalytic lifetime [61, 64, 110]. Research for a suitable replacement of mercury-containing catalysts for acetylene hydrochlorination continues to grow. Many studies, this one included, have focused on the use of Au^{3+} as a monometallic environmentally benign replacement [64-67]. There has been considerable further research interest on single metal catalysts such as Pd^{2+} [68, 69], Pt^{2+} [70, 71], Cu^{2+} [72], Ru^{3+} [73-75], and Bi^{3+} [76] and more recently, novel nonmetallic supports such as carbon nitride and boron doped carbon and graphene [73, 77, 78]. There are efforts at many levels to produce stable and environmentally friendly catalysts, where groups have looked at many different approaches of tuning these catalysts to improve stability, such as bimetallic systems, based on gold and ruthenium supported on carbon [61, 69, 75] or the addition of bismuth as a promoter to reduce the reduction of gold to Au^{+1} instead of Au^0 [111]. There is also significant work on the modification of the carbon support surface with oxygen-containing functional groups via chemical treatments with an oxidant, as well as thermal

treatments, to adjust the ratio of those groups on the surface to investigate their role in the reaction mechanism [65, 85, 112].

The goal of this study is to lay out a simple and repeatable synthesis method for the production of carbon and metal oxide supported gold nanoparticles with high dispersion and to better understand the role HCl plays in the growth of Au particles during the reaction. The timescale of particle growth was also of interest, as this reaction has a strong dependence on the concentration of HCl [113]. The role of the metal support interface is also explored in this study through the variation of untreated carbon supports and metal oxides coupled with the alteration of the carbon surface functional groups with an oxidizing agent, in the attempt to improve catalyst stability. There is some precedent in the literature for the addition of surface functional groups through the use of an oxidant or nitrogen modification for improving catalyst deactivation [80, 85, 86, 114]. However, these results have not produced results satisfactory for commercial production, due to stability problems that lead to rapid catalyst deactivation. Literature has indicated that carbon-supported gold catalysts offer high initial normalized activity up to an order of magnitude higher when compared to traditional mercuric chloride catalyst on a molar basis [64, 79]. Despite the high initial activity, the catalysts deactivate rapidly due to gold sintering on the support surface, coupled with the reduction of the oxidized active Au^{3+} species [3,5,6]. Further fundamental study of the cause for Au sintering on certain supports and the role of the support synthesis in producing stable active catalytic sites is needed.

Incipient wetness impregnation (IWI) is the most commonly employed method used to synthesize gold catalysts supported on carbon for acetylene hydrochlorination,

commonly using HAuCl_4 dissolved in aqua regia as the impregnation solution. The benefits of using this technique are the increase of surface gold oxidation of Au^0 to Au^{3+} from the HNO_3 , coupled with the possibility of increased surface functionalization of the carbon surface functional groups when compared to other preparation solvents [65]. One main drawback to common impregnation methods of synthesis is the resultant poor or inconsistent gold dispersion; one study [24] reports that altering the drying temperature from 110 to 140°C induces a change in particle size from <2 to 20 nm, and increasing it a further 40 degrees, brings it back to 3 nm. Another relative disadvantage is the need for a strong acidic solvent such as aqua regia in the preparation step [63-65, 113].

Other novel synthesis methods employed in recent studies include the MIV method, “M” for mixed solvents; “I” for impregnation; “V” for vacuum drying, which is a modification to traditional impregnation methods that uses solvents coupled with vacuum drying to produce effective Au^0 catalysts with relatively high dispersion that oxidize to the more active Au^{3+} species under reaction conditions [115]. Microwave and ultrasonic assisted methods that either involve the use of ultrasonic mixing of the aqua regia dissolved HAuCl_4 or microwave drying of the IWI prepared sample have been used in efforts to improve dispersion of the active sites. This led to improvements in the initial conversion, but similar long term deactivation trends occurred when compared to traditionally prepared catalysts [81].

In this work the synthesis method of Strong Electrostatic Adsorption (SEA) was applied for the preparation of highly dispersed Au^0 catalysts supported on low point of zero charge (PZC) supports employing the trivalent cationic gold(III) bis-ethylenediamine, $[\text{Au}(\text{en})_2]^{3+}$, species. SEA provides a highly reproducible synthesis

route to produce well dispersed gold nanoparticles supported on graphitic and activated carbons. Oxide supports, TiO_2 and SiO_2 , were also used to investigate the role of the gold-support interface in catalytic activity and long term deactivation. Catalyst activity for acetylene hydrochlorination was run for at least 20 hours at high gas hourly space velocities to fully evaluate deactivation trends. In this way, Au nanoparticles of almost precisely the same (small) size could be synthesized over a wide variety of supports, and the support surface composition could be correlated to reactivity, Au sintering, and deactivation.

3.2 Experimental

3.2.1 Materials

Bis(ethylenediamine)gold(III) chloride was used as the cationic gold precursor in all SEA experiments over low PZC supports as it has been shown previously to produce particles with high dispersion supported on carbon and a variety of oxide supports [106]. This gold precursor was synthesized fresh in lab by the method of Block and Bailar [116].

Low PZC supports i.e. oxidized carbon, graphitic carbon, silica, and titania were used as received from the manufacturer in this study to produce one weight percent gold catalysts. A table of the supports and the measured pore volume, PZC and BET measured surface area are given in Table 3.1. Vulcan XC-72 was oxidized using concentrated nitric acid at 85°C in reflux for 2 hours and then rinsed and filtered using DI water until a neutral pH of the filtrate was reached and then calcined in a muffle furnace for 3 hours at 400°C .

Table 3.1 Support materials used in catalytic testing, all supports were used as received, except for the oxidized VXC-72.

Support	Surface Area (m ² /g)	Pore Volume(ml/g)	(PZC)
HNO ₃ Oxidized Vulcan XC-72 (Cabot Corporation)	180	1.9	3.7
Vulcan XC-72 (Cabot Corporation)	254	2.3	8.5
Norit CA-1 (Norit Americas Inc.)	1400	1.7	2.6
Darco KB-M (Norit Americas Inc.)	1200	3.2	3.5
Darco KB-B (Norit Americas Inc.)	1500	4	4.8
Asbury grade 4827 (The Asbury graphite Mills Inc.)	115	0.4	4.7
Aersoil 300 fumed silica (Evonik Industries)	330	0.8	3.7
Aeroxide P25 (Evonik Industries)	35	0.7	4

3.2.2 pH shifts and PZC measurement

The PZC of the carbon and metal oxide supports were determined using a surface loading of 1000 m²/L (equation 1) with 50 mL of solution for each sample across all supports, to ensure an equal number of surface sites in solution. Solutions were made up at pH values over the range of 1–13 using HNO₃ and NaOH to adjust the initial pH. Then 50 mL of each pH-adjusted solution was added to the support in 60-mL polypropylene bottles. The solutions were shaken for 1 hour on an orbital shaker at 120 rpm. Final pH measurements were obtained using a general combination pH electrode. At high surface loadings, the plateau of the plotted pH shift corresponds to the PZC [32].

$$\text{Surface loading } \left(\frac{\text{m}^2}{\text{L}}\right) = \frac{\text{Surface Area of support } \left(\frac{\text{m}^2}{\text{g}}\right) * \text{grams of support(g)}}{\text{Volume of Precursor Solution (L)}} \quad (\text{Equation 1})$$

The adsorption of cationic [Au(en)₂]³⁺ onto these low PZC supports was determined as a function of the final pH of the adsorption solutions at constant initial gold concentration. The surface loading was kept constant at 1000 m²/L and the pH of a solution containing 160 ppm of freshly prepared Au(en)₂Cl₃, was adjusted over the pH range of 4-13, using NaOH and HNO₃ to adjust the pH, and the support was then added

to obtain the desired surface loading. The 60-ml polypropylene bottles containing 160ppm Au(en)₂Cl₃ solutions and support were shaken for 1 hour, after which 5 ml of filtered solution was analyzed for Au content via ICP-OES. The gold uptake was determined as the difference in Au concentrations in the pre and post contacted solutions and is reported as Γ shown in equation 2.

$$\Gamma(\mu\text{mol} / \text{m}^2) = \frac{(\text{Conc}_{\text{initial}}(\text{mg} / \text{L}) - \text{Conc}_{\text{final}}) * 10^6 (\mu\text{mol} / \text{mol})}{\text{Surface Loading}(\text{m}^2 / \text{L}) * \text{Mw of Metal}(\text{g} / \text{mol}) * 1000(\text{mg} / \text{g})} \quad (\text{Equation 2})$$

3.2.3 Catalyst preparation

After the amount of [Au(en)₂]³⁺ adsorbed at each pH was determined, 1 gram samples of catalysts at 1.0 weight percent were prepared at the determined pH of maximum uptake in Figure 3.1, where electrostatic forces are considered the strongest. The weight loading in the scaled up batches was confirmed via ICP-OES analysis of the pre- and post-adsorption solutions. To prepare these 1.0 weight percent gold catalysts, the support for 1000m²/l and Au solution were adjusted to the optimal pH were contacted for 1 hour on an orbital shaker at the optimal pH, then filtered and dried under vacuum overnight. The catalysts were then reduced in flowing 10% H₂ with a balance He at 180°C and a ramp rate of 3.0°C/min. Prepared catalysts are stored under vacuum at room temperature until reaction testing and characterization.

A catalyst of 1 weight percent Au/C catalyst was also prepared as a comparison via a conventional incipient wetness impregnation technique using aqua regia as a solvent using untreated VXC-72 carbon as support. A solution of HAuCl₄ (Sigma-Aldrich: 50% gold) was dissolved in aqua regia [HCl 37% (Aldrich): HNO₃ 67% (Aldrich) (3:1)] and this solution was added to the VXC-72 support drop-wise. The prepared catalyst samples were dried overnight and stored under vacuum.

3.2.4 Catalyst Characterization

Powder X-Ray diffraction (XRD) was used to investigate the crystalline characteristics and particle size of the supported gold metal catalysts with a Rigaku Miniflex-II instrument equipped with a D/Tex Ultra detector operating in Bragg–Brentano geometry. The radiation source was Cu-K α radiation ($\lambda = 1.5406 \text{ \AA}$) at operating condition of 30kV and 15mA. All patterns were taken at a scan rate of 0.5°/min and sampling width of 0.02 ° over the range of 10-80° 2 θ . The Scherrer equation was used to determine the Au crystalline size with a limit of detection for well-defined systems down to 1.5 nm [117]. This analysis was done before and after exposure to HCl and C₂H₂ in the reaction. The weight percentages of Au metal for each catalyst were measured by the inductively coupled plasma-optical emission spectroscopy (ICP-OES) technique on a Perkin Elmer Optima 2100DV. The analysis of elemental compositions and oxidation states of the catalyst surfaces was determined by x-ray photoelectron spectroscopy (XPS) using a Kratos Axis Ultra DLD instrument equipped with a monochromated Al K α x-ray source and hemispherical analyzer capable of an energy resolution of 0.5 eV.

3.2.5 Reaction and Particle Stability Testing

Acetylene hydrochlorination reaction testing was carried out in a fixed bed glass reactor (i.d. 3/8"). The acetylene gas was treated to remove major inhibiting impurities (acetone) by molecular sieve 5A and mixed with inert He as well as anhydrous hydrogen chloride gas (Praxair; 99.999%), before being fed to the reactor using calibrated mass flow controllers for each gas. Prior to the start of the reaction, the reduced catalysts were dried at 110°C for 60 minutes under flowing He and then pre-chlorinated with mixed

helium and hydrogen chloride gas at 1:1 flow ratios at 180°C for 1 hour. As previous work has shown, the initial surface composition ratio of $\text{AuCl}_x\text{:Au}^0$ can be maximized by prechlorination under reaction conditions [60, 63, 81]. Acetylene was then fed through the reactor containing the pre-chlorinated catalysts at the desired helium to acetylene to hydrochloride ratio of 1:1:1.1 at 180°C with a helium flow rate of 10 standard cubic centimeters per minute (SCCM) for a GHSV of 4500 hr^{-1} . The exit gas from the reactor was passed through a concentrated NaOH solution to eliminate non-reacted hydrochloric gas. The scrubbed gaseous products were analyzed by an on-line GC (HP5890 FID detector Column: Agilent J&W HP-Plot Q capillary Poraplot Q column). Acetylene conversion and VCM selectivity were calculated by mass balance method. The fractional conversion of C_2H_2 was determined using the standard formalism of $(\text{C}_2\text{H}_{2(\text{in})} - \text{C}_2\text{H}_{2(\text{out})})/\text{C}_2\text{H}_{2(\text{in})}$. VCM selectivity was calculated from the amount of VCM formed/amount of total products formed. All catalysts showed high selectivity to vinyl chloride (>99.5%) at a GHSV of 4500 hr^{-1} with only trace amounts of the C_2 side product 1-2 dichloroethane being observed. For gold particle stability testing the samples were dried under the same conditions as reaction samples and then HCl in He was added to the reactor cell for the desired time via calibrated MFC's. For low HCl concentration experiments, 100 ppm and 2000 ppm HCl diluted in a balance of He was used.

3.3 Results and Discussion

The PZC of carbons used in the present study ranged from 2.6 to 4.8; measured values of the support properties are given in Table 3.1. The PZC's were measured by equilibrium pH at high oxide loadings (EpHL) experiments, and confirmed via pH shift, [33]; details can be found elsewhere [118]. The typical SEA volcano shape plot for the

gold metal uptake (Γ vs pH_{final}) curves is shown in Figure 3.1, which indicates that the metal adsorption mechanism is electrostatic in nature. As the solution becomes highly basic, the increase in ionic strength of the solution retards the metal adsorption and for all complexes an optimal final pH near 12 is observed with maximum uptake values that range from 0.55-0.9 $\mu\text{mol}/\text{m}^2$. The metal uptake at values close to the acidic PZCs of the supports also gave limited uptake as there was insignificant surface charge and thus no driving force for electrostatic adsorption. Gold uptake for the activated and graphitic carbons (CA-1, KB-M, KB-B, and VXC-ox, 4827) is slightly higher compared to the oxide supports (A300 and P25), though they all have similarly acidic PZC's; this variance may have been a result of inaccuracies in the BET surface area measurements. There was a large difference in surface area between the carbons and TiO_2 and SiO_2 , and the difference in uptake was not likely due to a difference in the degree of hydration or support hydroxyl concentration as has been seen in some previous works in this research group [32, 34, 37, 119].

In Figure 3.2, the pH shifts in a metal free control experiment are compared to the metal-containing experiments for the different carbons and oxide supports. The proton exchange capacity of the surface hydroxyl groups buffers the solution pH leading to a plateau in the pH shift, which corresponds approximately with the PZC [33, 34, 119]. The pH final plateau corresponds approximately to the EpHL measured PZC. The system usually approaches the PZC of the support as surface loading increases. The plateau appears thin at the surface loading of 1000 m^2/L and becomes more broad as values approach incipient wetness, around 60,000-100,000 m^2/L .

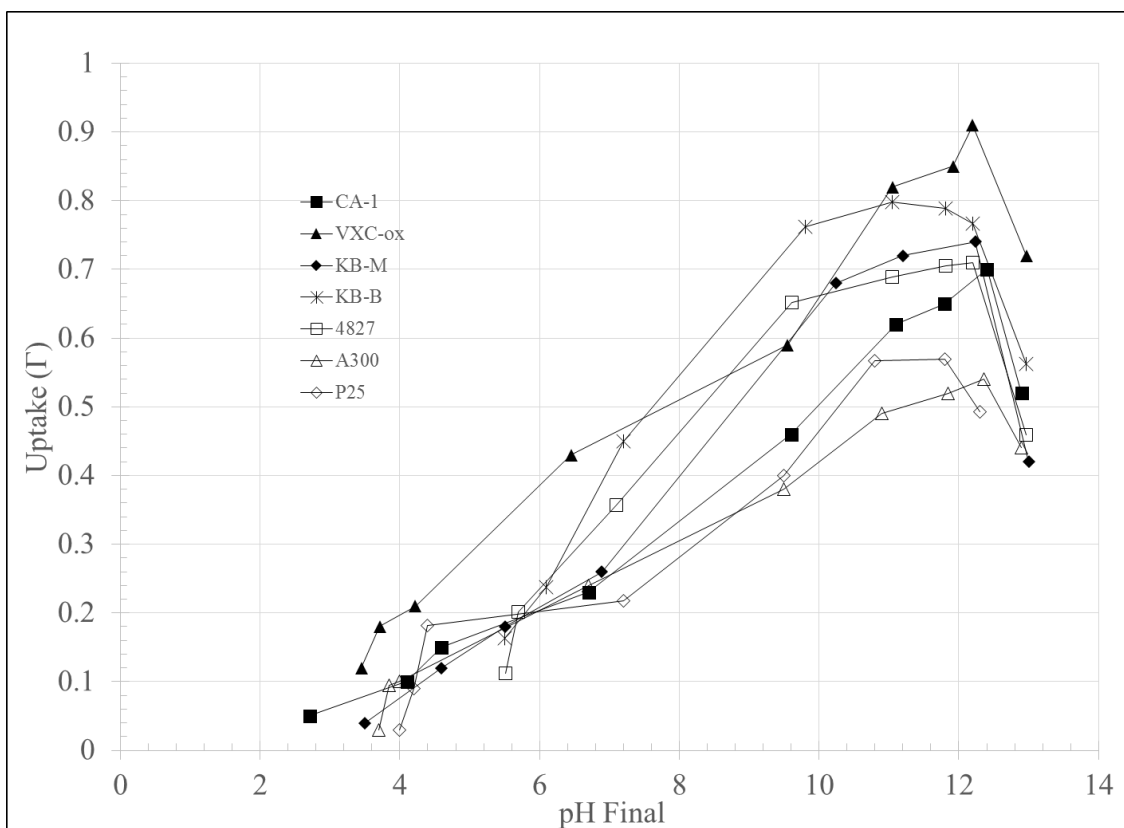


Figure 3.1 Au Metal uptake over the pH range of 2-13 for 160 ppm Au over 1000 m²/L of support for each sample, uptake was determined via ICP-OES of pre and post support contacted samples. NaOH and HNO₃ were used to adjust the initial pH of the samples.

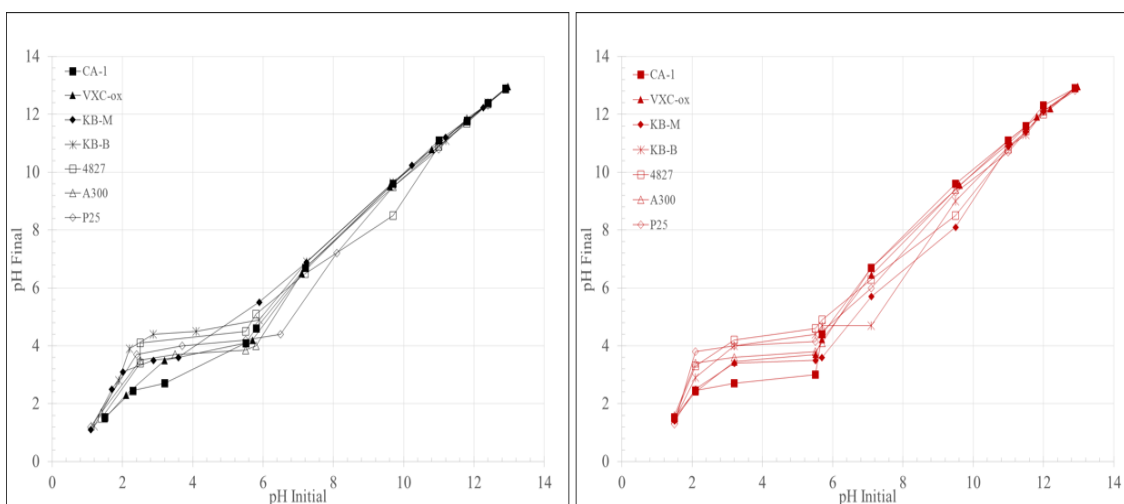


Figure 3.2 Metal Free control pH shift (black) over the pH range of 1-13 using NaOH and HNO₃ to adjust the initial pH with a surface loading of 1000 m²/L and the metal containing pH shift with 160 ppm of Au in solution (red) adjusted under the same conditions and

The similarity of the metal free control pH shift and the 160 ppm Au pH shift in Figure 3.2 indicated that electrostatic adsorption, in which surface charging is assumed to be independent of metal adsorption, appears to be the adsorption mechanism. The pH shifts for the carbon and metal oxides substantially overlap, further indicating that the mechanism of uptake is electrostatic for both types of surfaces.

As detailed in the experimental section, one gram batches of gold catalyst were synthesized using each support at the pH of optimum uptake to produce one weight percent samples. Powder x-ray diffraction experiments were conducted on the fresh, reduced samples before reaction (and prior to HCl contact), as well as on the spent catalyst after 20 hours of time on stream (TOS). These results for fresh and spent particle size are summarized in Table 3.2 and the corresponding XRD patterns are given in Figure 3.3.

Table 3.2 Particle size before and after 20 hours TOS for Au catalysts at a GHSV of 4500 hr⁻¹ with a 1.1:1:1 ratio of HCl:C₂H₂:He

Catalyst	Notation	Fresh Particle Size (nm)	Spent Particle Size (nm)
1 wt. % Au/ VXC-ox	VXC-ox	<1.5	12.3
1wt. % Au/VXC (IWI)	VXC	<1.5	16.4
1 wt. % Au/ CA-1	CA-1	2	20.1
1 wt. % Au/ KB-M	KB-M	3	17.5
1 wt. % Au/ KB-B	KB-B	2.1	22.2
1 wt. % Au/ 4827	4827	<1.5	3.7
1 wt. % Au/ A300	A300	<1.5	<1.5
1 wt. % Au/ P25	P25	<1.5	<1.5

The particle size of most of the fresh samples (the bottom pattern of each part of Figure 3.3) were below the limit of XRD detection; for the CA-1, KB-M and KB-B samples, broad peaks were observed with sizes estimated to be 2.0, 3.0, and 2.1 nm respectively. The small size of the fresh Au/KBB catalyst was confirmed by STEM

(Figure 3.4). The particle sizes of the spent catalysts are also given in Table 3.2, and their XRD patterns and STEM image are given in Figure 3.3 and 3.4. These will be discussed after the reactivity results are presented.

Reactivity results are shown in Figure 3.5. It is noticed immediately that the Au supported on the two oxides, P25 and A300, and on the non-oxidized carbon, 4827, had almost no activity. The non-graphitic carbon supported gold catalysts all had similar conversion patterns; initial high conversion likely stemming from completely oxidized Au^{3+} resulting from the HCl-rich pretreatment, followed by a rapid deactivation over the first 0-5 hours, followed by a slower decay over the length of the experiment. The VXC-ox and the VXC-iwi samples showed the highest initial activity with conversions of about 50 percent. However, the VXC-ox sample had the slowest conversion decay rate while the VXC-iwi sample exhibited the highest long term decay rate. The rest of the carbon supports i.e. CA-1, KB-M, and KB-B show similar trends to the VXC-ox carbon albeit with slightly lower conversion values, but similar, slow long term deactivation.

The long term activity seen here, about 30% conversion at a GHSV of 4500 h^{-1} , is about the same as that observed in an earlier work using the same flow system [5], in which long term conversions of about 80% were noted over the same weight loading (1 weight percent) Au catalyst at about a third of the space velocity (1480 h^{-1}) [29]. The activity appears to be much higher than aqua regia-derived 1 weight percent Au/C catalysts showing a conversion of 70% at a space velocity of 740 h^{-1} [63, 64]. The Au particle size in that study was relatively large and the number of active sites appear to have been much less than in the current catalysts.

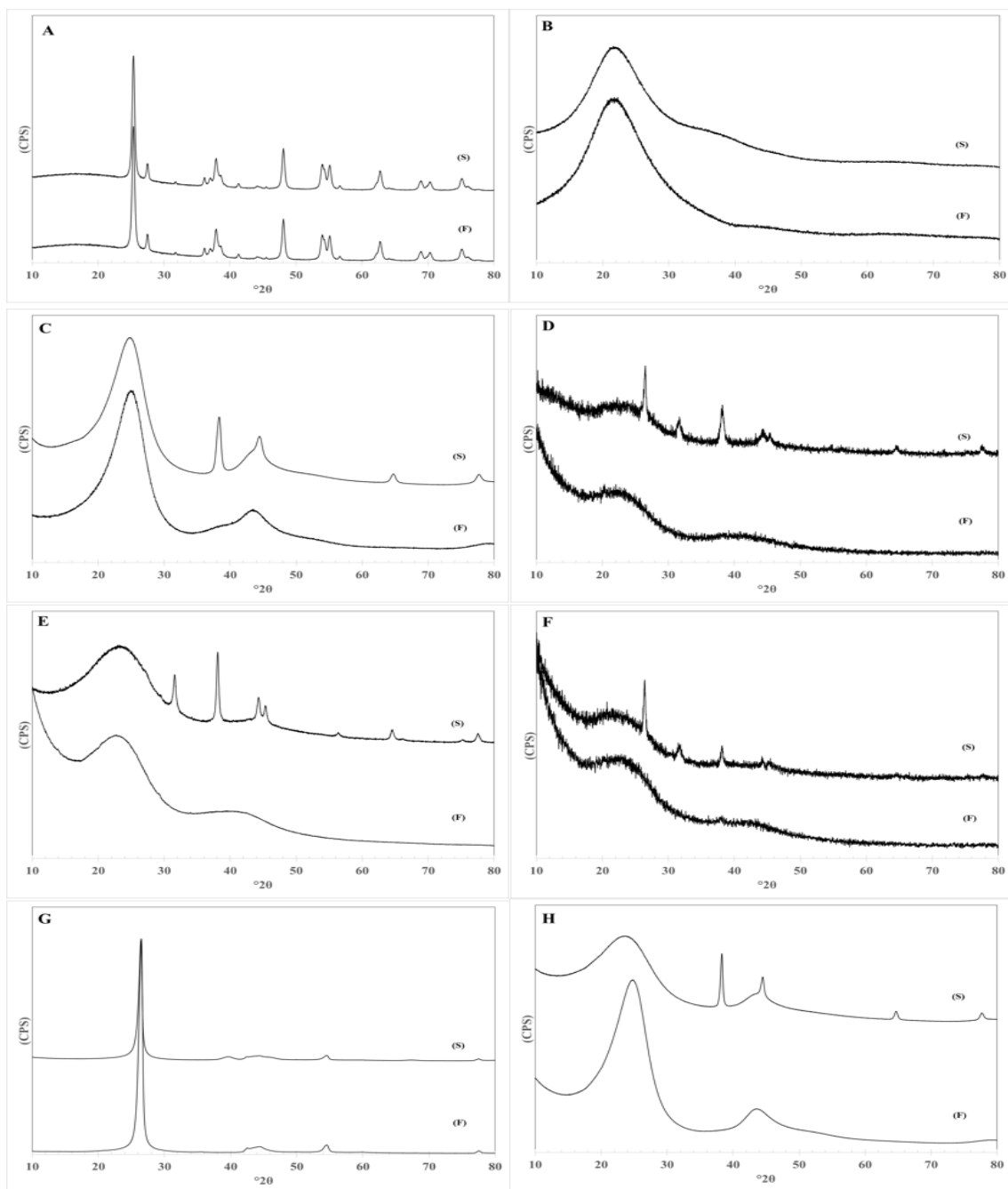


Figure 3.3 XRD patterns at operating condition of 30kV and 15mA. All spectra were taken at a scan rate of 0.5°/min and sampling width of 0.02° over the range of 10-80° 2θ for the fresh (F) and spent (S) catalyst samples. A) P25, B) A300, C) VXC-OX, D) KB-M, E) KB-B, F) CA-1, G) 4827 H) VXC-IWI.

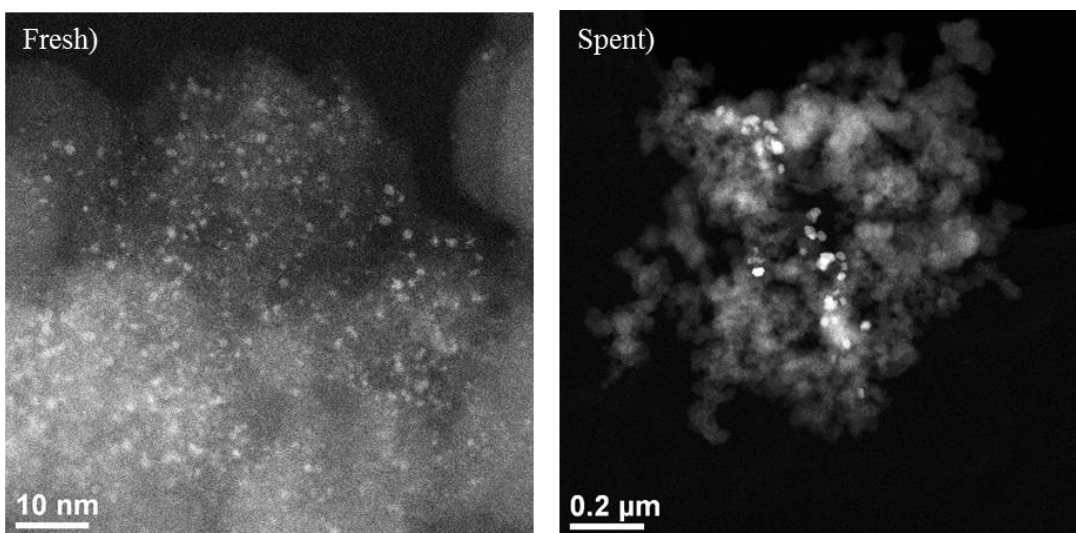


Figure 3.4 Representative stem images of Au/KBB fresh spent particles after 20 hours on stream

The larger space velocity was chosen to more closely mimic industrial conditions and to be able to better observe deactivation trends during time on line.

Characterization of the used catalysts is given in Figure 3.3 and 3.4, and summarized in Table 3.2. The XRD results reveal that the different supports exhibited vastly different anchoring ability. Sharp Au peaks indicated that extensive sintering occurred over all carbon supports except the graphitic carbon, which sintered mildly, whereas the absence of Au peaks over the oxide supports indicated the ability of these surfaces to anchor gold quite strongly. The STEM image of the aged Au/KBB catalyst in Figure 3.4 also confirms the sintering of the Au.

An intriguing trend is seen in comparing the post reaction characterization data to the activity data in Figure 3.5: the spent catalyst samples which gave the highest activity were in general the samples which sintered the most. The silica, titania, and graphitic carbon samples which showed little gold sintering were the least active catalysts for acetylene hydrochlorination.

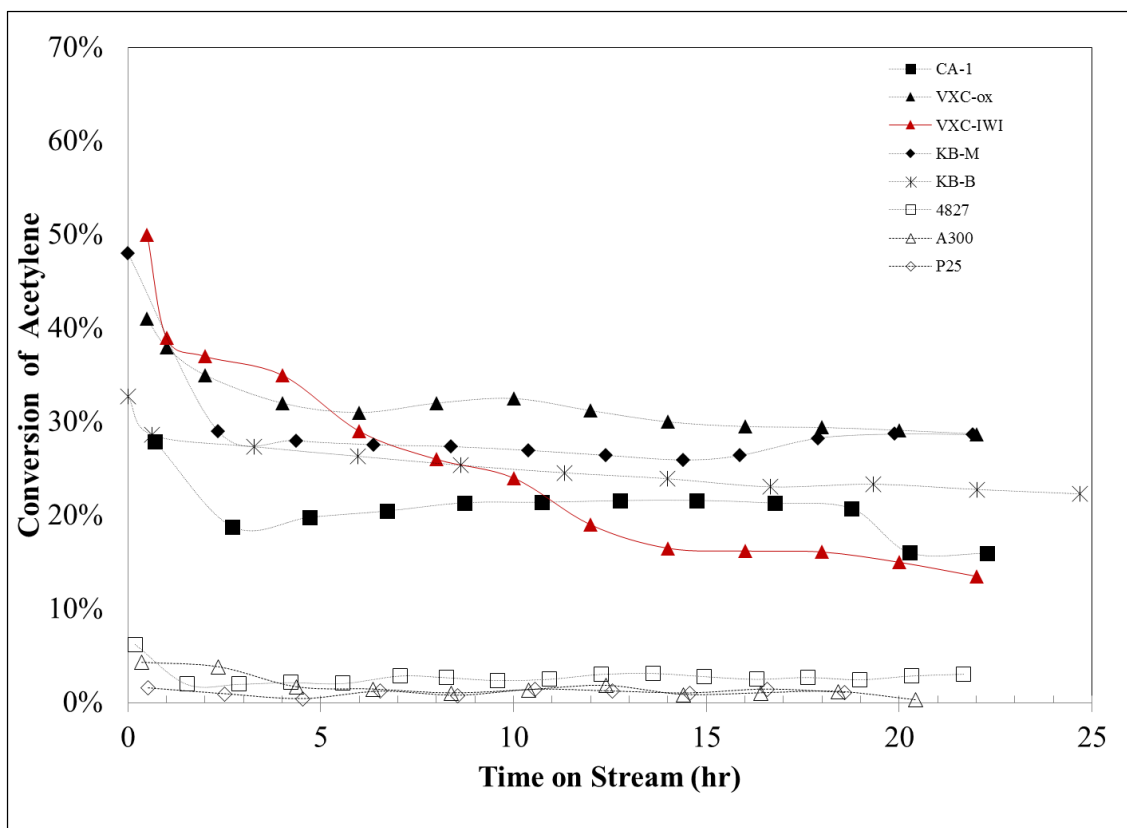


Figure 3.5 Conversion of acetylene based on $(C_2H_2(in) - C_2H_2(out))/C_2H_2(in)$ for each sample tested at a GHSV of 4500 hr⁻¹ the samples were dried for 1 hour at 110°C in the glass reactor and then prechlorided at 180°C for 1 hour prior to the beginning of catalytic testing.

This trend holds within this sub-group; of the three least active catalysts (bottom of Figure 3.5), that with the relatively highest activity, the graphitic carbon did show some degree of sintering; that with the relatively intermediate activity, the A300 silica, showed a trace of sintering, and that which showed virtually no activity, the P25 titania, showed virtually no sintering.

Of the group of most active catalysts (the activated carbons and carbon blacks), it is notable that activity is not precisely in line with particle size, for example, the KB-M and VXC-ox samples have similar values of conversion over 20 hours even though the particle size and so Au exposed area are about 50% different (12 to 18 nm, Table 3.2).

The activated carbons and the oxidized black all exhibit relatively slow rates of deactivation, while the unoxidized VXC catalyst displays a continual deactivation through 20 hours. This differs notably from the oxidized VXC-ox sample. A number of studies have related stability of carbon catalysts to the degree of oxidation of the support [65, 78, 80, 85, 120] and this data is consistent with them. A final observation from Figure 3.3 is that crystalline NaCl appeared in all the used activated carbons, undoubtedly from the Na impurity typical of this type of carbon.

Post-reaction size characterization has not been systematically carried out in most acetylene hydrochlorination studies of Au/C. Only one other study by Dai et al. have systemically considered the possibility of Au sintering as a possible deactivation mechanism past the loss of AuCl₃ on the surface. This work showed that similar results in that previously reduced Au/C catalysts were active for acetylene hydrochlorination but through STEM and XRD found that large particles formed via thermal treatment became less active as cluster size increased [120].

A final set of pre- and post-reaction characterization was performed by XPS (Figure 3.6) for the fresh and spent samples for the Au supported on (VXC-ox) SEA prepared sample and the HAuCl₄ impregnation prepared (VXC-iwi) sample after reduction but before reaction for both samples. The normal binding energy of Au⁰ is near 84 and 87 eV for Au4f_{7/2} and Au5f_{7/2}, while the position of Au4f_{7/2} and Au5f_{7/2} peaks for Au³⁺, widely held to be the active species in this reaction [65, 81] have binding energies of 86 and 89 eV [121].

No Au³⁺ was detected on the surface of the freshly reduced catalyst samples prepared via SEA or IWI as would be expected. Nor is Au³⁺ observed in the spent

catalysts; this observation is common for spent Au catalysts with large particle size [82, 120, 122]. These results imply that the number of active Au^{3+} sites must be small compared to the total number of Au sites and confirm that the deactivated catalysts are large particles of sintered Au^0 .

Further study of gold sintering in HCl rich reaction environments was conducted by isolating the effects of temperature and HCl; a first set of XRD results is shown in Figure 3.7. The fresh Au/KBB catalyst, which gave reasonably high long term conversion and exhibited a high degree of gold sintering, was reduced under standard conditions and then pretreated in flowing He (10 SCCM) for 20 hours at 180°C . This sample, the bottom pattern in Figure 3.7, showed no peak sharpening, indicating complete stability of the 2.1 nm gold nanoparticles in high temperature He. Additional samples were dried under standard conditions in the reactor cell and then contacted with 50% HCl/He for 5, 15, 45 and 60 minutes.

Size estimates from the sharpened XRD peaks are 21, 19, 20, and 21 nm for the respective time values. It is the hydrogen chloride which causes the Au particles to undergo dramatically rapid sintering to an apparently thermodynamically metastable particle size in the reaction atmosphere. While such sintering has not been reported to date, few other studies have begun with fresh Au particles as small as these. When catalysts are synthesized with small particle size, researchers must be aware of this rapid change in particle size. In the activity data of Figure 3.5, for example, it can be argued that the initial high rate of deactivation is due in significant part to sintering.

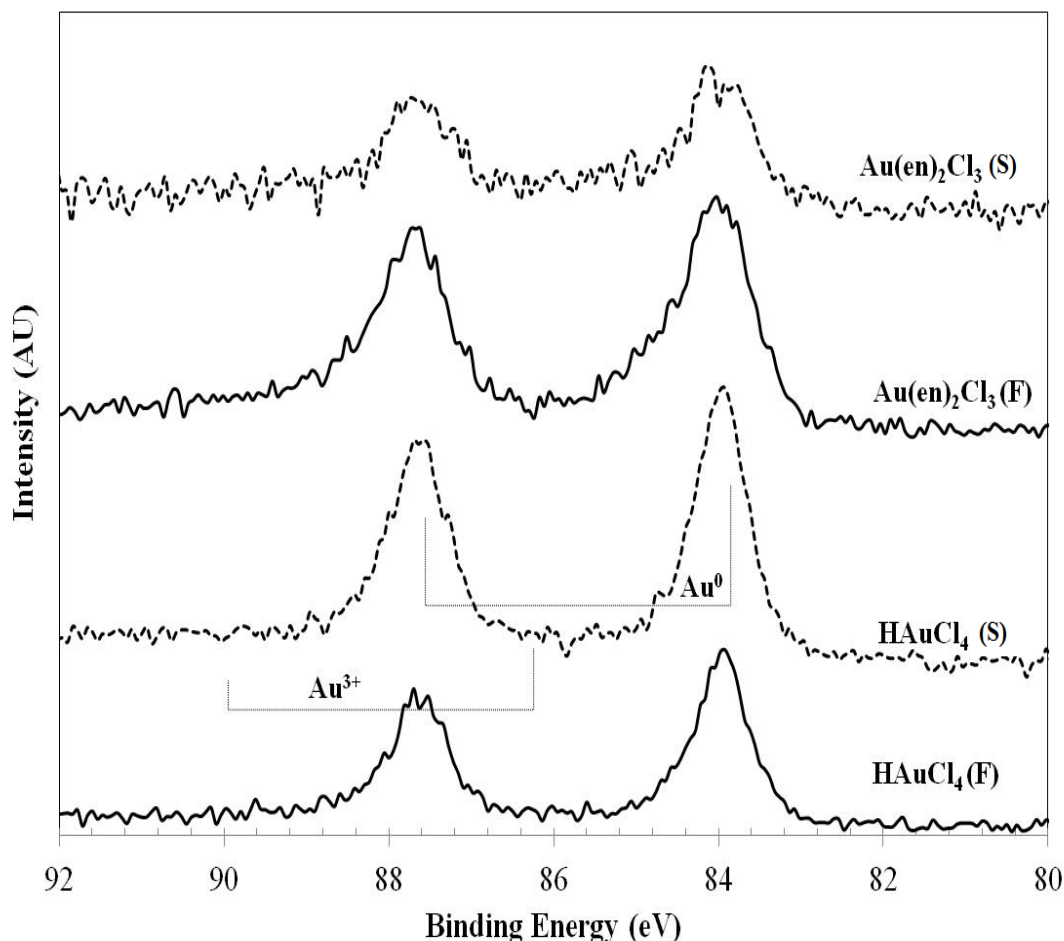


Figure 3.6 XPS spectra of fresh and used Au/C catalysts using HAuCl_4 prepared via IWI and $\text{Au(en)}_2\text{Cl}_3$ prepared via SEA. Fresh and spent catalysts denoted as F and S, respectively. Binding energy values have been referenced to C1s peak at 284.6 eV. Literature values for Au 4f_{7/2} binding energies of Au^0 , Au^+ , and Au^{3+} are 84, 85.0, and 86 eV, respectively [121]

A further study to more accurately determine the sensitivity of sintering to HCl was conducted by placing the Au/VXC-ox sample in dilute HCl (100 ppm and 2000 ppm) in a balance of He. For these experiments, the catalyst samples were dried in the reactor under flowing He at 180°C for 1 hour and then exposed to the dilute HCl gas for amounts of time corresponding to precise molar ratios of Au:HCl (using total atoms of gold). Once the desired ratio of Au:HCl was attained, the flow of HCl was stopped and the system

purged with nitrogen and the sample was removed for XRD analysis. Results are shown in Figure 3.8.

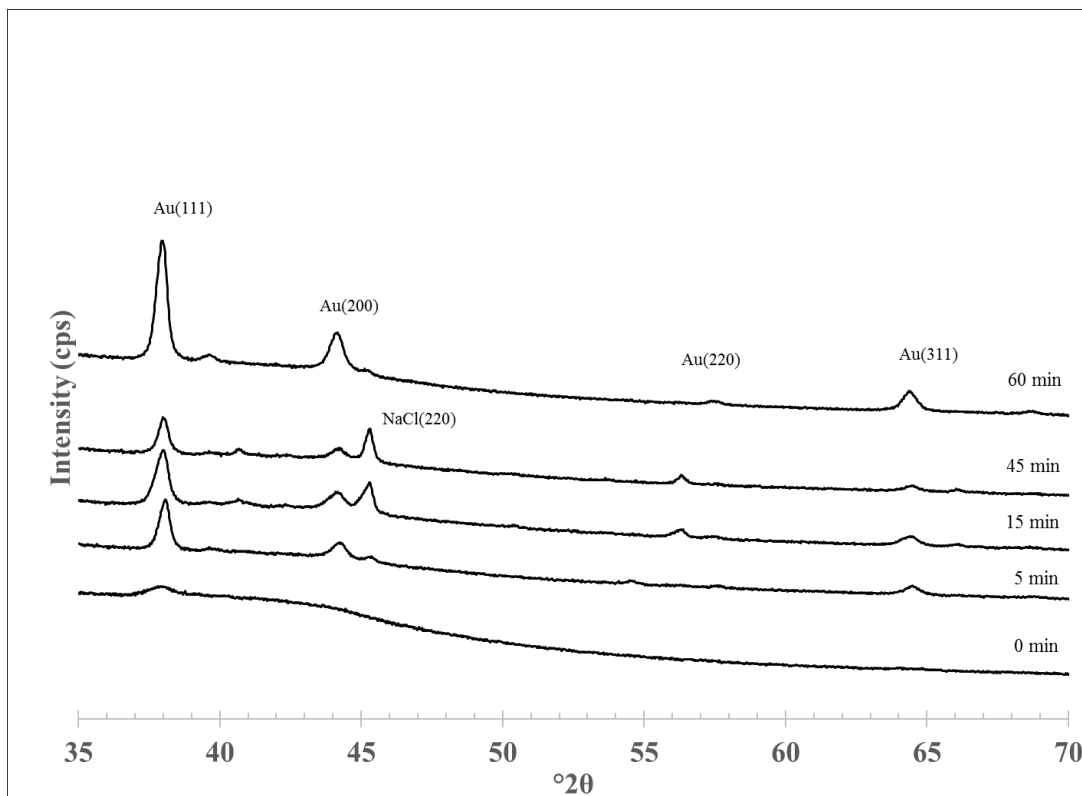


Figure 3.7 XRD patterns for Au/C samples exposed to 1:1 HCl:He at 180°C for times increasing to 60 minutes of pre chlorination at 10 SCCM after drying for 180°C in He (10 SCCM) for 1 hour.

XRD patterns of samples exposed to 1:3 and 1:9 Au:HCl ratios, over 10 and 30 minutes, showed no change from the stable, He-annealed sample. As the Au:HCl ratio increased from 1:170 to 1:2500 over 5 hours, there is a noticeable increase in Au particle size brought on by the HCl exposure. Particle sizes for the 1:630 case was 4.1 nm and for the 1:2500 case, 7.6 nm, which still did not approach the spent particle size observed for this VXC-ox catalyst after a 20-hour reaction run on stream in 33% HCl of 12 nm. While the sintering of Au is relatively very rapid, it would appear to be several orders of

magnitude slower than the production of a mobile intermediate formed via a stoichiometric reaction of Au with the reactant gas.

A more reasonable deactivation mechanism may involve a volatile active site such as the Au^{3+} dimer Au_2Cl_6 , shown to form when Au^0 is volatilized at the elevated reaction temperatures in the presence of HCl [123]. It has been suggested that the only active Au^{3+} species are those at the metal-support interface [80], and this suggestion is in line with computational work showing that a nitrogen containing dopant added to a graphene carbon model helps to stabilize the active Au_2Cl_6 gold species [112]. A volatile intermediate at the Au nanoparticle-support surface interface is consistent with the present results in a number of ways. First, activity does not appear to be strictly related to particle size; as Au nanoparticles sinter from 2 to 20 nm early on in Figure 3.5 corresponding to a 10 times loss in surface area, activity declines only about 50%. Second, the surfaces with the highest oxygen functionality show the least deactivation, as especially seen in the case of oxidized versus unoxidized VXC in Figure 3.5. The importance of the surface oxygen groups in stabilizing the active site for acetylene hydrochlorination has been reported numerous times [65, 86, 112].

Such an interfacial species might also explain the support effect on sintering and deactivation observed here. It is speculated that the dimer interacts very strongly with metal oxide and graphitic supports, to the extent that it is too strongly anchored to be reactive. Over unoxidized activated carbon, the species is very mobile, leading to volatilization, reduction, and extensive nanoparticle growth. Over oxidized carbon, the interfacial dimers would have the closest to the optimal interaction; weak enough to be reactive but strong enough to (at least partially) resist sintering.

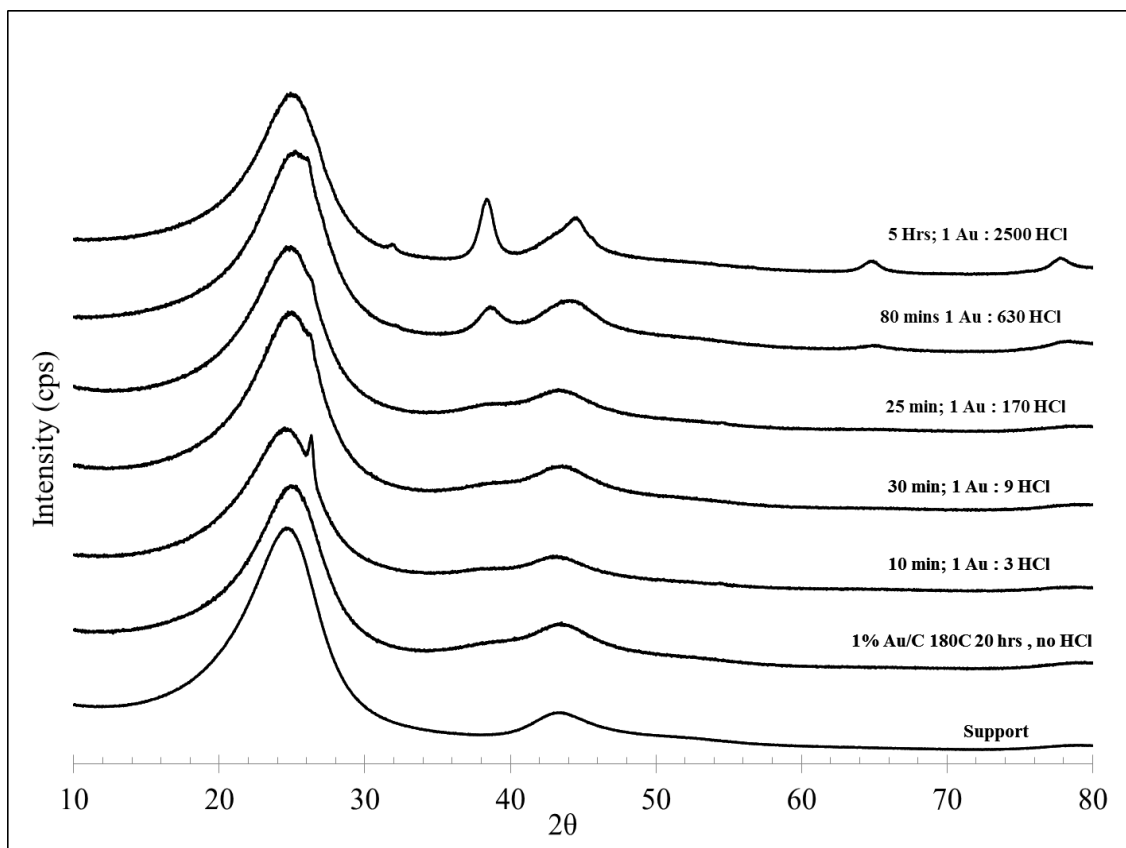


Figure 3.8 XRD patterns at operating condition of 30kV and 15mA. All spectra were taken at a scan rate of 0.5°/min and sampling width of 0.02° over the range of 10-80° 2θ. Profiles of samples after exposure to 10 SCCM total flow rate of HCl diluted in He at 180°C over time. For atomic ratios of 1:3 and 1:9 100 ppm HCl was used, for all other atomic ratios 2000 ppm HCl was used.

On a practical note, an active Au phase comprised of small nanoparticles – with large numbers of perimeter sites – may well be active if a support with the right Au³⁺ interaction can be found or engineered. If that is the case, strong electrostatic adsorption would be an excellent way to synthesize the nanoparticles. This is especially important if Au catalysts are to be commercialized for VCM production. Besides support engineering, reaction conditions may also be exploited to optimal catalyst stability. It has been shown, for example, that increased HCl:acetylene ratios larger than 1.15:1 showed a reduction in the rate of catalyst deactivation [113, 124].

3.4 Conclusion

Strong electrostatic adsorption has successfully been shown to produce effective Au supported catalysts for the hydrochlorination of acetylene to vinyl chloride. Highly dispersed gold particles can be synthesized across a variety of low PZC supports using $\text{Au(en)}_2\text{Cl}_3$ that give increased long term conversion when compared to a standard 1 weight percent IWI sample prepared over non-graphitic carbons. This preparation method is advantageous since this method does not require aqua regia, a fuming acid, to produce highly dispersed nanoparticles. These samples had a high degree of particle sintering, due to the presence of HCl in the reaction and not from the elevated temperature. This particle sintering occurs rapidly in the presence of HCl as the gold agglomerates to a more thermodynamically favorable metastable state. The sintering of the supported gold particles may play a more important role in loss of conversion of acetylene compared to just the loss of surface AuCl_3 as XPS has shown no AuCl_3 was present on the spent catalysts even though there was still considerable activity.

The type of support plays an important role in particle sintering during reaction. SiO_2 and TiO_2 supported gold was inactive for vinyl chloride synthesis, although the gold particles did not coalesce on these supports. When supported on activated carbon, a great degree of agglomeration occurs, yet these catalysts showed the highest activity. This phenomenon may be due to the strength of the bond of AuCl_3 - AuCl_3 dimers; on the surface of the metal oxides and graphitic carbons they may be too strongly bonded to be active.

The role of surface group functionalization is still unknown in this reaction, as is set forward in this study the catalyst with the highest long term stability was the 1 weight

percent Au/VXC-ox that was treated in nitric acid at elevated temperature. This sample showed limited sintering when compared to the untreated VXC-iwi sample. Further study will be conducted into the role of the carbon interface i.e. increasing the amount of Au-C interface through decreasing particle sizes that are stable in this chemically harsh environment. The degree of oxidation of the surface groups on treated carbons also can play a role to better tune the binding of the active species to the support without reducing it to Au⁰ to further increase stability of the active site. SEA provides another tool in the synthesis toolbox to rationally produce catalysts of high dispersion with a great degree of particle size control over low PZC supports that are favorable to more common or complicated impregnation preparation methods for the use in acetylene hydrochlorination.

CHAPTER 4: THE STABILIZATION OF AU SHELLS BY HIGH SURFACE FREE
ENERGY PT AND RU CORE, AND THE EFFECT ON ACTIVITY FOR
ACETYLENE HYDROCHLORINATION

To be submitted[K.C. O'Connell, J.R. Monnier, and J.R. Regalbuto]

4.1 Introduction

Polyvinyl chloride (PVC) is among the top three plastic polymers produced world-wide by volume, after polypropylene and polyethylene. It has been estimated that global demand for PVC will reach 40 million tons annually by 2016 [55]. Vinyl chloride monomer (VCM) is the monomer polymerized to produce PVC. The synthesis of VCM via acetylene hydrochlorination is a well-known vinyl chloride synthesis route most common in coal producing regions. This is a result of the abundance of acetylene, produced from calcium carbide, and limited need for separation of the product stream [57]. Approximately 70% of VCM produced in China, the world's largest producer, is synthesized via the direct method of acetylene hydrochlorination [110]. Commercially, the hydrochlorination of acetylene is catalyzed by a mercuric chloride catalyst supported on carbon. The reaction takes place at moderate temperature and pressure compared to the oxychlorination VCM process. The largest drawback for the industrially used mercuric chloride catalyst, is the short life span of the catalyst, due to rapid reduction of Hg^{2+} to Hg^0 and requisite sublimation of the mercury metal from the support under reaction conditions, which results in deactivation [58, 61].

As a result of the catalytic deactivation as well as environmental concerns of volatile Hg species, there has been substantial research interest in the synthesis and development of mercury-free catalysts for the hydrochlorination of acetylene. A multitude of research groups have made efforts to investigate novel alternative mercury free catalysts for acetylene hydrochlorination. Various mercury-free catalysts such as Au^{3+} [63, 66, 79], Cu^{2+} [125], Pd^{2+} [126, 127], Pt^{2+} [70, 71] and Bi^{3+} [76] have been studied. These results have not been satisfactory for commercial production due to stability

problems that lead to rapid catalyst deactivation and in the case of Au^{3+} containing samples, a large degree of particle sintering under reaction conditions [120]. Literature has indicated that carbon-supported gold offered high initial activity; however, the catalysts deactivate rapidly due to the poorly anchored Au species on the support surface, coupled with the reduction of the active species (Au^{3+}) [64, 113, 128]. The deactivation of the active gold chloride complex can be attributed to the reductive nature of acetylene, hence an oxidizing agent is often employed to regenerate the reduced gold metal to the active gold chloride complex on the carbon surface [66]. Additionally, on-line anhydrous hydrochloric acid has been shown to restore catalytic activity between reaction runs to near its initial reactivity after 6 hours of treatment [63]. Wittanadecha et al. studied the effect of catalyst pre-treatment with HCl and found that after 3 hours of reaction, time catalytic activity was similar for all species regardless of the initial surface Au^{3+} concentration and the sintering of gold particles occurs under reaction conditions. Similar concentrations of Au^{3+} were present on the surface, when comparing a fresh or pretreated catalyst [81, 122].

Metallic ions adsorbed on the carbon support as Au^{3+} are often reduced under reaction conditions and sinter to large deposits of bulk gold metal particles on the surface, which are thought to be catalytically inactive. Preserving the dispersion of the Au particles is of critical importance in producing a highly active and stable catalyst. As previous research has indicated, gold particles sinter rapidly under reaction conditions. This sintering is attributed to the presence of HCl and the mobility of the AuCl_3 phase at reaction conditions [129]. In our previous work the technique of Strong Electrostatic Adsorption (SEA) was used to increase initial particle dispersion in an attempt to increase

gold surface area to offset the reduction of active sites under reaction conditions, which happens rapidly in the presence of HCl and C₂H₂ [120, 129]. The results indicated that gold was stable when supported on metal oxides such as silica or titanium dioxide, but inactive. While gold supported on activated carbon was active for hydrochlorination while particles sintered rapidly, and there was monotonic long term deactivation up to 20 hours. This meant that the acidic metal oxide may have prevented the gold from forming the active Au³⁺ species and another method of stabilization is required

The hypothesis of the current work is that gold may be stabilized via anchoring onto a stable metal core possessing a surface free energy higher than metallic gold. It is expected that a precise synthesis route can produce bimetallic core-shell nanoparticles dispersed on a carbon support that will have improved resistance to particle coarsening under reaction conditions. For example, the surface free energy of metallic gold is lower than that of ruthenium or platinum, and higher than the carbon support. It would be thermodynamically favorable for gold atoms to cover the higher surface energy core metal atoms and exist as a thin shell, reducing the total surface energy of the system. Surface free energies of the species involved in this system are as follows: carbon: 0.506, Au: 1.626, Pt: 2.691, Ru: 3.409 (J/m²) [130].

Some precedence in literature exists for the use of bimetallic catalysts for the hydrochlorination of acetylene using co-impregnation to produce alloyed metal nanoparticles [61], though in these studies the bimetallic nanoparticle morphology is not well controlled nor well characterized. Gold is commonly alloyed via mixed impregnation or deposition with copper, which is claimed to act synergistically, or with bismuth or nickel, which may retard Au reduction to Au⁰ [61, 76, 111, 131].

The precision synthesis of Au shell-Pt or Ru core particles necessary to test our hypothesis will begin with strong electrostatic adsorption. SEA exploits the columbic interaction in aqueous solution between a protonated and positively charged surface and an anionic precursor, or a deprotonated and negatively charged surface and a cationic metal precursor to dramatically improve the adsorption of metal complexes onto the support surface [4, 30, 118]. This results, after precursor reduction, in more highly dispersed metal particles with a tight size distribution and hence an increased number of active sites. Highly dispersed platinum and ruthenium cores will be synthesized on carbon via strong electrostatic adsorption and tested for stability in the presence of HCl.

Once core particle stability is confirmed, gold shells will be selectively deposited on the higher surface free energy cores via Electroless Deposition (ED). If deposition of the gold precursor is not carefully controlled, the gold species may adsorb onto the support via deposition or precipitation. The clusters can further crystallize and grow yielding larger Au particles and a decreased active gold surface area. Electroless deposition of Au via a well-studied gold deposition developer bath [45, 132] has been demonstrated for a number of metal cores to produce well characterized bimetallic catalysts of a core-shell structure at various metal coverages [51].

In this study Au was deposited onto stable Pt and Ru cores at varying surface coverages. Aging in HCl as well as acetylene hydrochlorination as a probe reaction were used to test nanoparticle stabilization in a harsh chemical environment. The stabilization of Au shells on Ru and Pt cores was dramatic. The vastly higher number of Au sites available for the hydrochlorination reaction in stable gold shells, however, did not

translate into higher catalytic activity. The lack of activity must be related to the active site needed for the reaction not being accommodated by Au in its shell morphology.

4.2 Experimental

4.2.1 Catalyst preparation via SEA

The 1 weight percent carbon supported gold catalysts used in this study were synthesized via the electrostatic adsorption of Bis(ethylenediamine)gold(III)chloride $[\text{Au}(\text{en})_2\text{Cl}_3]$ onto Darco KBB carbon with a BET area of $1500 \text{ m}^2/\text{g}$. The point of zero charge (PZC) was measured to be 4.8. $[\text{Au}(\text{en})_2]$ was synthesized according to the method of Block and Bailar [116]. A solution of 160 ppm Au was prepared by dissolving freshly prepared $(\text{Au}(\text{en})_2\text{Cl}_3)$ into deionized water. A metal uptake survey was conducted to determine the pH of optimal metal uptake with precursor solutions containing 160 ppm of Au and the pH was adjusted over the range of 1-13, using 40ml of this gold solution, with a surface loading of $1000 \text{ m}^2/\text{L}$ carbon support added to the solution. A constant surface loading ensured a similar number of surface sites across all adsorption and pH shift experiments.

$$\text{Surface loading } \left(\frac{\text{m}^2}{\text{L}}\right) = \frac{\text{Surface Area of support } \left(\frac{\text{m}^2}{\text{g}}\right) * \text{grams of support(g)}}{\text{volume of precursor solution (L)}} \quad (\text{Equation 1})$$

Samples were mixed for 60 minutes after which a 10 mL aliquot of contacted solution was filtered. The gold concentration was measured of this, the post-contact sample as well as the parent solution using ICP-OES. Adsorption density was calculated by Equation 2 and is expressed as micromoles of Au adsorbed per square meter of support [133]. The optimal pH (pH of greatest metal uptake) was used to scale up to two gram batches of catalyst. For this, one liter of solution was prepared with the metal salt to

yield a final pH of optimal uptake and 1000 m²/L surface loading and mixed for one hour on an orbital shaker, then filtered and dried at room temperature for 24 hours under vacuum. The catalyst samples were reduced in flowing 10% H₂/He.

$$\text{Uptake } \Gamma \left(\frac{\mu\text{mol}}{\text{m}^2} \right) = \left(C_{\text{initial}} \left(\frac{\text{mg}}{\text{L}} \right) - C_{\text{final}} \left(\frac{\text{mg}}{\text{L}} \right) \right) * \frac{10^6 \left(\frac{\mu\text{mol}}{\text{mol}} \right)}{\text{surface loading} \left(\frac{\text{m}^2}{\text{L}} \right) * \text{M.W. of metal} \left(\frac{\text{g}}{\text{mol}} \right) * 1000 \frac{\text{mg}}{\text{g}}}$$

(Equation 2)

Uptake surveys and scaled up synthesis of Ru and Pt were also similarly performed at a loadings of 0.5 weight percent Ru and 1 weight percent Pt to ensure similar molar ratios of Au to the core metal. Tetraammine platinum(II) chloride (PTA), and hexaammine ruthenium(II) chloride were used as metal salts for preparation of the monometallic systems. Synthesis for these carbon supported catalysts can be found elsewhere in literature and have been shown to produce highly dispersed metal nanoparticles, when used in SEA preparations over low PZC carbons [134-136]. The reduction temperatures employed for the single metal Au, Ru, and Pt catalysts were determined by TPR and were 150, 250, and 250°C respectively.

4.2.2 Bimetallic Au catalyst preparation via electroless deposition

A series of Pt@Au/C and Ru@Au/C bimetallic catalysts were prepared by the electroless deposition of KAu(CN)₂ using hydrazine (N₂H₄) as the reducing agent. M@Au denotes a shell of Au deposited on the core metal M prepared via SEA. The ratio of reducing agent to metal salt in the bath was 10:1 (N₂H₄:KAu(CN)₂). The electroless developer bath volume was 200ml and 0.5 g of either the 0.5 weight percent Ru or 1.0 weight percent Pt/C was used as substrate for gold deposition. Deposition experiments were conducted at 313K by immersing the developer bath flask in temperature controlled oil baths. Initial pH of the baths was adjusted to pH 10 with concentrated NaOH and pH

was monitored and maintained during the experiment. Experiments were carried out for 180 minutes to ensure complete deposition of gold. Catalysts were then washed with 2 liters of DI H₂O to ensure removal of residual ligands and salts, then filtered and dried overnight at room temperature and stored under ambient conditions. Blank experiments were conducted to confirm that a solution of N₂H₄ and KAu(CN)₂ at pH 10 did not undergo reduction and deposition on the carbon support, which was expected, based on similar results of previous reports [45, 132]. After deposition, the samples were washed with 2 liters of DI water to remove any residual CN⁻ ligands and dried under vacuum overnight at room temperature and then stored under vacuum.

4.2.3 Catalyst Evaluation

Acetylene hydrochlorination reaction testing was carried out in a fixed bed glass reactor (i.d. 3/8"). The acetylene gas was treated to remove major inhibiting impurities (acetone) by molecular sieve 5A and mixed with inert helium as well as anhydrous hydrogen chloride gas (Praxair; 99.999%), before being fed to the reactor using calibrated mass flow controllers for each gas. Prior to the start of the reaction, reduced catalysts were pre-chlorinated with helium and hydrogen chloride gas at a 1:1 ratio at 180°C for 1 hour with a total flow of 20 SCCM. Acetylene was then fed through the reactor containing the pre-chlorinated catalysts at the desired helium to acetylene to hydrochloride ratio of 1:1:1.1 at 180°C with a helium flow rate of 10 sccm. The exit gas from the reactor was passed through a 5M NaOH solution to eliminate non-reacted hydrogen chloride gas. The gaseous products were analyzed by an on-line GC (HP5890 FID detector Column: Agilent J&W HP-Plot Q capillary Poraplot Q column). Acetylene conversion and VCM selectivity were calculated by the mass balance method; fractional

conversion of C_2H_2 to VCM was determined using the standard formalism of $(C_2H_{2(in)} - VCM_{(out)})/C_2H_{2(in)}$ and VCM selectivity was calculated from the amount of VCM formed/amount of total products formed. Each catalyst exhibited extremely high selectivity towards VCM - in excess of 99.5%.

4.2.4 Catalyst characterization

Powder X-Ray diffraction (XRD) was used to investigate the crystalline characteristics of the supported metal catalysts and particle size was determined by the Scherrer equation. The XRD spectra of catalysts was measured by a Rigaku Miniflex-II equipped with a D/TeX Ultra detector. The radiation source was Cu-K α radiation ($\lambda = 1.5406 \text{ \AA}$) at operating condition of 30kV and 15mA. All spectra were taken at a scan rate of $0.5^\circ/\text{min}$ and sampling width of 0.02° over the range of $20-80^\circ 2\theta$. An advanced x-ray detector, such as the D/TeX ultra, can output data with an excellent signal to noise ratio and accurate for particle size determination down to about 1.5 nm for well-defined carbon supported systems [137].

The amount of metal in solution as a function of time for the gold developer bath for each bimetallic preparation was measured by atomic absorption spectroscopy (PerkinElmer AAnalyst400). The amount of gold deposited on the monometallic substrate was used to determine the theoretical surface coverage of Au of the core metal. The concentration of metal for each catalyst prepared via SEA was measured by inductively coupled plasma-optical emission spectroscopy (ICP-OES) on a Perkin Elmer Optima 2100DV; pre- and post-support contacted samples were tested for metal concentration.

For chemisorption, Pt/C, Ru/C, and the bimetallic M@Au/C catalysts were characterized using H₂ titration of oxygen pre-covered Pt sites with a Micromeritics AutoChem 2920 Automated Analyzer. Catalysts were heated to 473K at a rate of 10K/min in 10% H₂/ Ar and held at 473K for 1 hr. Samples were then purged with argon for 30 min at 473K before cooling to 313K, for Pt, or heated at 10K/min to 523K for Ru. A 10% O₂/Ar mixture was then flowed over the catalyst for 30 min to saturate the surface with chemisorbed oxygen before purging in argon for 10 min to remove residual gas phase O₂. The catalysts were then dosed with a known volume (0.518 cm³) of 10% H₂/Ar until all oxygen on the Pt surface had been removed as water and replaced by chemisorbed hydrogen. Hydrogen consumption was quantitatively determined with a high sensitivity thermal conductivity detector downstream from the sample cell. Fractional coverage $\theta_{(Au)}$ of Au on Pt was determined by the difference of H₂ uptake, used for dispersion calculation, for the monometallic Pt catalyst with that for the Pt@Au or Ru@Au samples, since Au is not active for either O₂ or H₂ chemisorption at 313K. Reduction in dispersion was attributed to the coverage of Pt or Ru surface atoms by gold atoms [138].

STEM and EDXS analysis was performed using a JEM-ARM200CF that was used for images as well as elemental mapping of selected fresh and spent catalyst samples. The JEM-ARM200CF is a probe aberration corrected 200kV TEM with a cold field emission source and a 0.35 eV resolution. The microscope is also equipped with an Oxford X-max 80 SDD X-ray detector with a probe size of 1 angstrom and a current of 14 Pa, 20 μ . A resolution of 256-pixels and the dwell time is in microseconds; most maps are collected within 5 minutes to ensure the core shell structure remained intact.

4.3 Results and Discussion

Preparation and evaluation of monometallic catalysts

The metal uptake of Au(en)₂, PTA, and RuHA over carbon as a function of final pH is plotted in Figure 4.1. Typical volcano shaped curves were observed, which is an indication of electrostatic adsorption of the metal complexes on the support surface [4, 31, 32]. Maximum uptake of metal occurs at final pHs of 11 - 12 with an uptake of

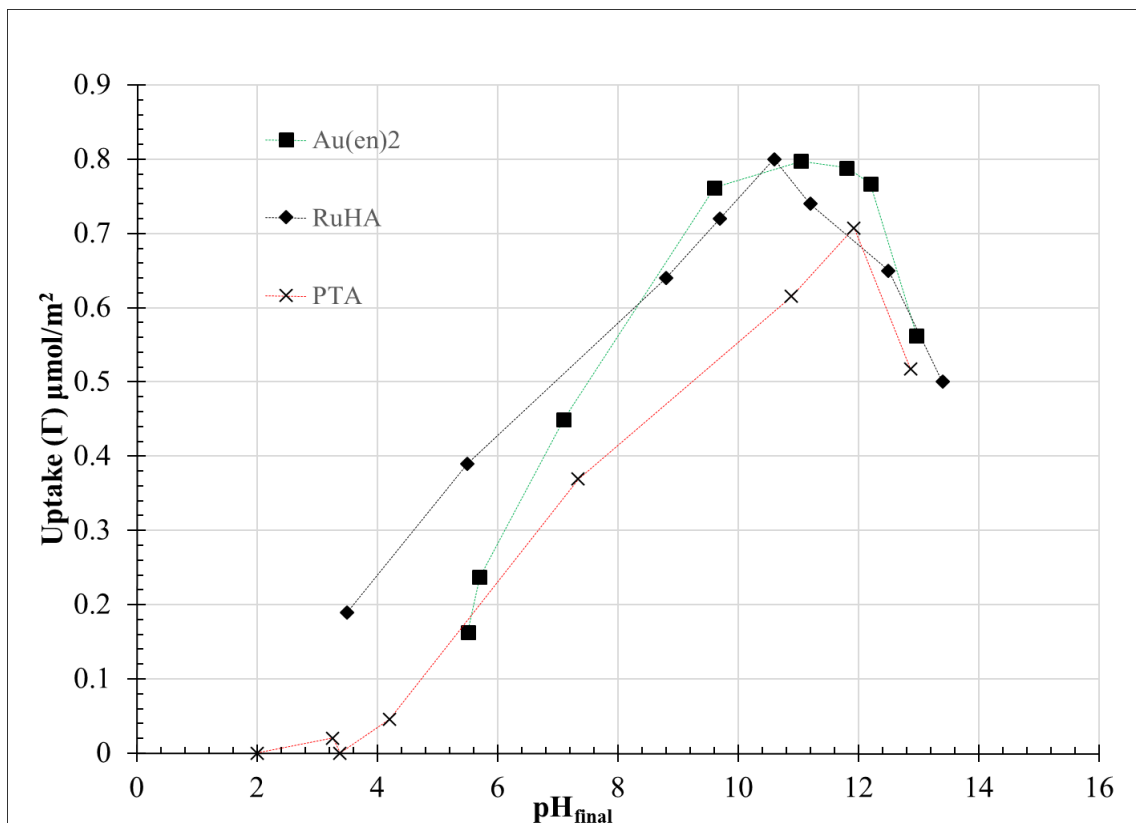


Figure 4.1 Uptake of Au Pt, and Ru over 1000 m²/L carbon as a function of the final pH of the adsorption solution

0.79 μmol/m² for gold, 0.82 μmol/m² for ruthenium, and 0.71 μmol/m² for platinum. Metal adsorption decreased at higher pH as the increase in ionic strength of the adsorption solution reduces the adsorption equilibrium constant due to double layer screening [34]. At low pH values near the PZC of the carbon support little uptake is also

low, as the surface charge is small; the charge difference between the metal complex and support surface is the driving force for electrostatic adsorption [32, 118].

Larger batches of single metal Au, Ru, and Pt catalysts were synthesized at the optimal pHs of 11.8, 10.5 and 12.0 respectively. The XRD characterization of these catalysts is shown in Figure 4.2a. The absence of fcc peaks for Ru indicates its very small size, which is below the approximately 1.5 nm limit of detection of the diffractometer. In the case of Pt, very broad fcc peaks can be observed; these were carefully deconvoluted from the background [137] and their average size is determined to be 1.8 nm. Small particle size of both metals is further confirmed by STEM images of the fresh single metal catalysts, shown in Figure 4.3. Not only are the metal particles small, each sample contains a significant fraction of isolated atoms.

The stability of these three catalysts to high (reaction) temperature HCl was examined next. To test particle growth as a function of time in anhydrous HCl, samples were dried at 180°C for 1 hour in 10 SCCM He to remove water and then subjected to a 1:1 ratio of HCl:He at 10 SCCM and 180°C for 15 hours. The system was thereafter purged with nitrogen and cooled to room temperature and the catalysts were removed for XRD analysis. These XRD results are shown in Figure 4.2b, and the size estimates summarized in Table 4.1. The Pt/C sample showed no detectable peak sharpening; the peak breadth again indicated an average particle size of 1.7 nm. The Ru/C sample showed only a trace (unquantifiable) amount of peak sharpening after the HCl exposure. As reported previously [129], Au sintered significantly after just 5 minutes of HCl exposure and not much more after an additional 100 hours (Table 4.1). This is also shown in the micrograph of the aged Au sample of Figure 4.3 and was agreement with XRD analysis.

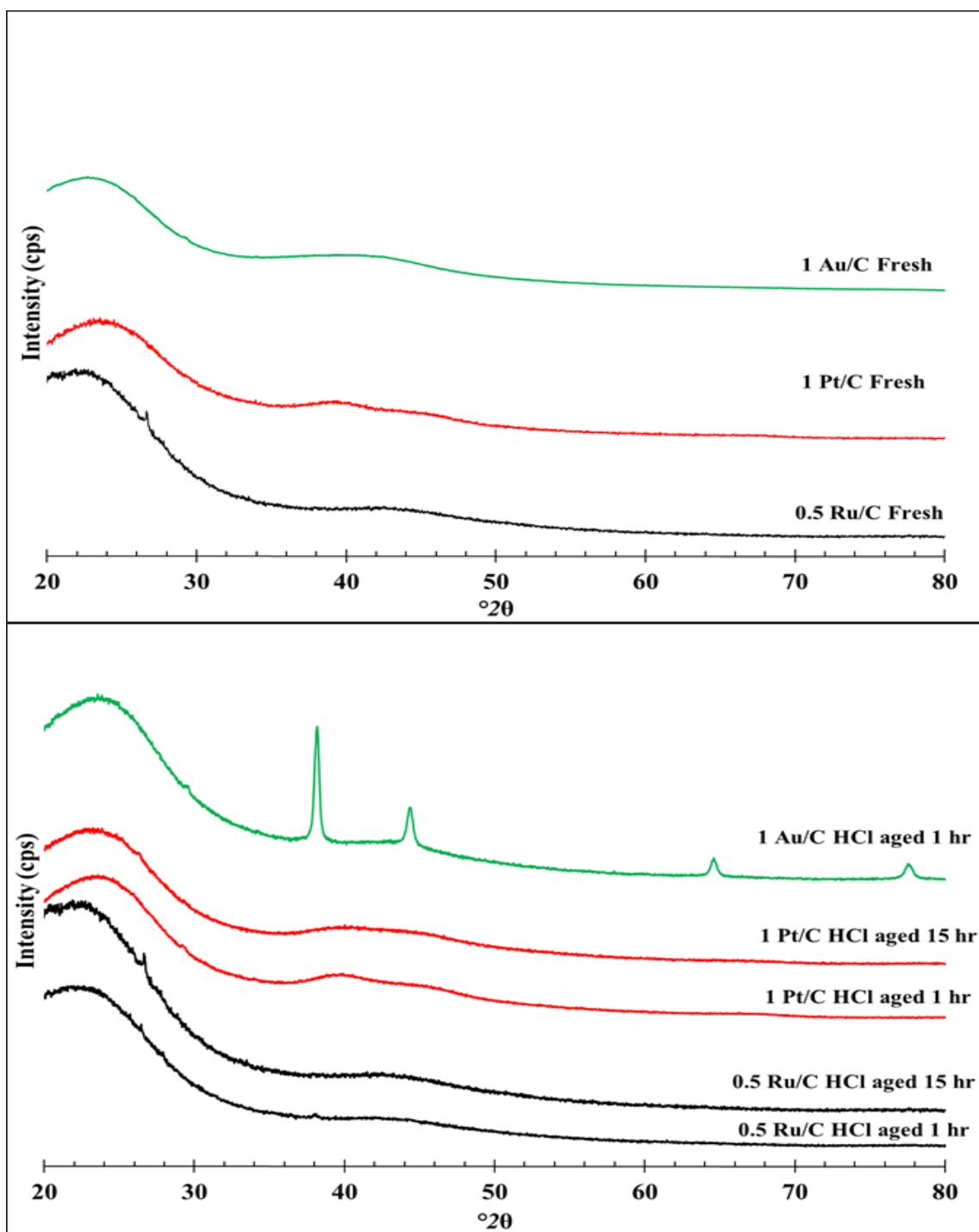


Figure 4.2 XRD patterns for all freshly prepared SEA catalysts after reduction(top) and XRD pattern of HCl aged catalysts at 180°C for 60 minutes and 15 hours at 1:1 HCl:He at 10 SCCM after drying at 180°C in flowing He for 60 minutes

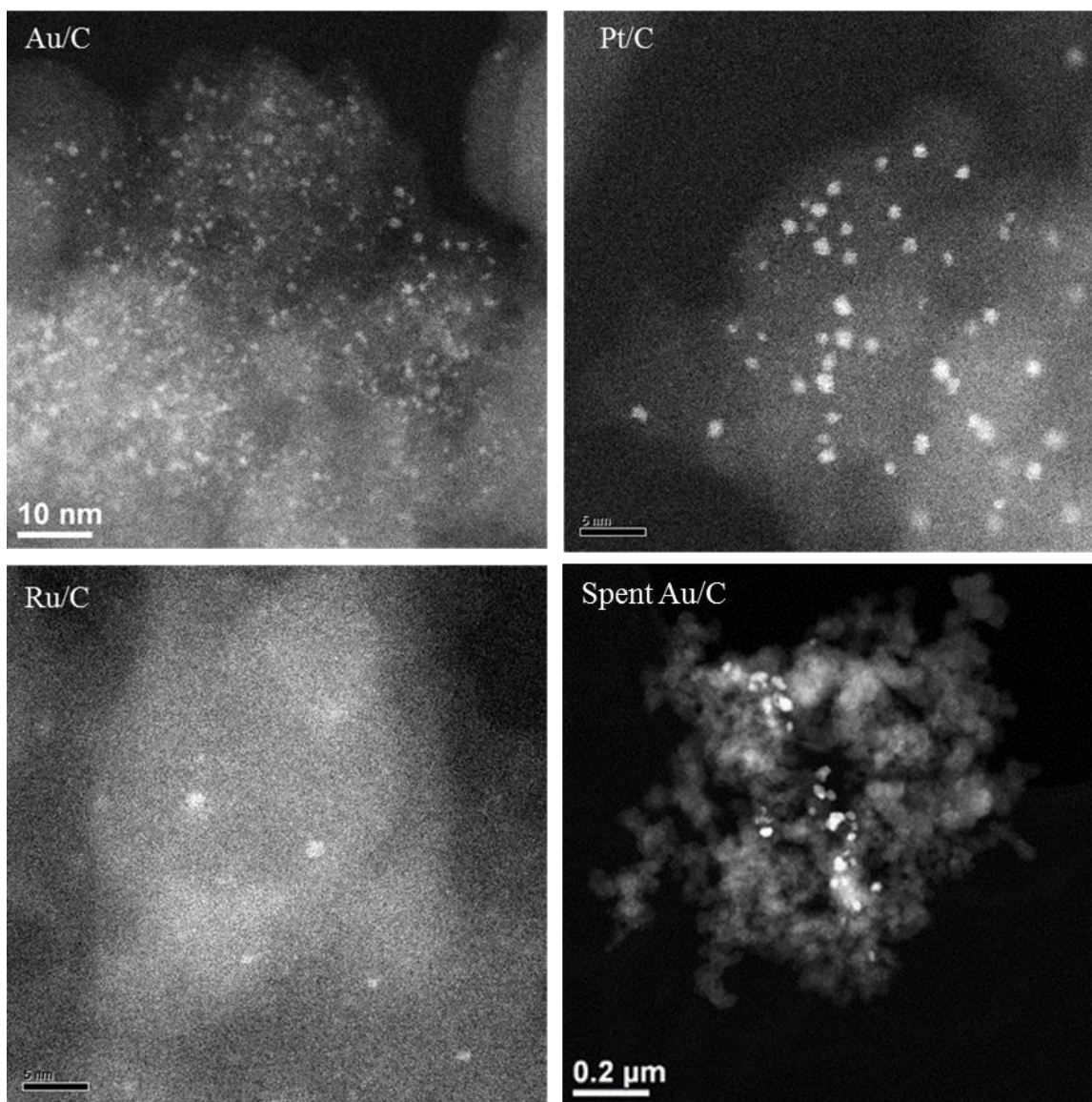


Figure 4.3 STEM of Fresh Au, Ru and Pt/C and a spent Au/C catalyst

An additional test run for the Au sample was to treat it in the inert carrier gas for one hour at 180°C; in this case (Figure 4.2) the gold nanoparticles did not sinter. Thus, it is the chemical environment and not the temperature causes gold to sinter. In the same environment, Ru and Pt are virtually impervious to sintering.

Table 4.1 Summary of metal particle size as a function of time in HCl for Au/C, Pt/C and Ru/C [129]

Catalyst	Particle size at 0 min (nm)	Time under HCl flow (min)	Final particle size(nm)
1 wt. % Au/C	<1.5	5	20.6
1 wt. % Au/C	<1.5	15	18.8
1 wt. % Au/C	<1.5	45	20.4
1 wt. % Au/C	<1.5	60	20.7
1 wt. % Au/C	<1.5	1200	19.5
1 wt. % Au/C	<1.5	6000	22.2
0.5 wt. % Ru/C	<1.5	60	<1.5
0.5 wt. % Ru/C	<1.5	900	<1.5
1 wt. % Pt/C	1.8	60	1.7
1 wt. % Pt/C	1.8	900	<1.5

Acetylene hydrochlorination activity of the monometallic catalysts is shown in Figure 4.4. The monometallic gold catalyst had the highest initial conversion of acetylene at 64%, which decayed to 44% after 15 hours of reaction time. These conversions were higher than the previous paper [129] since the space velocity is lower (4000 h^{-1} versus 4500 h^{-1} previously). The Pt/C and Ru/C catalysts prepared via SEA showed very little activity for conversion to VCM with a maximum conversion of acetylene that was less than 6 % for Pt/C and 4% for Ru/C.

The stability of each catalyst is inversely proportional to its activity; the post-reaction XRD patterns in Figure 4.2 reveal that while the Au catalyst sintered significantly over the 15 hours of reaction, the Ru and Pt catalysts were completely stable. This results is analogous to the support effect we reported previously [129]: Au supported on oxides (silica and titania) was not active and did not sinter. Coke buildup

on Pt and Ru was indicated by non-closure of the carbon balance predominantly at the beginning of each run (the carbon balance for Au was always very close to 100%). Platinum catalysts have also been cited as inactive for acetylene hydrochlorination due to the rapid deactivation due to the +4 oxidation state of Pt which is unlikely to form complexes with alkynes [139]. The Ru monometallic sample also had lower conversion than expected from the correlation of activity with electrode potentials [61]. A much lower space velocity of 180 hr^{-1} was used in that study (versus 4000 hr^{-1} employed here), and the different carbon support may have had a role in the production of more coke in the present study. RuO_2 has been reported to be the active site and no oxide species were observed in Figure 4.2 [74, 75].

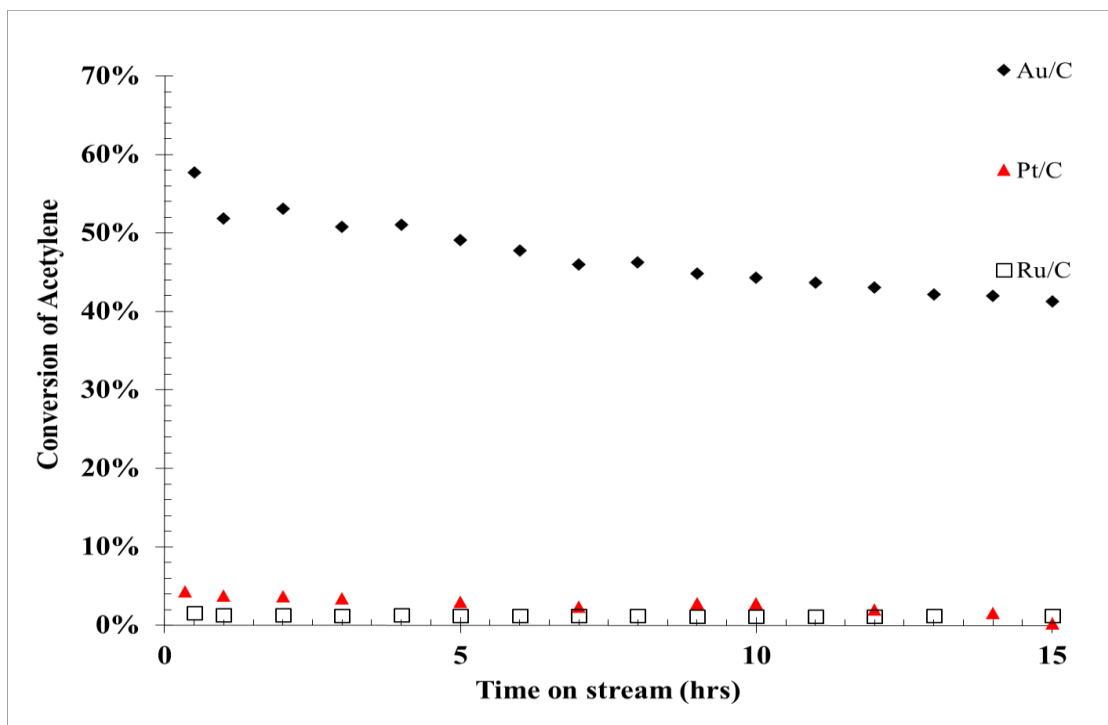


Figure 4.4 Conversion of Acetylene to VCM over monometallic carbon supported catalysts prepared via SEA at standard conditions, with a GHSV of 4000 hr^{-1}

Preparation and Evaluation of Core Shell Bimetallic Catalysts

Bimetallic catalysts were prepared using ED to deposit a thin shell of Au onto the core metal. Potassium dicyanoaurate, $\text{KAu}(\text{CN})_2$ was used in all cases as the gold metal salt for deposition onto the highly dispersed core metals, either Pt or Ru, at theoretical coverages of 1 and 2 monolayers. This corresponds to 0.5 and 1.0 weight percent gold for each sample. These values were chosen to ensure the gold loading was similar to other reactivity studies [61].

Electroless deposition of Au onto the metal cores was conducted in a developer bath at pH 10 using hydrazine as the reducing agent, at a 10:1 ratio of hydrazine to gold, and Au concentration was tracked over 180 minutes using AAS to ensure complete gold deposition. Figure 4.5a presents plots of the metal concentration of gold over time for the deposition of Au onto Pt at 1 and 2 theoretical monolayers. A control experiment with no reducing agent was performed to ensure there is no electrostatic adsorption of Au on the support; in the absence of the reducing agent no metal deposition occurred. For Au deposition, hydrazine was initially injected into with the pH adjusted Au solution and the core metal-containing catalyst was added only after 30 minutes, during which time the Au concentration remained constant and so demonstrated to be thermodynamically stable.

Employing initial Au concentrations of 13 and 25 ppm, the deposition of 1 and 2 theoretical monolayers of Au on Pt/C was complete within 70 and 120 minutes respectively. The rapid deposition of Au occurred quickly and completely in both cases without the need for an additional aliquot of reducing agent, as is sometimes required [refs]. As the control run with carbon and no substrate metal demonstrated that

electrostatic adsorption of the gold onto the carbon did not occur, the gold must have been deposited catalytically onto the Pt cores (or autocatalytically onto the Au depositing onto the Pt cores). Weight loadings for the samples were calculated to be 0.47 weight percent Au for the 1ML case and 0.95 weight percent for the 2ML preparation.

Figure 4.5b illustrates the deposition of 1 and 2 theoretical monolayers of Au onto the 0.5 wt% Ru/C. Deposition of Au occurred more slowly for both cases of Ru@Au/C than occurred over Pt, requiring 180 minutes for both loadings (the 1 ML or 0.51 wt% Au and the 2 ML, 1.02 wt% Au). No additional hydrazine was needed in these baths. The initial 30 minutes prior to the addition of the core metal catalysts again demonstrated that the KAu(CN)_2 salt was thermodynamically stable at the concentrations used in this bath, with a maximum concentration of 35 ppm. Deposition over either core metals may be slow due to the high formation constant of the cyanide-gold metal salt. In order to increase the rate of deposition the bath temperature may be increased, or additional aliquots of reducing agent may be added to the system during deposition [48].

The Pt@Au/C and Ru@Au/C catalysts were first characterized with chemisorption as a diagnostic of the Au coverage of core metal sites; these results are presented in Table 4.2. Au coverages were determined by the decrease in total hydrogen uptake compared to the monometallic catalysts as Au is inactive for hydrogen titration of O-precovered sites at these conditions. The reduction in Pt and Ru surface sites after the deposition of Au on the surface further indicated the gold was selectively deposited with a core@shell structure. The platinum catalyst of 1 weight percent and the 0.5 weight percent ruthenium catalysts resulted in coverages of 0.55 and 0.25 monolayers of base metal coverage after deposition of one theoretical monolayer.

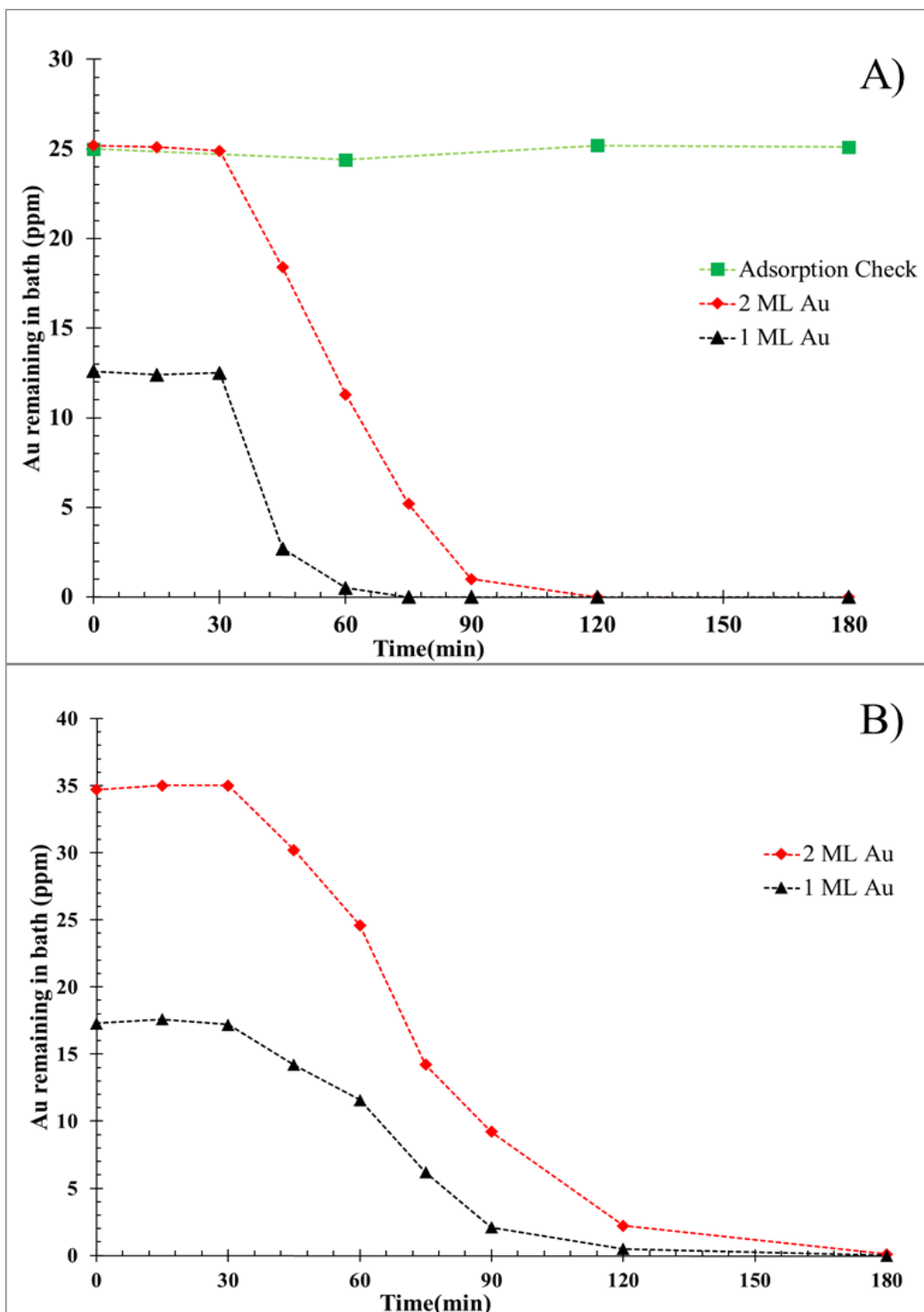


Figure 4.5 Concentration of Au remaining in the developer bath over time for the deposition of 1 and 2 monolayers of Au onto a) 1 wt. % Pt/C, b) 0.5 wt% Ru/C

The deposition of 2 theoretical monolayers corresponded to 0.85 and 0.53 actual monolayers of coverage for Pt and Ru samples. Au coverage less than theoretical indicates an appreciable amount of autocatalytic deposition of gold onto other gold. Autocatalytic deposition was also found in previous studies for the deposition of gold [45, 51].

Table 4.2 Summary of fractional coverage determined via chemisorption for the Pt@Au and Ru@Au bimetallic samples

Theoretical coverage (ML)	Hydrogen Uptake(cm³/g)	Fractional coverage	Total Au (wt. %)
0 (1% Pt/C)	0.485	0	0
1	0.217	0.55	0.47
2	0.073	0.85	0.95
2-Post	.020	0.96	
0 (0.5% Ru/C)	6.48	0	0
1	3.04	0.25	0.51
2	2.72	0.53	1.02
2-Post	0.164	0.94	

Au did not, however, auto-deposit to a significant extent, as the XRD profiles of the fresh core-shell catalysts given in Figure 4.6 showed no evidence of metallic gold. In fact, the patterns of the 1 and 2 ML Au on Ru and Pt core catalysts in Figure 4.6 appear identical to the single metal diffraction profiles of the fresh catalysts seen in Figure 4.2.

The catalytic activity of the core-shell catalysts is shown in Figure 4.7. Samples prepared with 1 and 2 monolayers of theoretical coverage of Au onto either Pt or Ru, prepared via ED, exhibited increased conversion of C₂H₂ to VCM when compared to the monometallic Pt or Ru catalysts, but lower activity than monometallic Au (Figure 4.5). In the case of Pt@Au/C, the 1ML sample had a maximum conversion of 18% while the 2ML maximum was 24% conversion of acetylene. The deactivation rate and the percent of initial activity lost (25 and 27% for the 1 and 2 ML catalysts, respectively) of these catalysts was the lowest of all catalysts tested.

The Ru@Au/C 1 and 2 ML catalysts exhibited higher initial activity, with maximum conversions of 38-40% for both samples, than the corresponding Pt@Au catalysts, but deactivated faster with a higher percentage of initial activity lost (about half) than either the Pt@Au catalysts or even the monometallic Au catalyst (29% loss in initial activity, Figure 4.4). Selectivity for both bimetallic systems was still high (> 99%). As with the monometallic Ru and Pt catalysts, coke formation was again suggested from the inability to close the initial carbon balance.

Insight into the deactivation mechanisms is found in post-reaction characterization. First, in the post-reaction XRD characterization in Figure 4.6, fcc Au peaks are absent, unlike the post-reaction monometallic Au sample in Figure 4.2 which exhibit very sharp Au peaks corresponding to particles of 20 nm average size. The absence of Au peaks in the post-reaction core-shell nanoparticles in Figure 4.6 reveals the striking stability of the Au in these catalysts, even at 1:1 atomic ratios with the core metals; the high surface free energy cores of Ru and Pt appeared to completely anchor the Au to sintering in the reactive HCl environment.

The reactivity of Au catalysts for acetylene hydrochlorination is clearly not a function of exposed metallic Au, as the area of metallic Au in well dispersed shells on the Ru and Pt catalysts is perhaps twenty times as high as the Au surface in the 20 nm, but relatively active, monometallic Au particles. Consensus in the literature is that activity depends on the amount of Au³⁺ present [83, 113, 139] and more recently it has been postulated that only Au³⁺ in the proximity of the carbon surface is active [63-65, 113].

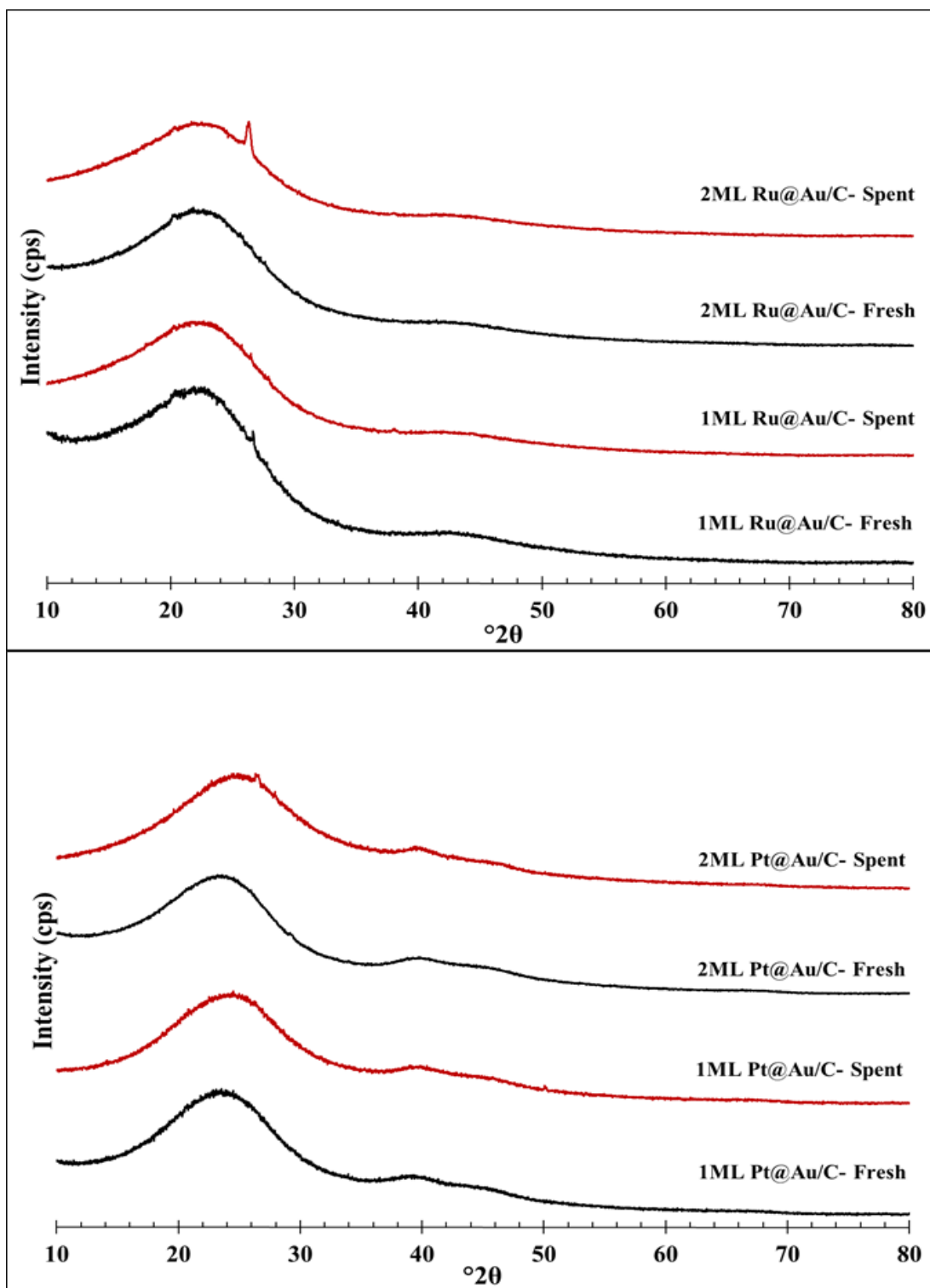


Figure 4.6 XRD pattern for Ru@Au/C and for Pt@Au/C fresh and spent catalysts 15 hours TOL

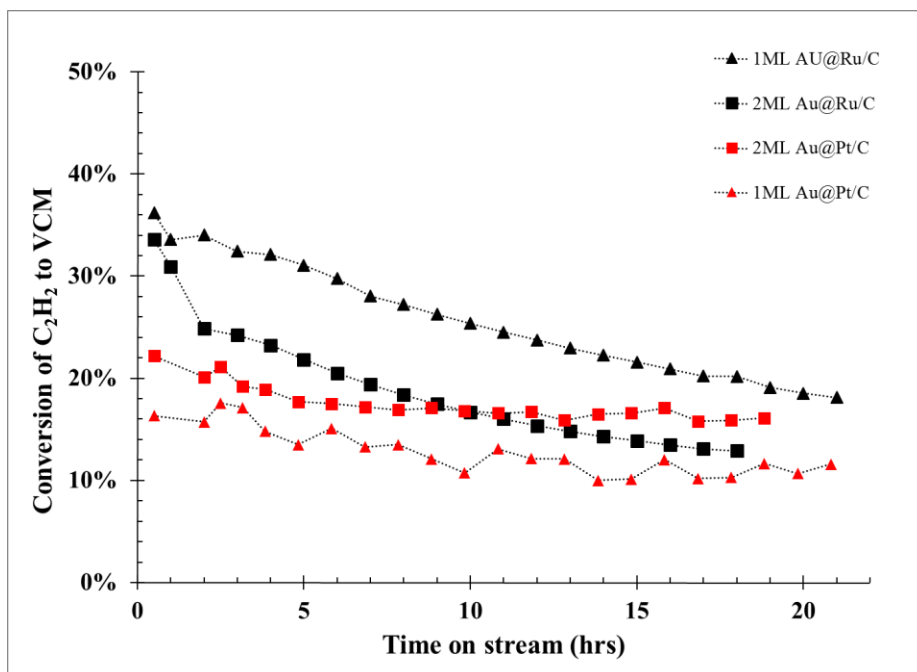


Figure 4.7 Conversion of acetylene to VCM using Ru@Au/C (Black) and Pt@Au/C (red). GHSV of 4000 hr⁻¹

In our previous work we postulated this active species to be volatile Au₂Cl₆ dimers, with oxidized carbon having the optimal strength of interaction with this species to permit its reactivity while preventing its sintering. It would appear that the association of Au with cores of Ru and Pt significantly deter the formation of this active species. Decreased amounts of Au³⁺ may be due to Pt or Ru spillover-assisted reduction of the AuCl₃ active sites to Au⁰ that has occurred with catalysts prepared via mixed impregnation, as previously demonstrated in literature via XPS study [61, 140]. Or, in its placement as a shell on a core metal, the Au species may be too far from the carbon surface for adequate interaction.

On the other hand, the stabilization of Au in a harsh chemical environment has been demonstrated. Any reaction, such as low temperature CO oxidation or water-gas shift [91, 141, 142], which depends on a metallic Au surface, would benefit from the

dramatically higher Au area available in the high surface free energy core-anchored Au shells.

Further insight into the acetylene hydrochlorination deactivation mechanism might be gained from the post-reaction chemisorption results (Table 4.2) which reveal significantly heightened blockage of Pt and Ru in the used catalysts. The post reaction coverage of the 2 ML samples increased to 0.94 and 0.96 monolayers, from pre-reaction values of .85 and .53 monolayers. This decrease can be explained by one of two causes; the spreading of autocatalytically-deposited Au during the reaction or Pt or Ru site blockage by coke as acetylene may interact strongly with the exposed Ru and Pt atoms and this oligomerization may block active Au sites [143, 144].

A final set of characterization was made with STEM imaging and mapping. Images of the fresh and post-reaction Ru@ 2 ML Au and the post-reaction Pt@ 2 ML Au catalysts are given in Figure 4.8. Comparison of the pre- and post-reaction images of the Ru@Au catalyst indicates not only no significant sintering, but also the presence of atomically distributed metals. The post-reaction Pt@Au catalyst also remains well dispersed, and especially with this sample, in which both metals are high Z, the presence of atomically distributed metal pairs are observed. The atomic dispersion of the monometallic samples (Figure 4.4) appears to have been substantially retained during ED, and it is speculated that the metal pairs are actually bimetallic. The presence of such sites can explain the inactivity of these catalysts as Au stabilized in this form would prevent the formation the active Au_2Cl_6 dimer.

Unfortunately, the spatial resolution of x-ray mapping is insufficient to identify individual atoms. The Au and Pt x-ray maps of small post-reaction Pt@Au nanoparticles

(Figure 4.8a) are consistent with Au shells on Pt cores, while the Ru and Au in the Ru@Au sample are too highly dispersed for strong enough signals to confirm co-location. Atom pairs are also seen clearly for the Pt@Au sample in Figure 4.9. The presence of bimetallic atom pairs, achievable by an initial deposition of atoms of Pt or Ru by SEA followed by ED of Au onto the metal, is particularly striking from a scientific point of view. Characterization with EXAFS is being planned to confirm the existence of such sites.

4.4 Conclusion

The coupling of SEA with ED gives an unprecedented degree of control for both particle dispersion and morphology of core-shell particles. Gold particles which sinter heavily under reaction conditions for the synthesis of vinyl chloride monomer, were stabilized via anchoring onto high surface free energy metal cores. These metal cores, prepared via SEA, can be synthesized with a high degree of dispersion, monodispersity, and shell composition. The 1 and 2 monolayer gold catalysts gave increased activity when compared to the Ru and Pt monometallic samples, but lower conversion compared to the Au/C monometallic sample. This may be due to reduction of the Au^{3+} by the substrate metal, removal of the Au shell from the necessary proximity of the surface, or the formation of metal atom pairs that are inactive for this reaction. All gold containing samples gave similar trends for long term deactivation an indication of the loss of the Au^{3+} surface species, regardless of increased gold surface area. The increased surface area for small particles in this study is up to two orders of magnitude larger than compared to 20 nm sintered particles studied previously, while the activity remained depressed due to either Ru and Pt assisted reduction or coking.

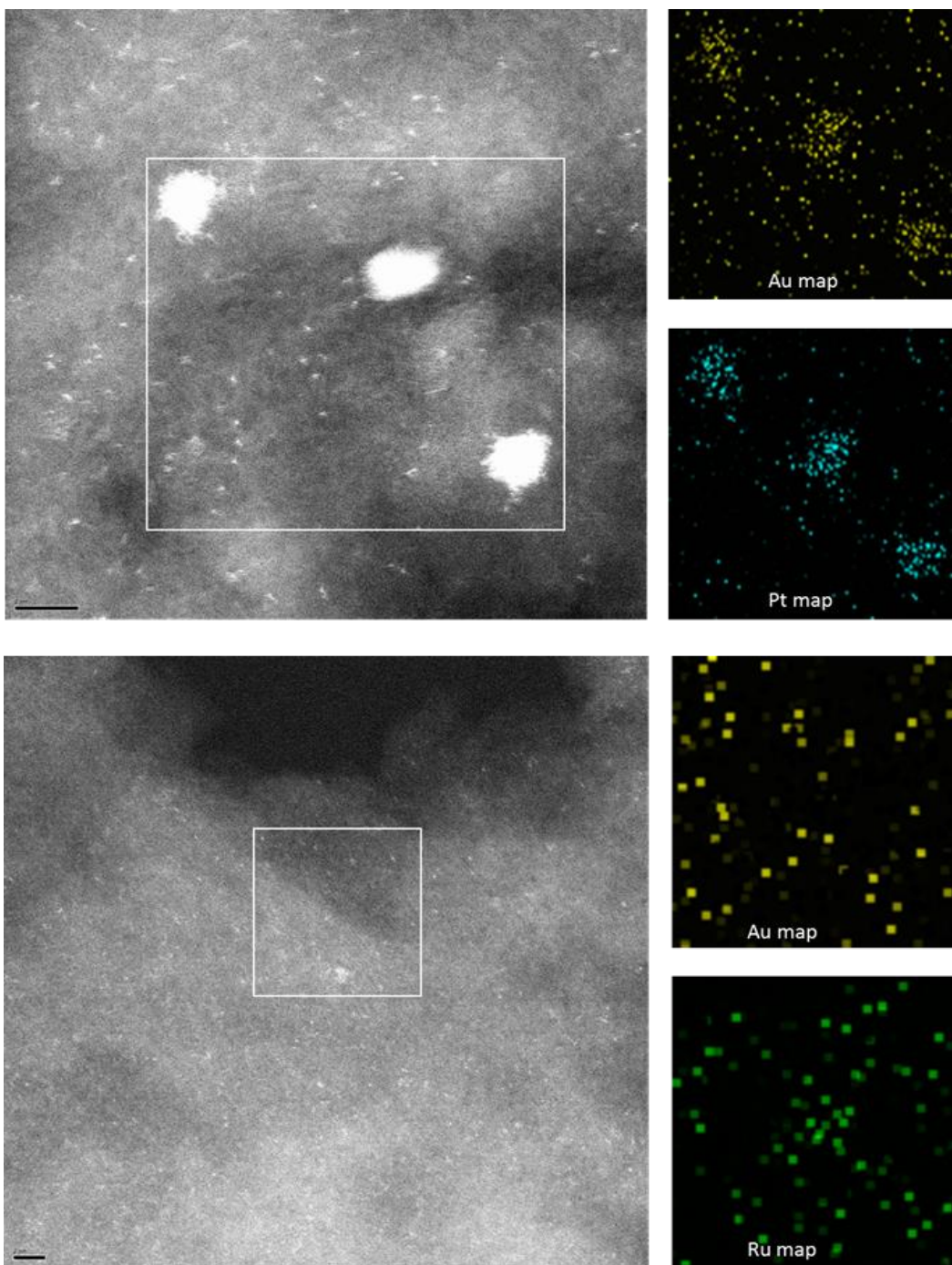


Figure 4.8 STEM images of 2ML Au over Pt (top) and Ru (bottom) after reaction. Scale bars are 2nm. EDXS maps of Au and either Pt or Ru particles for each image

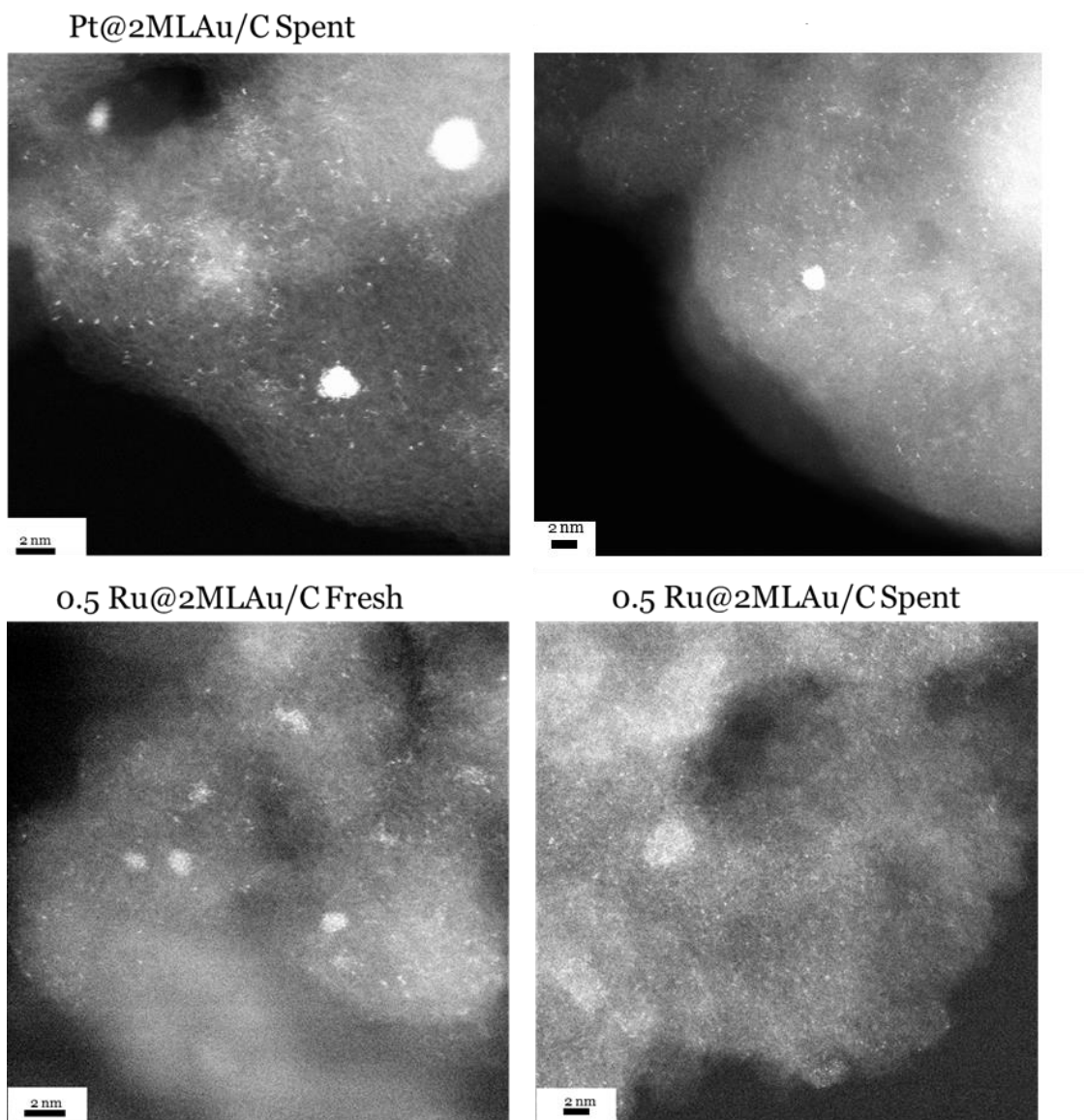


Figure 4.9 STEM images of the Spent Pt@2MLAu samples (a and b) and fresh (c) and spent (d) 0.5Ru@2MLAu samples

The ability to stabilize gold surfaces in harsh chemical environments allows further research to determine the effect of particle size on core@shell bimetallics for this reaction and others where particle sintering is a concern, such as the water-gas shift or low temperature CO oxidation. Coupling rational catalyst synthesis methods allows for the design of a stable gold bimetallic catalyst, although the particle size remained stable

there is still long term deactivation of the active species on the surface. This paves the way for the study of the addition of materials to retard gold reduction on particles that have a small stable particle size have synergistic effects for acetylene hydrochlorination. Further work is required to explore the effect of metal core size and gold shell thickness on activity for this reaction, including particle stability. The atomic dispersion of Au on either Pt and Ru on the surface, from STEM, and small particle size from XRD analysis (< 1.5 nm) lends support to the idea of a size effect for gold clusters in this reaction. Particles that are atomically dispersed either as monometallic gold or as bimetallic clusters may not be active for this reaction when compared to larger particles that are larger than 2 nm and smaller than aggregated 20 nm particles.

REFERENCES

- [1] F. Cavani, F. Trifiró, Classification of industrial catalysts and catalysis for the petrochemical industry, *Catalysis today*, 34 (1997) 269-279.
- [2] J. Hagen, *Industrial catalysis: a practical approach*, John Wiley & Sons, 2006.
- [3] J.T. Wroblewski, M. Boudart, Preparation of solid catalysts: an appraisal, *Catalysis today*, 15 (1992) 349-360.
- [4] J. Regalbuto, *Catalyst preparation: science and engineering*, CRC Press, 2006.
- [5] K.P. de Jong, *Synthesis of solid catalysts*, John Wiley & Sons, 2009.
- [6] A. Lekhal, B.J. Glasser, J.G. Khinast, Impact of drying on the catalyst profile in supported impregnation catalysts, *Chemical Engineering Science*, 56 (2001) 4473-4487.
- [7] J.A. Moulijn, P.W. van Leeuwen, R.A. van Santen, *Catalysis: an integrated approach to homogeneous, heterogeneous and industrial catalysis*, Elsevier, 1993.
- [8] J.A. Schwarz, C. Contescu, A. Contescu, Methods for preparation of catalytic materials, *Chemical Reviews*, 95 (1995) 477-510.
- [9] L. Hermans, J. Geus, Interaction of nickel ions with silica supports during deposition-precipitation, *Studies in Surface Science and Catalysis*, 3 (1979) 113-130.
- [10] R. Zanella, S. Giorgio, C.R. Henry, C. Louis, Alternative methods for the preparation of gold nanoparticles supported on TiO₂, *The Journal of Physical Chemistry B*, 106 (2002) 7634-7642.
- [11] K.P. de Jong, Synthesis of supported catalysts, *Current Opinion in Solid State and Materials Science*, 4 (1999) 55-62.
- [12] P. Burattin, M. Che, C. Louis, Characterization of the Ni (II) phase formed on silica upon deposition-precipitation, *The Journal of Physical Chemistry B*, 101 (1997) 7060-7074.
- [13] G.C. Bond, C. Louis, D. Thompson, *Catalysis by gold* (Catalytic Science Series, vol. 6), Ed. GJ Hutchings, Imperial College Press, London, (2006).

- [14] R. Zanella, C. Louis, S. Giorgio, R. Touroude, Crotonaldehyde hydrogenation by gold supported on TiO₂: structure sensitivity and mechanism, *Journal of Catalysis*, 223 (2004) 328-339.
- [15] G.L. Bezemer, P. Radstake, V. Koot, A. Van Dillen, J. Geus, K. De Jong, Preparation of Fischer–Tropsch cobalt catalysts supported on carbon nanofibers and silica using homogeneous deposition-precipitation, *Journal of catalysis*, 237 (2006) 291-302.
- [16] K. Qian, J. Fang, W. Huang, B. He, Z. Jiang, Y. Ma, S. Wei, Understanding the deposition–precipitation process for the preparation of supported Au catalysts, *Journal of Molecular Catalysis A: Chemical*, 320 (2010) 97-105.
- [17] M.K. van der Lee, J. van Dillen, J.H. Bitter, K.P. de Jong, Deposition precipitation for the preparation of carbon nanofiber supported nickel catalysts, *Journal of the American Chemical Society*, 127 (2005) 13573-13582.
- [18] A. Sandoval, C. Louis, R. Zanella, Improved activity and stability in CO oxidation of bimetallic Au–Cu/TiO₂ catalysts prepared by deposition–precipitation with urea, *Applied Catalysis B: Environmental*, 140 (2013) 363-377.
- [19] A. Sandoval, A. Aguilar, C. Louis, A. Traverse, R. Zanella, Bimetallic Au–Ag/TiO₂ catalyst prepared by deposition–precipitation: high activity and stability in CO oxidation, *Journal of Catalysis*, 281 (2011) 40-49.
- [20] M.E. Dry, The Fischer–Tropsch process: 1950–2000, *Catalysis today*, 71 (2002) 227-241.
- [21] J. Brunelle, Preparation of catalysts by metallic complex adsorption on mineral oxides, *Pure and Applied Chemistry*, 50 (1978) 1211-1229.
- [22] D.A. Sverjensky, Interpretation and prediction of triple-layer model capacitances and the structure of the oxide-electrolyte-water interface, *Geochimica et Cosmochimica Acta*, 65 (2001) 3643-3655.
- [23] D.A. Sverjensky, N. Sahai, Theoretical prediction of single-site enthalpies of surface protonation for oxides and silicates in water, *Geochimica et cosmochimica acta*, 62 (1998) 3703-3716.
- [24] D.A. Sverjensky, N. Sahai, Theoretical prediction of single-site surface-protonation equilibrium constants for oxides and silicates in water, *Geochimica et Cosmochimica Acta*, 60 (1996) 3773-3797.
- [25] D.A. Sverjensky, Zero-point-of-charge prediction from crystal chemistry and solvation theory, *Geochimica et Cosmochimica Acta*, 58 (1994) 3123-3129.
- [26] L.R. Radovic, *Chemistry and physics of carbon: a series of advances*, Marcel Dekker, Incorporated, 2001.

- [27] J. Solar, F. Derbyshire, V. De Beer, L. Radovic, Effects of surface and structural properties of carbons on the behavior of carbon-supported molybdenum catalysts, *Journal of Catalysis*, 129 (1991) 330-342.
- [28] J. Solar, C.L. y Leon, K. Osseo-Asare, L. Radovic, On the importance of the electrokinetic properties of carbons for their use as catalyst supports, *Carbon*, 28 (1990) 369-375.
- [29] F. Rodríguez-Reinoso, The role of carbon materials in heterogeneous catalysis, *Carbon*, 36 (1998) 159-175.
- [30] J.R. Regalbuto, A scientific method to prepare supported metal catalysts, *Surface and Nanomolecular Catalysis*, (2006) 161-194.
- [31] K.B. Agashe, J.R. Regalbuto, A revised physical theory for adsorption of metal complexes at oxide surfaces, *Journal of colloid and interface science*, 185 (1997) 174-189.
- [32] N. Santhanam, T.A. Conforti, W. Spieker, J.R. Regalbuto, Nature of metal catalyst precursors adsorbed onto oxide supports, *Catalysis Today*, 21 (1994) 141-156.
- [33] J. Park, J.R. Regalbuto, A simple, accurate determination of oxide PZC and the strong buffering effect of oxide surfaces at incipient wetness, *Journal of colloid and interface science*, 175 (1995) 239-252.
- [34] X. Hao, S. Barnes, J.R. Regalbuto, A fundamental study of Pt impregnation of carbon: Adsorption equilibrium and particle synthesis, *Journal of Catalysis*, 279 (2011) 48-65.
- [35] J.R. Regalbuto, 13. Strong Electrostatic Adsorption of Metals onto Catalyst Supports, Taylor and Francis/CRC, 2007.
- [36] W. Sachtler, Surface composition of alloys, *Applications of Surface Science*, 19 (1984) 167-180.
- [37] H. CHO, The Rational Synthesis of Supported Noble Single Or Bimetallic Catalysts by Electrostatic Adsorption, (2013).
- [38] T.E. Feltes, L. Espinosa-Alonso, E. de Smit, L. D'Souza, R.J. Meyer, B.M. Weckhuysen, J.R. Regalbuto, Selective adsorption of manganese onto cobalt for optimized Mn/Co/TiO₂ Fischer–Tropsch catalysts, *Journal of Catalysis*, 270 (2010) 95-102.
- [39] M. Heise, J. Schwarz, Preparation of metal distributions within catalyst supports. I. Effect of pH on catalytic metal profiles, *Journal of colloid and interface science*, 107 (1985) 237-243.

- [40] M. Heise, J. Schwarz, Preparation of metal distributions within catalyst supports: II. Effect of ionic strength on catalytic metal profiles, *Journal of colloid and interface science*, 113 (1986) 55-61.
- [41] J. Schwarz, M. Heise, Preparation of metal distributions within catalyst supports: IV. Multicomponent effects, *Journal of Colloid and Interface Science*, 135 (1990) 461-467.
- [42] G.O. Mallory, J.B. Hajdu, *Electroless plating: fundamentals and applications*, William Andrew, 1990.
- [43] K. Beard, D. Borrelli, A.M. Cramer, D. Blom, J. Van Zee, J.R. Monnier, Preparation and structural analysis of carbon-supported Co core/Pt shell electrocatalysts using electroless deposition methods, *ACS nano*, 3 (2009) 2841-2853.
- [44] K.D. Beard, J. Van Zee, J.R. Monnier, Preparation of carbon-supported Pt-Pd electrocatalysts with improved physical properties using electroless deposition methods, *Applied Catalysis B: Environmental*, 88 (2009) 185-193.
- [45] A.A. Rodriguez, C.T. Williams, J.R. Monnier, Selective liquid-phase oxidation of glycerol over Au-Pd/C bimetallic catalysts prepared by electroless deposition, *Applied Catalysis A: General*, 475 (2014) 161-168.
- [46] J. Rebelli, M. Detwiler, S. Ma, C.T. Williams, J.R. Monnier, Synthesis and characterization of Au-Pd/SiO₂ bimetallic catalysts prepared by electroless deposition, *Journal of Catalysis*, 270 (2010) 224-233.
- [47] M.T. Schaal, A.C. Pickerell, C.T. Williams, J.R. Monnier, Characterization and evaluation of Ag-Pt/SiO₂ catalysts prepared by electroless deposition, *Journal of Catalysis*, 254 (2008) 131-143.
- [48] Y. Zhang, W. Diao, J.R. Monnier, C.T. Williams, Pd-Ag/SiO₂ bimetallic catalysts prepared by galvanic displacement for selective hydrogenation of acetylene in excess ethylene, *Catalysis Science & Technology*, 5 (2015) 4123-4132.
- [49] W. Diao, J.M.M. Tengco, J.R. Regalbuto, J.R. Monnier, Preparation and Characterization of Pt-Ru Bimetallic Catalysts Synthesized by Electroless Deposition Methods, *ACS Catalysis*, 5 (2015) 5123-5134.
- [50] Y. Zhang, W. Diao, C.T. Williams, J.R. Monnier, Selective hydrogenation of acetylene in excess ethylene using Ag-and Au-Pd/SiO₂ bimetallic catalysts prepared by electroless deposition, *Applied Catalysis A: General*, 469 (2014) 419-426.
- [51] J. Rebelli, A.A. Rodriguez, S. Ma, C.T. Williams, J.R. Monnier, Preparation and characterization of silica-supported, group IB-Pd bimetallic catalysts prepared by electroless deposition methods, *Catalysis Today*, 160 (2011) 170-178.
- [52] S.S. Djokić, Electroless deposition of metals and alloys, in: *Modern aspects of electrochemistry*, Springer, 2002, pp. 51-133.

- [53] J. Rebelli, Preparation, Characterization, and Evaluation of Bimetallic Catalysts Prepared by Electroless Deposition Methods, in, UNIVERSITY OF SOUTH CAROLINA, 2011.
- [54] I. Ohno, O. Wakabayashi, S. Haruyama, Anodic oxidation of reductants in electroless plating, *Journal of The Electrochemical Society*, 132 (1985) 2323-2330.
- [55] Y. Saeki, T. Emura, Technical progresses for PVC production, *Progress in polymer science*, 27 (2002) 2055-2131.
- [56] Global demand for PVC to rise by about 3.2%/year to 2021, *Additives for Polymers*, 2014 (2014) 10-11.
- [57] J.G. Speight, *Chemical and process design handbook*, McGraw-Hill, (2002) 2.20-22.22.
- [58] J. Agnew, H. Shankar, Catalyst deactivation in acetylene hydrochlorination, *Industrial & engineering chemistry product research and development*, 25 (1986) 19-22.
- [59] H. Bremer, H. Lieske, Kinetics of the hydrochlorination of acetylene on HgCl_2 /active carbon catalysts, *Applied catalysis*, 18 (1985) 191-203.
- [60] G.J. Hutchings, Vapor phase hydrochlorination of acetylene: Correlation of catalytic activity of supported metal chloride catalysts, *Journal of Catalysis*, 96 (1985) 292-295.
- [61] M. Conte, A.F. Carley, G. Attard, A.A. Herzing, C.J. Kiely, G.J. Hutchings, Hydrochlorination of acetylene using supported bimetallic Au-based catalysts, *Journal of Catalysis*, 257 (2008) 190-198.
- [62] X. Zhang, H. Shi, B.-Q. Xu, Vital roles of hydroxyl groups and gold oxidation states in Au/ZrO_2 catalysts for 1, 3-butadiene hydrogenation, *Journal of Catalysis*, 279 (2011) 75-87.
- [63] B. Nkosi, M.D. Adams, N.J. Coville, G.J. Hutchings, Hydrochlorination of acetylene using carbon-supported gold catalysts: A study of catalyst reactivation, *Journal of Catalysis*, 128 (1991) 378-386.
- [64] B. Nkosi, N.J. Coville, G.J. Hutchings, M.D. Adams, J. Friedl, F.E. Wagner, Hydrochlorination of acetylene using gold catalysts: A study of catalyst deactivation, *Journal of Catalysis*, 128 (1991) 366-377.
- [65] M. Conte, C.J. Davies, D.J. Morgan, T.E. Davies, D.J. Elias, A.F. Carley, P. Johnston, G.J. Hutchings, Aqua regia activated Au/C catalysts for the hydrochlorination of acetylene, *Journal of Catalysis*, 297 (2013) 128-136.
- [66] G.J. Hutchings, Catalysis by gold, *Catalysis Today*, 100 (2005) 55-61.

- [67] G.J. Hutchings, Gold catalysis in chemical processing, *Catalysis today*, 72 (2002) 11-17.
- [68] S. Mitchenko, T. Krasnyakova, I. Zhikharev, Catalytic hydrochlorination of acetylene on mechanochemically-activated K_2PdCl_4 , *Theoretical and Experimental Chemistry*, 44 (2008) 316-319.
- [69] S. Wang, B. Shen, Q. Song, Kinetics of Acetylene Hydrochlorination over Bimetallic Au-Cu/C Catalyst, *Catalysis Letters*, 134 (2010) 102-109.
- [70] S.A. Mitchenko, T.V. Krasnyakova, R.S. Mitchenko, A.N. Korduban, Acetylene catalytic hydrochlorination over powder catalyst prepared by pre-milling of K_2PtCl_4 salt, *Journal of Molecular Catalysis a-Chemical*, 275 (2007) 101-108.
- [71] R.S. Mitchenko, A.A. Shubin, T.V. Krasnyakova, Mechanism of the catalytic action of the mechanoactivated salt K_2PtCl_4 in the gas-phase hydrochlorination of acetylene, *Theoretical and Experimental Chemistry*, 42 (2006) 314-319.
- [72] J. Ma, S. Wang, B. Shen, Study on the effects of acetylene on an Au-Cu/C catalyst for acetylene hydrochlorination using Monte Carlo and DFT methods, *Reac Kinet Mech Cat*, 110 (2013) 177-186.
- [73] G. Li, W. Li, H. Zhang, Y. Pu, M. Sun, J. Zhang, Non-mercury catalytic acetylene hydrochlorination over Ru catalysts enhanced by carbon nanotubes, *RSC Advances*, 5 (2015) 9002-9008.
- [74] Y. Pu, J. Zhang, L. Yu, Y. Jin, W. Li, Active ruthenium species in acetylene hydrochlorination, *Applied Catalysis A: General*, 488 (2014) 28-36.
- [75] J. Zhang, W. Sheng, C. Guo, W. Li, Acetylene hydrochlorination over bimetallic Ru-based catalysts, *RSC Advances*, 3 (2013) 21062-21068.
- [76] K. Zhou, J. Jia, X. Li, X. Pang, C. Li, J. Zhou, G. Luo, F. Wei, Continuous vinyl chloride monomer production by acetylene hydrochlorination on Hg-free bismuth catalyst: From lab-scale catalyst characterization, catalytic evaluation to a pilot-scale trial by circulating regeneration in coupled fluidized beds, *Fuel Processing Technology*, 108 (2013) 12-18.
- [77] B. Dai, K. Chen, Y. Wang, L. Kang, M. Zhu, Boron and nitrogen doping in graphene for the catalysis of acetylene hydrochlorination, *ACS Catalysis*, 5 (2015) 2541-2547.
- [78] X. Li, Y. Wang, L. Kang, M. Zhu, B. Dai, A novel, non-metallic graphitic carbon nitride catalyst for acetylene hydrochlorination, *Journal of Catalysis*, 311 (2014) 288-294.
- [79] G.J. Hutchings, Gold catalysis in chemical processing, *Catalysis Today*, 72 (2002) 11-17.

- [80] M. Conte, C.J. Davies, D.J. Morgan, T.E. Davies, A.F. Carley, P. Johnston, G.J. Hutchings, Modifications of the metal and support during the deactivation and regeneration of Au/C catalysts for the hydrochlorination of acetylene, *Catalysis Science & Technology*, 3 (2013) 128-134.
- [81] W. Wittanadecha, N. Laosiripojana, A. Ketcong, N. Ningnuek, P. Praserttham, J.R. Monnier, S. Assabumrungrat, Preparation of Au/C catalysts using microwave-assisted and ultrasonic-assisted methods for acetylene hydrochlorination, *Applied Catalysis A: General*, 475 (2014) 292-296.
- [82] X. Tian, G. Hong, B. Jiang, F. Lu, Z. Liao, J. Wang, Y. Yang, Efficient Au/C catalyst synthesized by a new method for acetylene hydrochlorination, *RSC Advances*, 5 (2015) 46366-46371.
- [83] S. Chao, Q. Guan, W. Li, Study of the active site for acetylene hydrochlorination in AuCl₃/C catalysts, *Journal of Catalysis*, 330 (2015) 273-279.
- [84] J.L. Figueiredo, M.F.R. Pereira, M.M.A. Freitas, J.J.M. Órfão, Modification of the surface chemistry of activated carbons, *Carbon*, 37 (1999) 1379-1389.
- [85] X. Li, M. Zhu, B. Dai, AuCl₃ on polypyrrole-modified carbon nanotubes as acetylene hydrochlorination catalysts, *Applied Catalysis B: Environmental*, 142-143 (2013) 234-240.
- [86] J. Zhao, J. Xu, J. Xu, T. Zhang, X. Di, J. Ni, X. Li, Enhancement of Au/AC acetylene hydrochlorination catalyst activity and stability via nitrogen-modified activated carbon support, *Chemical Engineering Journal*, 262 (2015) 1152-1160.
- [87] H.P. Klug, L.E. Alexander, X-ray diffraction procedures: for polycrystalline and amorphous materials, *X-Ray Diffraction Procedures: For Polycrystalline and Amorphous Materials*, 2nd Edition, by Harold P. Klug, Leroy E. Alexander, pp. 992. ISBN 0-471-49369-4. Wiley-VCH, May 1974., 1 (1974).
- [88] B.E. Warren, *X-ray Diffraction*, DoverPublications. com, 1969.
- [89] R. Szczygiel, P. Grybos, P. Maj, A. Tsukiyama, K. Matsushita, T. Taguchi, Low-noise multichannel ASIC for high count rate X-ray diffractometry applications, *Nuclear Instruments and Methods in Physics Research Section A: Accelerators, Spectrometers, Detectors and Associated Equipment*, 607 (2009) 229-232.
- [90] T. Taguchi, A new position sensitive area detector for high-speed and high-sensitivity X-ray diffraction analysis, *Powder Diffr.*, 21 (2006) 97-101.
- [91] M. Haruta, Size- and support-dependency in the catalysis of gold, *Catalysis Today*, 36 (1997) 153-166.
- [92] N. Lopez, J.K. Nørskov, Catalytic CO oxidation by a gold nanoparticle: A density functional study, *Journal of the American Chemical Society*, 124 (2002) 11262-11263.

- [93] M. Haruta, T. Kobayashi, H. Sano, N. Yamada, Novel gold catalysts for the oxidation of carbon monoxide at a temperature far below 0 °C, *Chemistry Letters*, (1987) 405-408.
- [94] M. Haruta, K. Saika, T. Kobayashi, S. Tsubota, Y. Nakahara, Preparation and catalytic properties of gold dispersed on beryllium oxide, *Chemistry Express*, 3 (1988) 159-162.
- [95] M. Haruta, When gold is not noble: catalysis by nanoparticles, *The Chemical Record*, 3 (2003) 75-87.
- [96] G.J. Hutchings, M. Haruta, A golden age of catalysis: a perspective, *Applied Catalysis A: General*, 291 (2005) 2-5.
- [97] M. Valden, X. Lai, D.W. Goodman, Onset of Catalytic Activity of Gold Clusters on Titania with the Appearance of Nonmetallic Properties, *Science*, 281 (1998) 1647-1650.
- [98] M. Haruta, Catalysis of Gold Nanoparticles Deposited on Metal Oxides, *CATTECH*, 6 (2002) 102-115.
- [99] C.L. Cleveland, U. Landman, T.G. Schaaff, M.N. Shafigullin, P.W. Stephens, R.L. Whetten, Structural evolution of smaller gold nanocrystals: The truncated decahedral motif, *Physical review letters*, 79 (1997) 1873-1876.
- [100] J.T. Miller, A.J. Kropf, Y. Zha, J.R. Regalbuto, L. Delannoy, C. Louis, E. Bus, J.A. van Bokhoven, The effect of gold particle size on Au-Au bond length and reactivity toward oxygen in supported catalysts, *Journal of Catalysis*, 240 (2006) 222-234.
- [101] S. Komaba, Y. Matsuura, T. Ishikawa, N. Yabuuchi, W. Murata, S. Kuze, Redox reaction of Sn-polyacrylate electrodes in aprotic Na cell, *Electrochemistry Communications*, 21 (2012) 65-68.
- [102] Z. Bakenov, I. Taniguchi, Electrochemical performance of nanocomposite LiMnPO₄/C cathode materials for lithium batteries, *Electrochemistry Communications*, 12 (2010) 75-78.
- [103] P. Riello, P. Canton, A. Benedetti, Au/C Catalyst: Experimental Evidence of the Coexistence of Nanoclusters and Larger Au Particles, *Langmuir*, 14 (1998) 6617-6619.
- [104] B. Block, J.C. Bailar Jr, The Reaction of Gold (III) with Some Bidentate Coordinating Groups, *Journal of the American Chemical Society*, 73 (1951) 4722-4725.
- [105] L.K. Minacheva, A.S. Gladkaya, V. Sakharova, G. Don, R. Shchelkov, M. Porai-Koshits, Structure of bis (ethylenediamine) gold (III) determined by single-crystal X-ray Diffraction, *Zh. Neorg. Khim*, 233 (1988) 683-687.
- [106] S.E. Barnes, Optimization of Single and Bimetallic Noble Metal Catalysts by Strong Electrostatic Adsorption, 2011.

- [107] M. Brust, M. Walker, D. Bethell, D.J. Schiffrin, R. Whyman, Synthesis of thiol-derivatised gold nanoparticles in a two-phase liquid–liquid system, *J. Chem. Soc., Chem. Commun.*, (1994) 801-802.
- [108] M.M. Maye, Y. Lou, C.-J. Zhong, Core-shell gold nanoparticle assembly as novel electrocatalyst of CO oxidation, *Langmuir*, 16 (2000) 7520-7523.
- [109] M.M. Maye, W. Zheng, F.L. Leibowitz, N.K. Ly, C.-J. Zhong, Heating-Induced Evolution of Thiolate-Encapsulated Gold Nanoparticles: A Strategy for Size and Shape Manipulations, *Langmuir*, 16 (1999) 490-497.
- [110] N.L. Jinli ZHANG, Wei LI, Bin DAI, Progress on cleaner production of vinyl chloride monomers over non-mercury catalysts, *Front. Chem. Sci. Eng.*, 5 (2011) 514-520.
- [111] K. Zhou, W. Wang, Z. Zhao, G. Luo, J.T. Miller, M.S. Wong, F. Wei, Synergistic Gold–Bismuth Catalysis for Non-Mercury Hydrochlorination of Acetylene to Vinyl Chloride Monomer, *ACS Catalysis*, 4 (2014) 3112-3116.
- [112] J. Gu, Q. Du, Y. Han, Z. He, W. Li, J. Zhang, Nitrogen-doped carbon supports with terminated hydrogen and their effects on active gold species: a density functional study, *Physical Chemistry Chemical Physics*, 16 (2014) 25498-25507.
- [113] M. Conte, A.F. Carley, C. Heirene, D.J. Willock, P. Johnston, A.A. Herzing, C.J. Kiely, G.J. Hutchings, Hydrochlorination of acetylene using a supported gold catalyst: A study of the reaction mechanism, *Journal of Catalysis*, 250 (2007) 231-239.
- [114] J. Xu, J. Zhao, J. Xu, T. Zhang, X. Li, X. Di, J. Ni, J. Wang, J. Cen, Influence of Surface Chemistry of Activated Carbon on the Activity of Gold/Activated Carbon Catalyst in Acetylene Hydrochlorination, *Industrial & Engineering Chemistry Research*, 53 (2014) 14272-14281.
- [115] X. Tian, G. Hong, B. Jiang, F. Lu, Z. Liao, J. Wang, Y. Yang, Efficient Au 0/C catalyst synthesized by a new method for acetylene hydrochlorination, *RSC Advances*, 5 (2015) 46366-46371.
- [116] B.P. Block, J.C. Bailar, The Reaction of Gold(III) with Some Bidentate Coördinating Groups¹, *Journal of the American Chemical Society*, 73 (1951) 4722-4725.
- [117] K. O’Connell, J.R. Regalbuto, High Sensitivity Silicon Slit Detectors for 1 nm Powder XRD Size Detection Limit, *Catalysis Letters*, 145 777-783.
- [118] W. Spieker, J. Regalbuto, A fundamental model of platinum impregnation onto alumina, *Chemical Engineering Science*, 56 (2001) 3491-3504.
- [119] X. Hao, W. Spieker, J. Regalbuto, A further simplification of the revised physical adsorption (RPA) model, *Journal of colloid and interface science*, 267 (2003) 259-264.

- [120] B. Dai, Q. Wang, F. Yu, M. Zhu, Effect of Au nano-particle aggregation on the deactivation of the AuCl₃/AC catalyst for acetylene hydrochlorination, *Scientific reports*, 5 (2015).
- [121] Z. Chen, Q. Gao, Enhanced carbon monoxide oxidation activity over gold–ceria nanocomposites, *Applied Catalysis B: Environmental*, 84 (2008) 790-796.
- [122] W. Wittanadecha, N. Laosiripojana, A. Ketcong, N. Ningnuek, P. Praserttham, J. Monnier, S. Assabumrungrat, Preparation of Au/C catalysts using microwave-assisted and ultrasonic-assisted methods for acetylene hydrochlorination, *Applied Catalysis A: General*, 475 (2014) 292-296.
- [123] D.S. Rustad, N.W. Gregory, The ultraviolet-visible absorption spectrum of dimeric gold(III) chloride in the gas phase. An equilibrium study of vapours formed by gold-chlorine-water mixtures, *Polyhedron*, 10 (1991) 633-643.
- [124] J. Zhang, Z. He, W. Li, Y. Han, Deactivation mechanism of AuCl₃ catalyst in acetylene hydrochlorination reaction: a DFT study, *RSC Advances*, 2 (2012) 4814-4821.
- [125] J. Ma, S. Wang, B. Shen, Study on the effects of acetylene on an Au–Cu/C catalyst for acetylene hydrochlorination using Monte Carlo and DFT methods, *Reac Kinet Mech Cat*, (2013) 1-10.
- [126] Q.L. Song, S.J. Wang, B.X. Shen, J.G. Zhao, Palladium-Based Catalysts for the Hydrochlorination of Acetylene: Reasons for Deactivation and Its Regeneration, *Petroleum Science and Technology*, 28 (2010) 1825-1833.
- [127] S.A. Mitchenko, T.V. Krasnyakova, I.V. Zhikharev, Catalytic hydrochlorination of acetylene on mechanochemically-activated K(2)PdCl(4), *Theoretical and Experimental Chemistry*, 44 (2008) 316-319.
- [128] G.J. Hutchings, M. Haruta, A golden age of catalysis: A perspective, *Applied Catalysis a-General*, 291 (2005) 2-5.
- [129] K. O'Connell, J.R. Monnier, J.R. Regalbuto, In Preparation, in, 2016.
- [130] W. Tyson, W. Miller, Surface free energies of solid metals: Estimation from liquid surface tension measurements, *Surface Science*, 62 (1977) 267-276.
- [131] S. Wang, B. Shen, Q. Song, Kinetics of acetylene hydrochlorination over bimetallic Au–Cu/C catalyst, *Catalysis letters*, 134 (2010) 102-109.
- [132] M.B. Griffin, A.A. Rodriguez, M.M. Montemore, J.R. Monnier, C.T. Williams, J.W. Medlin, The selective oxidation of ethylene glycol and 1,2-propanediol on Au, Pd, and Au–Pd bimetallic catalysts, *Journal of Catalysis*, 307 (2013) 111-120.
- [133] N. Job, S. Lambert, M. Chatenet, C.J. Gommès, F. Maillard, S. Berthon-Fabry, J.R. Regalbuto, J.-P. Pirard, Preparation of highly loaded Pt/carbon xerogel catalysts for

Proton Exchange Membrane fuel cells by the Strong Electrostatic Adsorption method, *Catalysis Today*, 150 (2010) 119-127.

[134] S. Cao, Effect of Nanoparticle Size, Support, and Potassium Dopant on Ruthenium Activity for Levulinic Acid (LA) Hydrogenation to γ -Valerolactone (GVL), (2013).

[135] H.-R. Cho, J.R. Regalbuto, The rational synthesis of Pt-Pd bimetallic catalysts by electrostatic adsorption, *Catalysis Today*, 246 (2015) 143-153.

[136] X. Hao, L. Quach, J. Korah, W. Spieker, J.R. Regalbuto, The control of platinum impregnation by PZC alteration of oxides and carbon, *Journal of Molecular Catalysis A: Chemical*, 219 (2004) 97-107.

[137] K. O'Connell, J. Regalbuto, High Sensitivity Silicon Slit Detectors for 1 nm Powder XRD Size Detection Limit, *Catalysis Letters*, 145 (2015) 777-783.

[138] A.G. Sault, R.J. Madix, C.T. Campbell, Adsorption of oxygen and hydrogen on Au(110)-(1 \times 2), *Surface Science*, 169 (1986) 347-356.

[139] M. Conte, G.J. Hutchings, Hydrochlorination of Acetylene Catalyzed by Gold, in: *Modern Gold Catalyzed Synthesis*, Wiley-VCH Verlag GmbH & Co. KGaA, 2012, pp. 1-26.

[140] S.P. Mehandru, A.B. Anderson, Acetylene adsorption on Pt(111) and unreconstructed (110) and (100) surfaces, *Applications of Surface Science*, 19 (1984) 116-134.


[141] M. Shekhar, J. Wang, W.-S. Lee, W.D. Williams, S.M. Kim, E.A. Stach, J.T. Miller, W.N. Delgass, F.H. Ribeiro, Size and Support Effects for the Water-Gas Shift Catalysis over Gold Nanoparticles Supported on Model Al₂O₃ and TiO₂, *Journal of the American Chemical Society*, 134 (2012) 4700-4708.

[142] M. Haruta, S. Tsubota, T. Kobayashi, H. Kageyama, M.J. Genet, B. Delmon, Low-temperature oxidation of CO over gold supported on TiO₂, α -Fe₂O₃, and Co₃O₄, *Journal of Catalysis*, 144 (1993) 175-192.

[143] J. Parmeter, M. Hills, W. Weinberg, Interaction of acetylene with the ruthenium (001) surface, *Journal of the American Chemical Society*, 108 (1986) 3563-3569.

[144] M. Abon, J. Billy, J.C. Bertolini, Ethylene and acetylene adsorption on a Pt(111) face: Comparative $\Delta\phi$ and coverage measurements, *Surface Science*, 171 (1986) L387-L394.

APPENDIX A: PERMISSION TO REPRINT



[My Orders](#) [My Library](#) [My Profile](#) Welcome [oconneco@email.sc.edu](#) [Log out](#) | [Help](#)

My Orders > Orders > All Orders

License Details

This is a License Agreement between Kerry C O'Connell ("You") and Springer ("Springer"). The license consists of your order details, the terms and conditions provided by Springer, and the [payment terms and conditions](#).

[Get the printable license.](#)

License Number	3771890560414
License date	Dec 18, 2015
Licensed Content Publisher	Springer
Licensed Content Publication	Catalysis Letters
Licensed Content Title	High Sensitivity Silicon Slit Detectors for 1 nm Powder XRD Size Detection Limit
Licensed Content Author	K. O'Connell
Licensed Content Date	Jan 1, 2015
Volume number	145
Issue number	3
Type of Use	Thesis/Dissertation
Portion	Full text
Number of copies	1
Author of this Springer article	Yes and you are the sole author of the new work
Title of your thesis / dissertation	Characterization, synthesis, and optimization of Au based bimetallic catalysts for the hydrochlorination of acetylene to vinyl chloride
Expected completion date	Mar 2016
Estimated size(pages)	120
Total	0.00 USD

BACK